ABSTRACT

Title of Dissertation: THERMO-MECHANICAL FATIGUE OF STEEL PILES IN
                            INTEGRAL ABUTMENT BRIDGES

                             Jafar Razmi, Doctor of Philosophy, 2012

Dissertation Directed By: Professor M. Sherif Aggour

                            Department of Civil and Environmental Engineering

        The issue of fatigue in steel piles of Integral Abutment Bridges (IABs) is investigated. A

three-dimensional, non-liner finite element (FE) model is constructed for a bridge located in a

harsh climate. Historic temperature data for the region is obtained and a sinusoidal model was

developed to represent the daily and seasonal temperature changes. The FE is parametrically run

for 5 cases with bridge lengths varying between 400 and 1800 feet under the cyclic load of daily

and seasonal temperature variations. The pile behavior and stresses in the piles are evaluated and

a fatigue model is used to determine the fatigue life of the piles. The Palmgren-Miner rule is used

to evaluate the combined effects and contribution of both types of temperature cycles. The

critical location of the pile is modeled locally utilizing a global-local modeling approach.

"Successive initiation" in conjunction with a strain-based fatigue damage model is implemented

in the local model to determine the thermo-mechanical fatigue crack initiation site, propagation

path, and rate in the piles.

The results show that maximum stress occurs in the pile furthest from the center of the bridge in

its flange right below the concrete abutment. Plastic deformation is observed in all the piles and

in all the cases studied indicating the possibility of low cycle fatigue. Lateral displacement and

maximum plastic deformation in the piles increases as the length of the bridge increases. A linear

relationship was found between the length of the bridge and the lateral displacement for both seasonal and daily temperature variations.

The longer the bridge is the shorter the fatigue life. The crack modeling results indicate that the crack initiates in the tip of the flange. Multiple cracks form in the flange, which causes an increased propagation rate. The propagation rate decreases when the crack reaches the web. The crack could initiate in the pile in the first decade, but it will take several decades to reach the web. The final failure of the pile may not occur for several decades.

THERMO-MECHANICAL FATIGUE OF STEEL PILES IN INTEGRAL ABUTMENT
BRIDGES

by

Jafar Razmi

Dissertation submitted to the Faculty of the Graduate School of the
University of Maryland, College Park in partial fulfillment
of the requirements for the degree of
Doctor of Philosophy
2012

Advisory Committee:
Professor: M. Sherif Aggour, Advisor and chair
Professor: Amde A. Amde
Associate Professor: Dimitrios G. Goulias
Professor: Chung C. Fu
Professor: Sung Lee

DEDICATION
To my wife, my son and my daughter

Acknowledgments

First and foremost I must thank my advisor, Professor Sherif Aggour. Without his dedication, his deep insight and guidance during the research and course of my studies at the University of Maryland and his support this simply would never have happened.

I would also like to thank Professor Amde for his efforts towards making this project a success. I extend my sincere appreciation to my other committee members for serving on my committee.

Finally, I sincerely express my appreciation to my wife, Leila, for her help, companionship, understanding and continuous encouragements throughout this challenging endeavor.

Table of Contents

LIST OF TABLES

LIST OF FIGURES

Chapter 1. Introduction and background

Fatigue is the cause of approximately 50-90% of all metallic failures [1]. It has recently been estimated that the annual cost of premature failures due to fatigue is well over 100 billion dollars per year. It is one of the design factors considered in many structures, buildings, bridges, aerospace machinery and even pavements. However, it has not been considered in the design of piles for integral abutment bridges (IABs). Several sources have indicated the importance of fatigue and the increased level of stress on piles in fully integral bridges [2-3]. Fatigue failure can occur even if the stress in the material is below the yield stress. The failure typically happens due to damage accumulation. In many studies that have been conducted on IABs, stresses measured or analytically calculated exceed the yield stress, indicating that low cycle fatigue is likely. However, fatigue of piles has not been considered and studied systematically, and there is no standard procedure available for piles evaluation for fatigue and crack. The main design resource for civil engineers, the American Association of State Highway and Transportation Officials (AASHTO) 17th edition (2002), explains the importance of the fatigue issue in structures only [4], but does not provide any guidelines for fatigue design and its consideration in pile structures. As bridge structures become longer and new types of materials are used for jointless bridges, the issue of fatigue becomes even more critical.

It is necessary to scientifically understand the behavior of piles under cyclic lateral loads and determine the most likely locations for crack initiation and propagation. It will also provide insights for inspectors and maintenance crews to be able to inspect the bridges and piles intelligently. In many cases these piles are covered with soil and it is very difficult to find the cracks in those locations.

1.1. Problem statement

Integral bridges are bridges without expansion joints between the abutment and the superstructure. Because there are no expansion joints in IABs, as temperatures change daily and seasonally, the length of the bridge increases and decreases cyclically for many daily and seasonal cycles. This causes the bridge superstructure, the abutment, the approach fill, the foundation piles, and the foundation soil to be subjected to cyclic load. This cyclic load could cause fatigue in piles, and joints. Cyclic tension-compression stresses are developed in piles as schematically shown in Figure 1-1. The thermal expansion is linearly proportional to the bridge length according to the following formula [5]:

$$\Delta L = \alpha_{eff}\, L\, \Delta T \qquad\qquad\qquad\qquad \text{Eq. 1-1}$$

Where L is the length of the bridge, ΔL is the change in bridge length, α_{eff} is the effective coefficient of thermal expansion (CTE), and ΔT is the change in temperature. As implied from this equation ΔL has a direct relationship with L (length of the bridge). Therefore, as a bridge gets longer the load on the piles increases proportionally. Bridges have complex structures and consist of many different materials. Determining their effective properties may not be straight forward and one may need complex simulation and numerical techniques to quantify it.

Furthermore, this equation is based on the assumption that the bridge is not constrained. In reality the bridge is constrained by piles and the backfill soil. As a result, when the bridge expands, large amounts of force may develop in the slab. This force is transferred to the top of the piles causing the piles to deform.
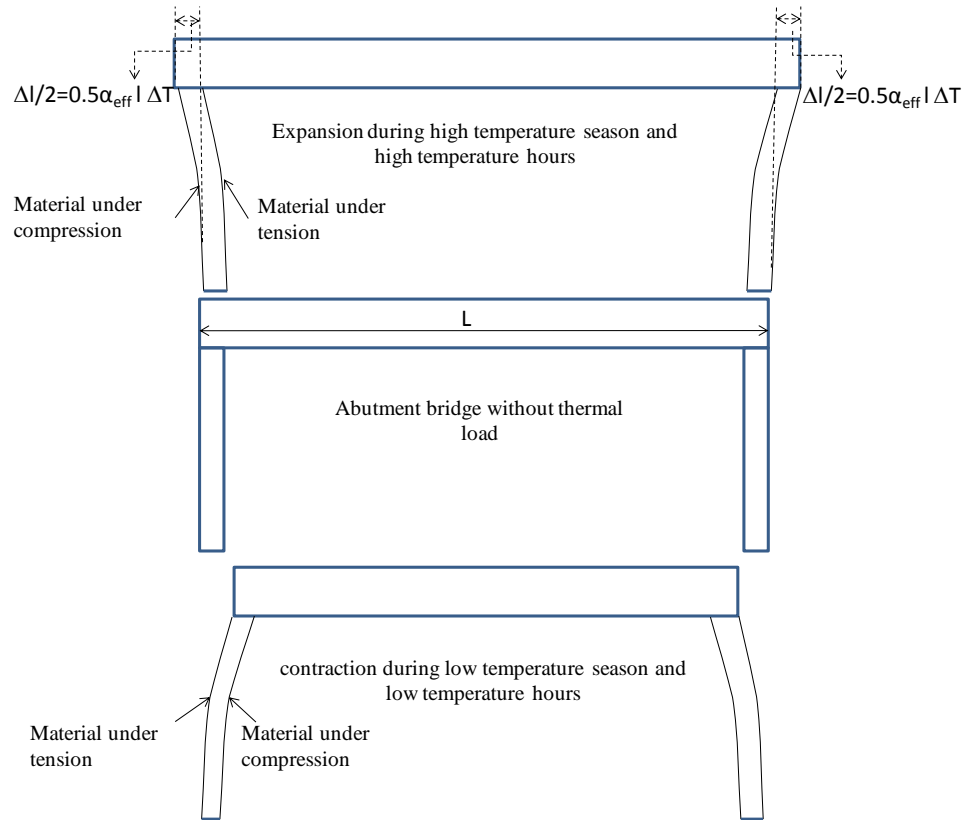
Figure 1-1: Schematic of tension and compression of Abutment Bridge due to temperature variations.

The amount of loads that act on the piles depend on the soil type and profile, the backfill soil, pile material, length of the bridge, material used for the bridge, and daily and seasonal temperature amplitudes.

Equation 1-1 also indicates that the change in the length is directly related to the change in temperature. In harsh environments with large amplitudes of daily and seasonal temperatures, as the bridges get longer, the load amplitude induced in the piles will increase. This may cause cyclic fatigue failure even if the loads are below the yield stress in piles. In some cases (as will be discussed in the literature review section) it was shown that the stress may exceed the yield

stress in a single cycle, thereby increasing the likelihood of low cycle fatigue failure.

Furthermore, the stress distribution in piles and stress concentration at joints and other sharp edges may well exceed the yield stress and cause low cycle fatigue.

1.2. Fatigue

A component or structure, which is designed to carry a single monotonically increasing application of static load, may fracture and fail if the same load or even smaller load is applied cyclically a large number of times. For example, a thin rod bent back and forth fails after a few cycles of such repeated bending. This is termed 'fatigue failure'. Examples of structures prone to fatigue failure are bridges, cranes, offshore structures, and slender towers, etc., which are subjected to cyclic loading. Fatigue crack in steel structures has been a very critical issue for many years. In particular, steel bridges have suffered immensely. Different steel members of the bridge are prone to failure including girders, bracings, eyebars, and welded joints, etc. Examples of fatigue failures include failure of the Point Pleasant Suspension Bridge in West Virginia (1967) due to fatigue of an eyebar, and failure of the Mianus River Bridge in Connecticut (1958) due to fatigue crack growth in the hanger assemblies. One of the most recent examples is the failure of the I-35 Mississippi River Bridge in Minnesota in 2007. Although the definite cause of failure is not yet known, fatigue failure was suspected to be one of the reasons [6].

The fatigue failure is due to progressive propagation of flaws in steel under cyclic loading. This is partially enhanced by the stress concentration at the tip of such a flaw or crack.

The fatigue failure occurs after three different stages, namely:

a. Crack initiation at points of stress concentration

b. Crack propagation

c. Final rupture

Fatigue failure can be defined as the number of cycles, and hence time taken to reach a pre-defined or a threshold failure criterion. Fatigue failures are classified into two categories namely high cycle and low cycle fatigue failures, depending upon the number of cycles necessary to create rupture. Typically, if the stress's amplitude exceeds the yield stress the fatigue is called low cycle fatigue (Figure 1-2). In metals and alloys, the low cycle fatigue process starts with plastic deformation due to dislocation movements, eventually forming persistent slip bands that nucleate short cracks (micro cracks). The micro cracks typically form at the surface mainly because the stresses are higher at the surface. Existing flaws and surface asperities assist formation of these micro cracks. These micro cracks themselves then act as stress concentration points at which the stress exceeds the yield stress and causes more plastic deformation. Accumulation of these micro cracks that nucleate and grow over time results in formation of a large crack that will eventually result in the failure of the structure.
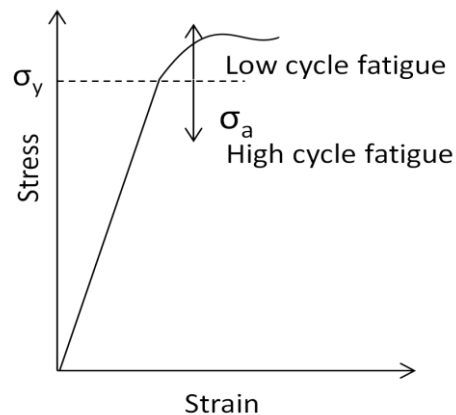
Figure 1-2: Stress limits for different fatigue regimes.

Fatigue damage is of particular concern where members are not accessible for inspection.

1.3. Integral abutment bridges (IAB)

IABs are bridges that do not have joints between the superstructure and abutment piles. In IABs the superstructure and substructure move together to accommodate the required translation and rotation. There are no bridge expansion joints, and no bearings in the case of fully IABs. In the U.S. there are more than 9,000 fully IABs and 4,000 Semi-IABs [7]. Integral Abutment Bridges have proven to be less expensive to construct, easier to maintain, and more economical over their life span [8].

Figure 1-3 shows the normal bridge and integral abutment bridge. As seen in this figure the expansion joints on both sides of the superstructure accommodates the expansion and contraction of the bridge. Therefore, no forces are developed in the superstructure due to expansion and contraction of the bridge.
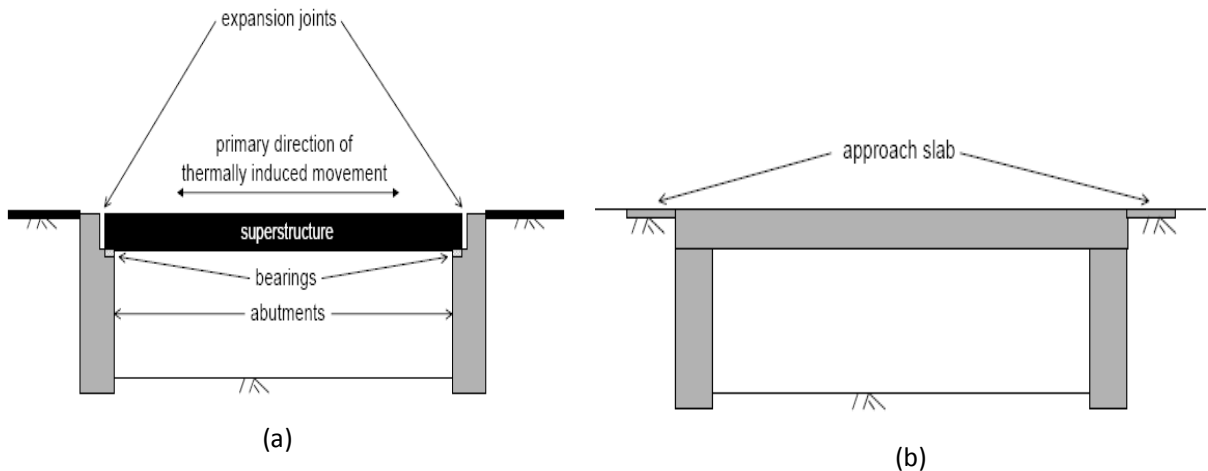
Figure 1-3: (a) A normal bridge versus (b) Integral Abutment Bridge [7].

1.4. Advantages and disadvantages of IABs

The main advantages of IABs over bridges with expansion joints are [9-12]:

- No cost for maintenance or replacement of faulty expansion joints.

- Low initial cost of design, manufacture, and installation due to the simplicity of the abutment and wing wall design.

- Fewer piles are required for foundation support and no battered piles are needed.

- Improved seismic performance.

- Greater end-span ratios are achievable.

- Smooth, uninterrupted deck of the integral bridge is aesthetically pleasing and improves vehicular riding quality.

The disadvantages of IABs [12-13] are:

- Increased earth pressure can cause abutment cracking.

- Cracks developed in the asphalt back face of the abutments, as a result a bump at the end of the bridge or approach slab could appear.

- There is lack of rational methods for predicting behavior.

- Thermal stresses are unknown.

- Temporary shoring will be required in precast bridges.

- Cranes cannot go close to placed precast beams, since backfill is put in after the beams have been placed. Therefore, cranes with large booms are required.

- Longer than normal approach slab is required.

- The proper compaction of backfill is critical.

- It limits future modifications, such as widening.

- Cracks in slab, end diaphragm or wing walls are possible.

- Erosion of the approach embankment may be caused by water intrusion.

- Field problems exist when constructing a bridge on a steep slope.

- Drill shafts cannot be used.

- The effects of elastic-shortening after post-tensioning should be carefully considered.

- Wing walls may need to be designed for heavier loads to prevent cracking.

- Adequate pressure relief joints should be provided in the approach slab to avoid overstressing of the abutments.

However, in most cases, the IABs have not had major structural damage affecting the long-term serviceability of these structures.

1.5. Pile orientation

Maruri and Petro [14] conducted a survey of all 50 states (as a follow-up to a 1995 survey) to examine how IAB design and construction had evolved over the decade. The investigators reported that:

- The majority of states that responded did not limit the maximum span within the bridge, but they did limit the total bridge length and skew angle.

- The majority of states used steel piles for the foundations, but Hawaii and Nevada also used drilled shafts.

- 33% of states reported orienting steel piles for strong axis bending (with respect to the longitudinal axis of the bridge) while 46% reported orienting piles for weak axis bending

(with respect to the longitudinal axis of the bridge).

Interestingly, over 60% of the states reported that they have not changed their design procedures in the past decade regarding loads, substructures, backfill/abutments, and approach slabs, despite the observed settlement and cracking damage. Overall, Maruri and Petro [14] noted that IAB design approaches were very inconsistent, and they recommended that more uniform guidelines be developed based on the research performed by various states.

The Idaho Department of Transportation indicates [15] that "abutments shall be supported on a single row of steel H-piles, steel smooth hollow pipe pile or steel-encased concrete piles utilizing smooth steel tubes. The preferred orientation of the piles is for bending about the strong axis."

It is also recommends that H-piles are oriented such that thermal expansion and contraction causes bending about the strong axis. This may cause higher resulting forces induced in the abutment, however the pile itself will handle larger deflections without flange buckling.

Dicleli [16] also indicates that in general, piles oriented to bend about their strong axis can accommodate larger displacement than those oriented to bend about their weak axis. The larger bending capacity of the piles about their strong axis relative to the bending capacity about their weak axis allows the bridge to accommodate larger cyclic displacement before fatigue failure of the pile takes place. The difference is more pronounced especially in stiff soil conditions.

In general, there have been different opinions about how single symmetric integral abutment piles, like H-piles, should be oriented. In the early 1980's more than half of the states in the USA, which allowed integral bridges, oriented their piles for strong-axis bending due to the thermal movements [17]. In a survey ordered by the US Federal Highway Administration in year

9

2004, the Departments of Transportation were asked how they oriented the piles in their integral bridges. The result from this survey is quite different compared to the study from the early 1980´s, which Abendroth and Greimann [17] refer to. Nowadays, most of the states are orienting integral abutment piles for weak axis bending, see Figure 1-4. But it is obvious that there are no uniform rules that are applied all over the USA. Each state makes their own decisions. Australia follows the main trend in the USA and orientates their piles for weak axis bending [18]. Figure 1-5 shows how the orientation of piles was varying from state to state in 2004 [14].
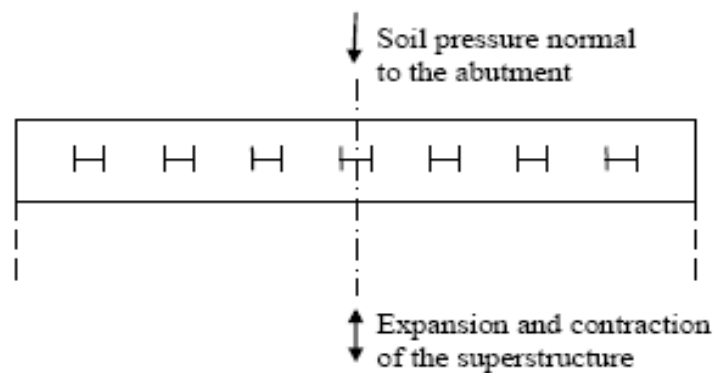
Figure 1-4: Schematic illustration of an abutment with H-piles oriented for weak axis bending, seen from above.
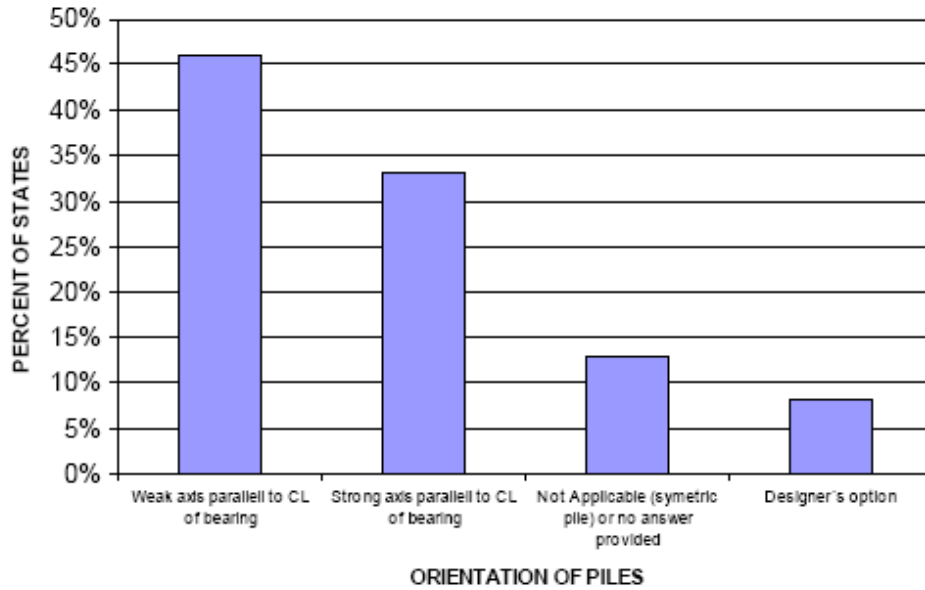
Figure 1-5: Pile orientations in the USA, according to Maruri and Petro [14].

The reason to orient the pile for weak axis bending is mainly to minimize the stresses in the abutments. For a given displacement of the abutment, a pile oriented for strong axis bending will induce higher stresses in the abutment than a pile oriented for weak axis bending. It is also done in order to make sure that local buckling of the flanges shall not occur, even if the soil is not supporting the pile laterally. Arsoy [2], Huckabee [19] Dicleli and Albhaisi [16] have studied the effect of cyclic thermal loading on the performance of steel H-piles in integral bridges with stub-abutments. One of their conclusions is that the orientation of the piles has only a negligible effect on the displacement capacity of the integral bridge. Their study was made on bridges with stub-abutments, and it is possible that this conclusion is not valid for bridges with larger abutment heights.

1.6. Pile-abutment-girder interaction

The pile-abutment-girder interaction is very important in the design of the piles. Rigid connections will transfer all forces and movements down into the piles. Hinged connections can be used in order to transfer only vertical and shear forces to the piles, and no moments.

1.7. Rigid joints

One method for building rigid connections between piles and girders is to cover the top of the piles with a cap. Leveling bolts anchored in the pile cap are then used to connect to girders (see Figure 1-6(a)). The ends of the girders are later surrounded by concrete, when the top of the abutment backwall is cast. Some states prefer welded joints for connecting steel piles and girders (see Figure 1-6(b)). This technique is used nowadays, for example in Maine, and has previously been used in many other states. New York state routinely used welding for connecting the piles and girders. However they experienced some problems with this technique and now prefer other types of connections. When the piles are driven they have to be very close to their planned position if the girders are to be welded on top of them. This means that piles often must be driven within a tolerance of 2-3 cm, and this can be hard to achieve in difficult pile driving conditions [20-21].

(a): Girder mounted on levelling bolts on top of a pile cap.　　　(b): Welded connections between piles and girders.
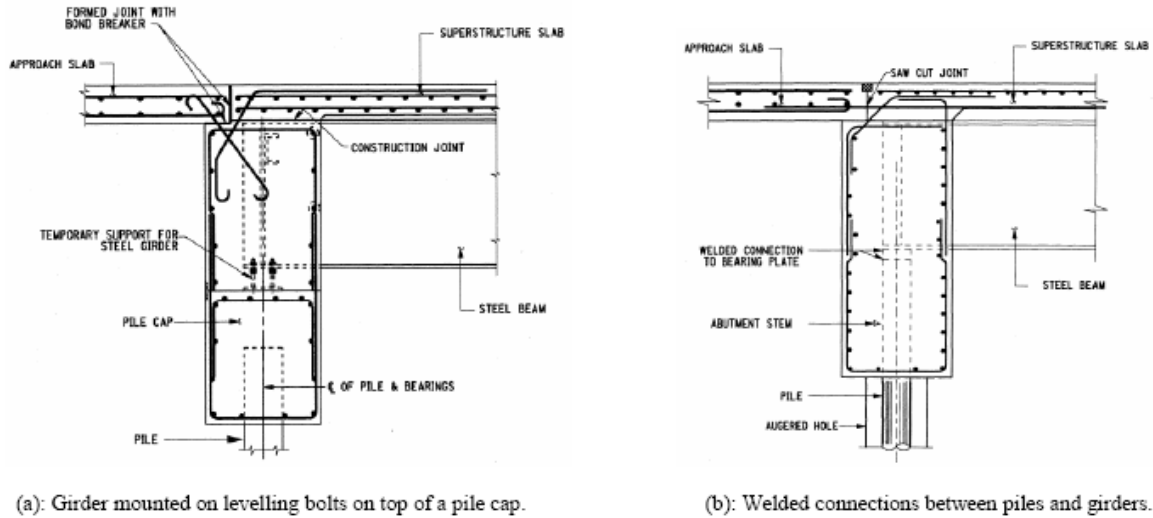
Figure 1-6: Illustrations of two different techniques of designing the pile-abutment-girder connection for steel bridges with integral abutments [21] (a) girders mounted on leveling bolts on top of a pile, (b) welded connections between piles and girders.

Connections without welds between piles and girders are easier to construct, and no differences in performance have been detected [20]. Due to these facts, it is hard to understand why some states are still using welded connections.

1.8. Hinged joints

Another approach is to use a hinge between abutment and piles. The hinge transfers only vertical and shear forces to the piles. No bending moment is transferred. An example of a bridge with abutments constructed with this technique is Gillies Street Bridge in Australia.

Figure 1-7 shows one of the abutments from that bridge and the hinged connection between the abutment and the concrete piles that was used [18].
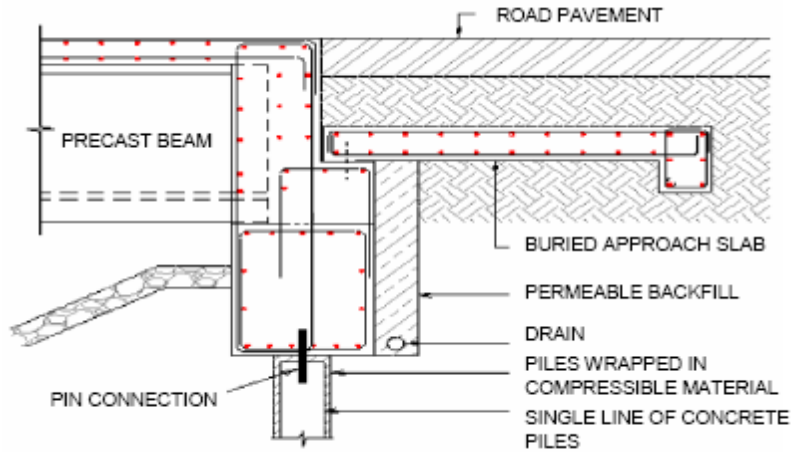
Figure 1-7: Abutments with hinged-piles [18].

The pin connection used in the Gilles Street Bridge is illustrated in more detail in Figure 1-8. The pin connection was made of galvanized dowel bars, which was anchored in both the concrete pile and the pile cap. Polystyrene sheets were used as joint filling in order to avoid crushing of the concrete when the pile cap is rotating due to the applied moments. To make sure that the lateral forces were not getting too high in the top of the concrete piles, the upper 2 m were wrapped with 50 mm thick compressible foam.
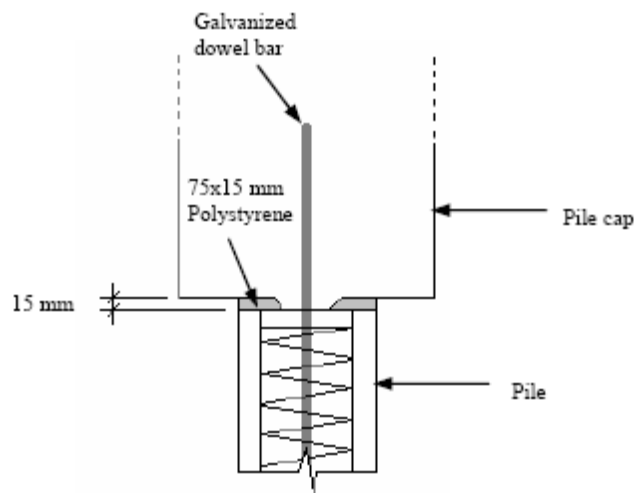
Figure 1-8: Illustration of the pin connection used in Gilles Street Bridge [18].

The Virginia Department of Transportation (VDOT) has been working a lot with jointless bridges and has had a very good experience with these types of bridges. VDOT prefers steel H-piles oriented in weak axis bending, and the abutments are designed in a way that reduce the pile stresses. One way of reducing the pile stresses is to construct a moment relief hinge in the abutment wall. VDOT has been developing a moment relief hinge based on a shear key along the joint. This type of hinge has been modified after some tests made by Arsoy [2]. Figure 1-9 illustrates both the original and the modified hinge [22].
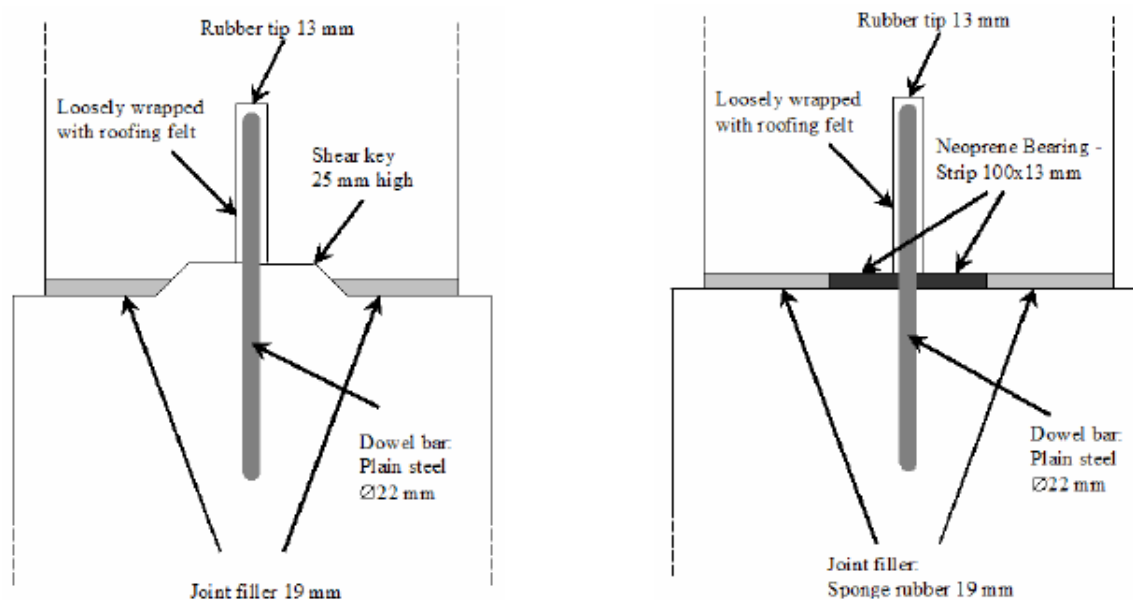
Figure 1-9: Original hinge to the left and modified hinge to the right, redrawn from Weakley [22], and Arsoy [2].

The modified hinge is more flexible to rotation and consists of strips of neoprene along both sides of the line of dowels. The rest of the joint is filled with some joint filler, for example sponge rubber. The vertical forces will be transferred from the upper part of the abutment, through the neoprene, and down into the pile cap. The dowels will transfer the shear forces.

Arsoy [2] performed full scale laboratory tests of the original hinge construction and the modified hinge. The hinges were tested both with static and cyclic lateral loadings. The shear key in the original hinge construction had already failed at the static test. Analysis of the data showed that the hinge did not work as a hinge. The abutment and the pile cap rotated as one singular unit until the shear key failed. The bond between the upper and lower part was almost as strong as if they had been cast together. The modified hinge did not show such behavior in the tests. It behaved more as a hinge. The cyclic load test showed no sign of fatigue failure after more than 27,000 cycles, which should simulate the thermal movements over 75 years. The bending stress during theses cycles was a bit higher than the yield strength of the dowel bars. The original hinge with the failed shear key did not show any further damage after the cyclic test. A failure of the shear key is therefore not expected to result in a collapse of the bridge.

The rotational stiffness of the hinged abutments seems to be dependent on the abutments rotation angle. When the rotation gets larger, the rotational stiffness seems to go towards a low constant. Arsoy [2] drew the conclusion that hinged abutments actually reduce the pile moments significantly. This technique can therefore be useful in order to construct longer bridges with integral abutments, without getting bending moments that are too large in the piles.

Chapter 2. Literature review

This chapter summarizes the findings in the literature on fatigue in IABs. Lateral displacements at the top of the piles will lead to varying stresses in the H-piles. It is possible that these stresses will exceed the yield strength now and then during the bridge lifetime. The tip of the flanges will then yield, and plastic deformations take place. The frequency at which plastic deformations may occur depends on climate, soil properties, bridge length, pile cross-section, etc. Low-cycle fatigue failure will start with small cracks that appear at the tip of the flanges. These cracks will propagate towards the web under further cyclic loading, see Figure 2-1. The width of the flanges that can transfer axial loads becomes smaller and smaller, and the web has to support a greater axial load. The part of the pile where the cracks are propagating starts to work more as a hinge, until ultimate failure of the web takes place [23].
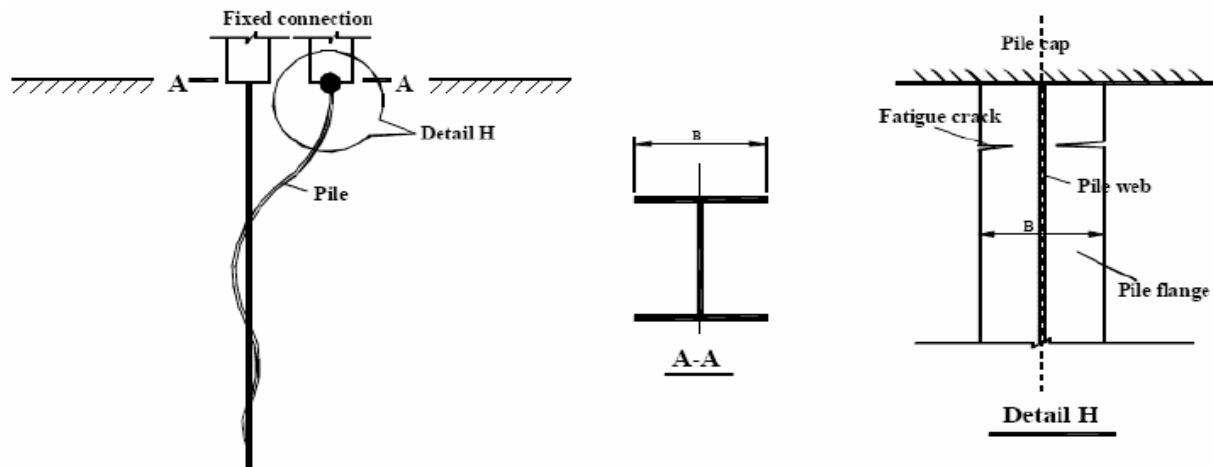
Figure 2-1: Illustration of low-cycle fatigue failure in a steel H-pile [23].

One way of estimating the time until low-cycle fatigue failure is to use a strain-based approach. In this approach, the number of displacement cycles that a structural unit can withstand is

formulated as a function of the plastic strains in the studied area of a structural member. Piles in integral abutments will be subjected to lateral movements. In many cases these movements are quite large and plastic deformations are expected. Dicleli and Albhaisi [24] stated that a strain-based approach was an appropriate way of estimating the number of cycles until low cycle fatigue failure for steel piles in integral abutment bridges. Several other researchers have investigated the cyclic lateral load and fatigue in piles.

Narong and Amde found that steel piles of such an abutment are routinely subjected to axial and flexural stresses approaching, equaling, or exceeding yield stresses [25]. The stress at the top of the pile is sufficient to initiate a yield stress in the steel, but not sufficient to cause the formation of a plastic hinge [26-27]. However, for longer integral abutment bridges, such piling stresses, if large enough, will result in the formation of plastic hinges that will limit the flexural resistance of the piles to additional superstructure elongation. Lack of movement of the abutments can cause higher stresses in the deck than it is designed to sustain, due to the bridge attempting to expand or contract while being restrained.

One of more important works that has been completed was Arsoy and Duncan's work, done at the Virginia Institute of Technology in 2000 [2]. In this work, Arsoy experimentally investigated the interaction between the soil and piles for semi-integral abutment bridges for a daily temperature cycle. An experiment was conducted on three different pile types, in which a constant lateral load was applied cyclically for 27,000 cycles, which replicates 75 years of daily temperature variations. The test was conducted for both semi-integral and fully-integral abutment types. The experimental results showed no appreciable change in the pile behavior. They also conducted a numerical analysis of the pile-abutment-soil interaction. To save time, the structures

were simplified and used a two-dimensional plane strain case. This analysis provided the displacements and moments induced in piles. Two different softwares, LPILE and SAGE were used. Two main relevant conclusions that were made are:

- Stiffer piles increase the stress on piles.
- Cyclic damage to steel piles may not be an issue, as long as stress induced in the piles is less than yield stress. However concrete piles were not recommended, because under lateral loads tension cracks may develop and progressively worse, thereby significantly reducing the vertical load carrying capacity of these piles.

The study was for a specific geometry and weather, so it may not be applicable if the length of the bridge is increased or the environment is made harsher. Integral abutment bridges longer than 180 m have already been built and longer bridge spans may also be under consideration for future constructions. Arsoy's investigation was more experimental. It is not possible to always run an experiment for all the bridges. Furthermore in the experiment he did not simulate the complex three-dimensional state of stress. A simplified experiment was used in which load was applied in one dimension only. In cases that fatigue is likely, there is also need to predict the crack initiation, propagation site, and path. Arsoy's investigation does not provide any tool for that.

In another study conducted in Europe, Hallmark investigated low cycle fatigue for one specific bridge in Sweden, with a span length of 40 m [3]. Limited parametric studies were conducted on parameters such as soil stiffness, pile cross section, and length of the bridge. It was found that in the European climate, and under their traffic load, fatigue may not become an issue up to lengths of 100m. However it did not study bridge spans longer than 100m. Furthermore, in a much

harsher environment, the temperature range is larger, and therefore the deformation range becomes larger, which in turns increases the load on the piles and may cause failure.

Additionally, separate cycles of traffic and thermal cycles were assumed, whereas these two types of cyclic loads are occurring simultaneously and should be counted together. Rain-flow method can be used to count the number of cycles. Another shortcoming of this research was that it only proposed to estimate the number of cycles, and have no way of determining the crack initiation and propagation site. Furthermore, a simplified analytical approach was used to calculate the effective coefficient of thermal expansion and deformation in piles. The approach was not capable of capturing a complex three-dimensional load condition. A finite element model should be able to correct both of these short comings.

An overall assessment of abutment bridges was done by Wiss, Janney, Elstner Associates [4]. According to this study, abutment bridge behavior is not yet well understood. Several hypotheses were proposed that were to be investigated. On page 26 of the report where the influence of cyclic load due to thermal variations was mentioned, this hypothesis is stated: "Hypothesis: Changes in soil-structure interaction under cyclic loading produces corresponding changes in bridge behavior, the result of which may result in cracking or yielding of substructure elements." Within the paragraph before this hypothesis sentence: "Ultimately, the variations in soil-structure interaction over time can lead to cracking in concrete bridge abutments and yielding of piles." was noted. Furthermore, it was stated that "Steel piles in integral bridges could be subjected to fatigue related distress due to the cyclical nature of the environmental loads. The following rationalization was given by Loveall (1985), who reported that fatigue research conducted under stress ranges well below yield stress indicates that fatigue cracking should occur at a low number

of stress cycles. For piles in weak axis bending, fatigue cracking will commence at flange tips and propagate toward the web when the flexural component of stress sufficiently exceeds the axial component along the flange edge in tension. Because the flexural component is proportional to the effective width of the flange, cracking of the flange will reduce the effective width and the flexural component, thereby producing a hinge-like condition where the axial compression protects the piles from further crack growth. Loveall (1985) recommended additional research to describe the behavior of piles and to determine if there are sufficient stress cycles to result in the fatigue crack growth just discussed. Observations of fatigue cracking of piles have not been reported in the literature.

In a study conducted by Health and Safety Executives (HSE) in United Kingdom [28], the damage due to driving in mono-tower offshore structures was calculated, and remaining life of the piles was also calculated using standard curves (C and F_2) for sand and clay. These curves were developed by HSE as standard for fatigue measurements. It was concluded that fatigue damage of piles due to in-place conditions and driving was significant. Although in-place stresses due to utilization of the piles in this study were low, the environmental fatigue damage was relatively high.

Dicleli et al. conducted analysis of maximum lateral displacement in abutment bridges based on displacement capacity of H shaped steel piles in sand [16]. A life of 75 years was assumed and a fatigue model was used to determine the maximum deformation that an H pile can stand to have that life. It was recommended that the maximum lengths of concrete integral bridges be limited to 190 m in cold climates and 240 m in moderate climates, and that of steel integral bridges are limited to 100 m in cold climates and 160 m in moderate climates. This study was conducted

only in sand. According to previous studies conducted by Arsoy, stiffer soil increases the stress on the piles. Therefore, the fatigue life may be shorter in the case of clay and stiff clay. Dicleli et al. did not conduct analysis of crack initiation and propagation predictions. So it is not clear where the fatigue crack in piles may start.

Dunker and Abu-Hawash in a study conducted in Iowa, acknowledged, that there are several fatigue considerations in design of abutment bridges. First, there is the high-stress–low-cycle condition caused by annual thermal expansion and contraction of the bridge. Second, there is a low stress– high-cycle fatigue condition caused by live and impact loads on the end span. However, According to these researchers, AASHTO allowable fatigue stress for the base metal in the pile is 24 ksi for more than 2 million cycles. Bending stresses in the pile due to these conditions, fluctuating live plus impact load on the end span, are unlikely to exceed this value if the pile is required to meet ordinary service load column checks. Evidently, there is no known field evidence to date of fatigue damage for any of the conditions mentioned. However, this analysis is not based on systematic calculation of stresses and fatigue damage.

The Federal Highway Administration and AASHTO [30 & 5] talk about the allowable stresses in piles. According to the first one, depending on the hidden defect factor, the stresses could be lower than 0.3 F_y for ideal (defect factor of 1) or 0.25F_y for normal hidden (defect factor of 0.85). The second document stresses on the same load. But this time summation of both live and dead loads must be lower than 0.25 F_y. Current design approaches require the stress to be 0.25 of yield stress (σ_y). However, this does not invalidate the concern about fatigue, as fatigue can happen at loads much lower than the yield strength of the material. Assuming even under lateral load this stress does not exceed 0.25σ_y, fatigue can still happen. If the stresses are below the yield stress,

the fatigue is called high cycle fatigue.

Jorgensen made measurements on an abutment bridge for a one year period [31]. Readings of the bridge length, gap between the soil backfill and backside of the abutment, openings in expansion joints on the concrete approach slabs, and vertical elevation of abutments and piers were made, This study was conducted on The Case County Bridge about 2 miles north of Fargo. The author used an analytical approach to calculate the stresses in the piles. These stresses were found to result in the same pile displacement that was measured using slope indicator. It was found that stresses at the top of the pile were sufficient to initiate a yield stress in the steel. It was also found that the two parameters that had the most influence on pile stresses are the amount of abutment movement and the modulus of subgrade reaction near the upper portion of the pile. In summary, It was concluded that stresses in piles may get as high as yield stress in abutment bridges and therefore increase the possibility of having low cycle fatigue. In this study fatigue analysis was not conducted.

Girton et al. [32] studied two skewed bridges in Iowa. An experiment was designed and thermocouples and strain gauges were installed on these bridges, and thermal expansion and strains on weak and strong axis of the piles were measured. In this study the authors found that stress may reach 60% to 75% of yield stress, based on the amount of strain that they measured on the bridge over a one year period. The measured strains (at the location of strain gauges) on the piles were in order of 600 to 900 microstrains and the yield strain of steel was about 1200 micro strain. The thermal strains at the flange tips (beyond the strain gauge and below abutment) are larger than the measured strain (600-900 microstrain). So most likely yielding and low cycle fatigue will happen at the flange tips. Cyclic measurement or fatigue analysis was not conducted.

Hoppe and Gomez [33] analyzed an integral backwall bridge that was instrumented during construction and monitored for 2.5 years. Field instrumentation included strain gages, temperature probes, and earth pressure cells. Data were collected continuously using electronic data loggers. The results demonstrated a satisfactory performance of the structure; however, some maintenance problems associated with excessive approach settlement were observed. Soil pressures exerted on the back of the integral backwall showed significant daily variation as a result of ambient air temperature fluctuation. This study mostly focused on stresses in girders. Stresses in piles have not been reported.

Lawver et al. monitored a bridge near Rochester Minnesota for several years of service, and used over 180 instruments to monitor several effects such as abutment rotation, abutment pile strains, steel reinforcement strains, etc [34]. The most important relevant conclusion that this study made was that abutment piles appeared to be deforming in double curvature, with pile strains on the approach panel sides of the piles indicating the start of yielding.

Alizadeh and Davisson conducted a study as part of the comprehensive pile testing program initiated by U.S. Army Engineer District, Little Rock, Corps of Engineers, in connection with Arkansas River Navigation Project [35]. The goal of this project was to understand the effect of repetitive loading on the batter and vertical piles. The main relevant conclusion made in this study was that repeated loading caused an increase in total deflection at a given load level of 70% to 90% over that for the first cycle of load. This is a significant change over repetitive cycles of load that may be even larger in abutment bridges. This may indicate that cyclic fatigue may also happen in regular types of bridges. It also found that maximum stresses in piles could reach 80% of nominal yield stress.

Matlock et al focused on behavior of soil and soil pile interactions rather than stresses developed in piles [36]. In the study static and cyclic loads were conducted on single piles and a group of piles. Large groups of piles (10 piles) showed increased deflection and bending moment in cyclic loads. Smaller groups (5 piles) had roughly the same behavior of a single pile.

Meimon et al. was also focused on the behavior of single piles, groups of piles, and soil-pile interactions [37]. The stresses in piles were not studied. The main conclusion in the cyclic test was that soil reaction breakdown was recorded near the surface, while the soil reaction increased at lower levels of soil.

Brown et al. studied a group of nine piles that were subjected to two way cyclic lateral loading [38]. The piles were pinned in stiff over-consolidate clay with water above the surface, in Huston Texas. The piles were instrumented so that the soil resistance could be monitored. The results emphasize the highly non-linear nature of the pile-soil-pile interaction. A substantial reduction in ultimate soil resistance was measured in the group of piles relative to that of a similarly loaded single pile for both the first cycle and for 100 cycles of load.

Brown et al. also studied a large scale group of steel pipe piles and single isolated piles that were subjected to two way cyclic lateral loading [40]. The variation of soil resistance was measured experimentally. The main relevant conclusions that were made are: deflection of the piles in the experimental group was significantly greater than that of a single pile under load equal to the average load per pile, and that cyclic loading in two directions had a relatively small effect on pile response relative to similar tests conducted in clays. Some softening of the response of the piles in the group was observed at large loads (approaching pile failure); almost no effect occurred at small loads.

2.1. Objectives and scope

Based on the extensive literature review conducted in this study, it was found that the issue of fatigue is important in IABs, particularly the new generation that are made longer and may be built in a harsh climate. Many researchers have stressed the importance of understanding the stresses in piles and many have shown that stresses in piles may exceed the yield stress of steel which could result in low cycle fatigue of the piles. However, no comprehensive study has so far been conducted in order to determine with certainty the displacement in piles, the stress-strain behavior of piles, possibility of crack initiation due to fatigue and the location of possible fatigue cracks.

The objectives of this dissertation are first to evaluate the displacement behavior of piles of IABs due to seasonal and daily temperature variations, understand the significance of each type of temperature variation and determine the stresses that develop in these piles. The aim is to understand whether the stresses exceed the yield strength of the piles and evaluate the possibility of fatigue failure due to daily and seasonal temperature variations and as a result of combination of these two loads. Furthermore, because currently, universal guidelines to determine the maximum fatigue life and length of integral bridges do not exist, it is intended to develop a guideline that can be used by bridge engineers to determine the fatigue life of IABs and also evaluate the life expectancy of existing IABs.

Additionally, none of the analysis conducted so far in the literature have been able to find the location of maximum damage and possible crack initiation and propagation site and path. In this study, "successive initiation", a continuum damage modeling approach combined with finite element analysis, which will allow for prediction of the location of maximum damage and

possible crack propagation site, will be used to determine these effects. This method can also determine the crack initiation time and propagation path. This will facilitate the work of inspectors and maintenance crews in inspecting and maintaining the piles and bridges. In particular it helps in structural health monitoring for parts that are not visible and may be covered with soil. To understand the effect of the bridge length, we will conduct a parametric study with bridge length varied between 400ft and 1800 ft. This analysis will show the relationship of fatigue life with the length of the bridge.

2.2. Proposed guidelines for determining fatigue life of piles

Currently, universal guidelines to determine the maximum fatigue life and length of integral bridges do not exist. Generally, bridge engineers depend on the performance of previously constructed integral abutment bridges to specify the maximum length for their new designs and since there are no field data available that can be used to determine the safety and fatigue credibility of existing bridges, no standard method exists to determine if the current designs and existing bridges are fatigue resistant for a long period of time. In 1982 [39], a study of integral bridge lengths in the USA revealed that continuous steel bridges with integral abutments have performed successfully for years in the 91 m (299 ft) range in North Dakota, South Dakota, and Tennessee and continuous concrete integral bridges, in the range of 152–183 m (499-600 ft) long have been constructed in Kansas, California, Colorado, and Tennessee. For years, bridge design engineers have depended on similar data to determine the maximum life of integral bridges. Bridge engineers did not conduct fatigue analysis to ensure the long term safety and reliability of the IAB piles. This chapter presents a procedure that can be used for any bridge at the design stage or for existing bridges to determine the fatigue life of the piles in IABs

as well as determine possible fatigue crack location. It will provide insights for bridge engineers for the design and inspection of the IABs. The procedure is used to evaluate fatigue life of bridges with lengths of 400, 600, 800, 1200 and 1800 ft. The procedure is outlined using a flowchart shown in Figure 2-2. The steps of the process are elaborated in the next section.

```
┌─────────────────────┐
│   Design capture    │
└─────────────────────┘
           │
┌─────────────────────────┐
│ Determine the thermal load │
└─────────────────────────┘
           │
┌─────────────────────────────┐
│ Develop mathematical model for │
│         thermal load          │
└─────────────────────────────┘
           │
┌─────────────────────────────┐
│  Develop finite element model │
└─────────────────────────────┘
           │
┌─────────────────────────────┐
│ Extract stress-strain history from │
│         finite element        │
└─────────────────────────────┘
           │
┌─────────────────────────────┐
│     Determine an appropriate    │
│      fatigue damage model      │
└─────────────────────────────┘
           │
┌─────────────────────────────┐
│  Determine the fatigue life of the │
│             piles             │
└─────────────────────────────┘
```
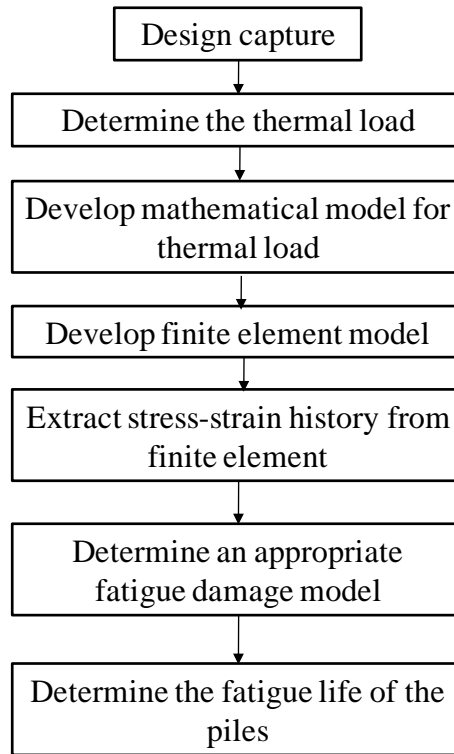
Figure 2-2: Procedure for determining the fatigue of piles in IABs.

2.2.1. Design capture

The procedure starts with design capture. This includes obtaining information on the bridge geometry, dimensions, materials, architecture, foundation properties (soil type, pile depth, type of pile, pile materials, etc.). This information will be used to construct the finite element (FE) model. The architecture of the bridge and symmetries may be utilized to reduce the size of the model. This is illustrated in the case study presented in a later section of this paper.

2.2.2. Determine the thermal load

To study the thermo-mechanical fatigue of piles, the thermal load is to be determined. In a case where other types of load may exist, all the loads and environmental conditions must be determined as well and included in the FE model. Thermal loads depend on the ambient temperature in the region that the bridge is or will be located. Typically, there are climate centers that collect hourly and daily temperature data in each region. These data are usually available and can be extracted for a long period of time (e.g., 10 years). The temperature data will provide information on the pattern of daily and seasonal temperature variations and will be used as a baseline to develop a mathematical model that can be input into the FE simulation.

2.2.3. Develop mathematical model for thermal load

Due to the random nature of the temperature data, this data may not be easily applied to the model. Typically a mathematical model needs to be created based on the historical data. There are several different techniques that can be used to model the historical data. Polynomial or sinusoidal types [2-3 & 16] of models can be fit to historical data. However, sinusoidal models are more common due to their cyclic nature and the fact that they can easily be fit to the extreme values of the temperature. The extreme values have a much more pronounced effect than the other parameters in the model.

2.2.4. Develop FE model

A FE model of the superstructure and substructure is then built. It is essential that the

model is conducted in three dimensions to capture the three dimensional state of stress and be able to determine the location of maximum stress or strain amplitudes. Commercial software or programming languages can be used to build and run the FE model. In order to determine the fatigue life, it is necessary to model the non-linear and plastic behavior of materials. For common types of bridges made with steel and concrete, it is usually reasonable to only include inelastic behavior of the steel, since plastic deformation of concrete is typically negligible compared to steel. Loads, such as thermal loads modeled using a mathematical model, traffic loads, and other dead and live loads are implemented in the FE model. Modeling the superstructure and substructure typically involves hundreds of thousands of elements and millions of degrees of freedom. To reduce the size of the model, several strategies can be utilized, e.g., using shell elements rather than using solid elements in sections with small thicknesses compared to other dimensions, or utilizing the symmetry condition of the bridge to model half or a quarter of the bridge. Since shell elements are planar elements, their number of degrees of freedom are smaller than the degrees of freedom for solid elements. Meshing is one of the most important steps in FE modeling. The type of elements that are selected depends on many different factors, e.g., type of material, type of load, compatibility with elements in different sections, etc. The final goal of conducting FE modeling is to determine the stress and strain distribution and history of the entire model and use the stress and strain history to determine the fatigue life.

2.2.5. Extract stress and strain history from FE model

Since in most cases the material experiences three dimensional state of stress, a yield criterion such as von-Mises or Tresca is needed to determine the state of deformation (elastic vs.

plastic). Depending of the state of deformation either a stress-based, strain-based or energy-based fatigue model is used to determine the fatigue life. The piles typically consist of many elements. To determine the fatigue life, the section of the pile that experiences the largest amount of cyclic stress or strain amplitude or largest amount of energy released in one cycle of loading needs to be identified. The value of stress or strain amplitude or strain energy released over one cycle of load is the value that will be used in the fatigue model to determine the fatigue life.

2.2.6. Determine appropriate fatigue damage model

Depending on the type of deformation, an appropriate type of fatigue model needs to be selected. Many different types of fatigue damage models are available in the literature. A list of models based on the damage criteria are provided in section 3.2. Depending on the type of deformation (elastic, plastic or creep) and availability of a model for a certain material a model can be selected from literature to calculate the fatigue life.

2.2.7. Determine fatigue life of the piles

Fatigue life is then determined by substituting the values of stress, strain or energy obtained from the FE into the fatigue model. Depending on how the failure is defined, one may take an average of the values of stress, strain or energy over the elements across a section in the critical location of the pile and use that value to calculate fatigue life or simply use the values of stress, strain or energy in a certain element.

Chapter 3. Cyclic fatigue modeling and analysis

3.1. Fatigue life analysis

Avoiding or controlling fatigue damage is a major issue in the design and inspection of structures subjected to cyclic loading. Fatigue life analysis or life predictions are usually used for safe life analysis, i.e., for verifying that it is very unlikely that fatigue damage will occur during the target service life of a structure. Damage tolerance analysis is used for predicting the behavior of a fatigue crack and for planning the in-service scheduled inspections. It should be a high probability that any cracks appearing are detected and repaired before they become critical. In both safe life analysis and the damage tolerance analysis there may be large uncertainties involved that have to be treated in a logical and consistent manner by stochastic modeling.

Fatigue life analysis is determining the number of cycles to failure using a fatigue model based on the material that we have in the structure. The model that is used to relate the stress amplitude to the number of cycles to failure is called a fatigue model. An example of a model is shown in Figure 3-1. This graph is often called S-N curve where S stands for stress or strain and N stands for number of cycles to failure. More advanced models may also use strain energy instead of stress or strain. However, since the term S-N curve has been used for many years, even for energy-based models the same term is typically used. The S-N curve is typically represented using the fatigue model equation. An example of a fatigue model is given below:

$$N_f = C\,(\sigma_a)^n \qquad\qquad\qquad\qquad\qquad\qquad\qquad \text{Eq. 3-1}$$

Where N_f is the number of cycles to failure, σ_a is the stress amplitude of the cyclic load (refer to Figure 3-2), C and n are constant and are called the fatigue coefficient and exponent that are

found through experiment.
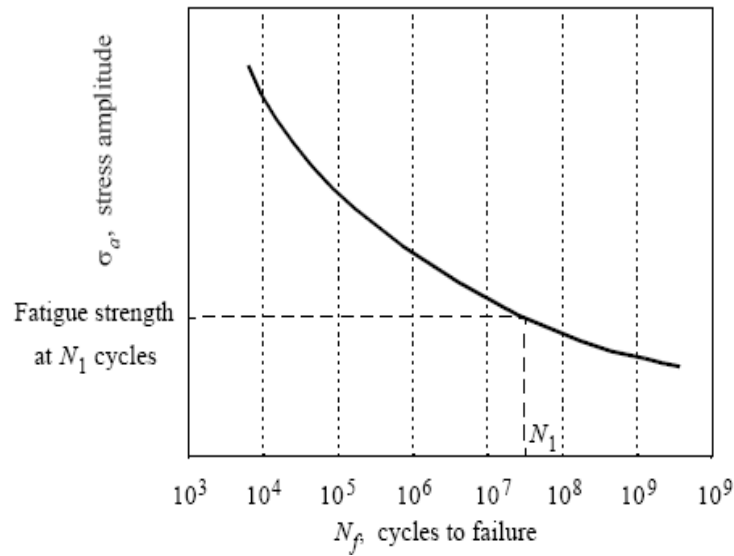
Figure 3-1: Example of S-N curve.
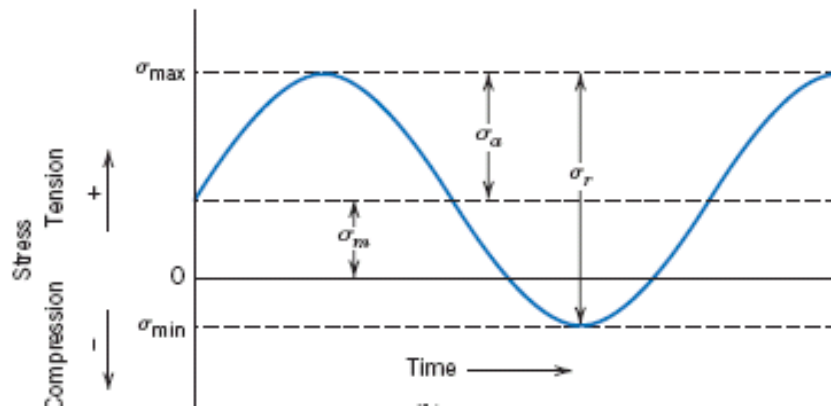
Figure 3-2: Illustration of cyclic load, stress amplitude, stress range and mean stress

The stress amplitude is defined as:

$$\sigma_a = \frac{\sigma_{max} - \sigma_{min}}{2}$$ Eq. 3-2

where σ_{max} is the maximum stress and σ_{min} is the minimum stress. Stress amplitude is usually

33

used to do fatigue life analysis.

3.2. Fatigue models

Fatigue behavior of material is usually classified into two regimes, low cycle fatigue and high cycle fatigue. Low cycle fatigue occurs when the cyclic deformations are so large that they are predominantly inelastic (plastic). If the cyclic deformations are small enough to be predominately elastic, the fatigue is called high cycle fatigue. Low-cycle fatigue is fatigue caused by strain cycles involving plastic deformations. Large temperature displacements and cyclic loading of integral abutment piles can cause plastic deformations and lead to low-cycle fatigue failures. Thermal movements of the abutments can cause elastic as well as plastic deformations in the piles, depending on how long the bridge is and how large the variations in effective bridge temperature are. Rotations of the abutments due to varying traffic loads and temperature gradients will also cause deformations of the piles. These deformations must also be taken into account in an analysis of a possible low-cycle fatigue failure.

Fatigue failure has been the subject of numerous studies and various mechanisms and techniques are proposed to evaluate failure in brittle and ductile fatigue. Brittle fatigue fracture is typically evaluated using Linear Elastic Fracture Mechanics (LEFM) or Elastic-Plastic Fracture Mechanic (EPFM), using approaches such as J-integral [40], or Crack-Tip Opening Displacement (CTOD) [41]. These techniques have proven efficient and reliable when examining the fracture process in cases where there is a limited amount of yielding or if a sharp crack exists [42]. If large amounts of yielding occur, however, the basic assumptions that build the governing equations of these techniques do not hold. Furthermore, they typically need the assumption of having a pre-existing crack in the structure. Additionally, Both LEFM and EPFM address the problem of crack

initiation and growth based on far-field stresses. In situations of large-scale yielding, these far-field stresses often lose correlation with the near crack tip stresses and strains, consequently invalidating the use of either LEFM or EPFM [43].

In situations where plastic deformation and distributed damage is expected, continuum damage modeling techniques tend to predict the extent of damage and cracks more reliably. When large stresses exist in the structure, steel elements can exhibit ductile yielding and ductile fatigue fracture. Ductile fracture typically occurs by microvoid nucleation, growth and coalescence. Voids may form at the grain boundaries, triple junctions in particular or around the secondary particles and inclusions [43]. After nucleation, plastic strain and hydrostatic stress cause the voids to grow. Upon further growth these voids join and create a microcrack that further join and create macro-cracks and fracture. The continuum damage modeling approach is based on the assumption of ductile and distributed damage, first introduced by Kachanov [44]. Long before, Rabotnov [45] introduced the effective stress concept when studying the creep rupture of metals under uniaxial loading. Later this concept was used to study fatigue by Chaboche and Lesne [46] and Dufailly and Lemaitre [47]; creep by Hayhurst [48], Cocks and Leckie [49] and Kruch et al.[50]; creep-fatigue interaction by Lemaitre and Plumtree [51] and Chaboche [52]; and ductile plastic damage by Lemaitre [53], Rousselier [54] and Lemaitre and Marquis [55]. Most of these concepts are built upon the thermodynamics of irreversible processes and internal state variable theory [56]. If the damage is considered isotropic and homogeneous a scalar quantity can represent the damage in the material. Then the damage variable can be defined as [44]

$$D = \frac{A}{A_0}$$ Eq. 3-3

A is the load bearing area after damage has developed and A_0 is the original load bearing area

before any damage has occurred. D is a positive, monotonically increasing function, with values ranging in the interval $0 < D < 1$. $D = 0$ identifies the initial undamaged state and $D = 1$ identifies complete mechanical failure (loss of load-bearing capability) of the material.

Assuming that the structure accumulates damage at a constant rate, meaning that the amount of damage per cycle, D_{cycle} is constant and equal in each cycle, if the material reaches the total damage of 1 and fails after N_f number of cycles, at the end of the life the following equation stands:

$$D = 1 = D_{cycle} \times N_f$$
Eq. 3-4

This means that if the number of cycles to failure, N_f, is known, damage per cycle can be obtained using the following equation:

$$D_{cycle} = \frac{1}{N_f}$$
Eq. 3-5

Continuum damage modeling approaches have been classified into several groups: stress based approach, strain based approach, and energy based approach.

3.2.1. Stress based approaches

The stress based approach to life prediction is the oldest method used in fatigue modeling [57]. In this method the fatigue life is expressed as function of a strength parameter. Basquin [57] proposed the following equation:

$$\sigma_a = \sigma_f'(2N_f)^b$$
Eq. 3-6

In which, σ_a is the stress amplitude, σ_f' is called the fatigue strength coefficient, and b is the fatigue strength exponent.

3.2.2. Strain based approaches

The strain based approach to fatigue modeling is one of the most widely used approaches for predicting the life in different structures. It is especially useful in the case of low cycle fatigue, because it uses plastic inelastic deformation amplitude. This method has been used by several researchers for fatigue life analysis of bridges and structures [57-60]. Most cases in nature involve a strain controlled environment. For example, the abutment bridge usually goes under cyclic load for which the strain is defined by the length of the bridge and the temperature change. If only plastic strain is considered, the function that correlates the number of cycles to plastic strain is called the Coffin–Manson [61-62] relation, and is as follows:

$$\frac{\Delta_{\varepsilon p}}{2} = \varepsilon_f'(2N_f)^c \qquad\qquad \text{Eq. 3-7}$$

Where $\Delta_{\varepsilon p}$ is plastic strain amplitude, ε_f' fatigue ductility coefficient and c is the fatigue ductility exponent. Sometimes the Basquin equation is combined with the Coffin-Manson equation to obtain a generalized fatigue model based on total strain as follows [63]:

$$\frac{\Delta_{\varepsilon t}}{2} = \frac{\sigma_f'}{E}(2N_f)^b + \varepsilon_f'(2N_f)^c \qquad\qquad \text{Eq. 3-8}$$

where $\Delta\varepsilon_t$ is the total strain amplitude, σ_f' is the fatigue strength coefficient, ε_f' is fatigue ductility coefficient, E is the Young's modulus, N_f is the number of cycles to failure and b and c are damage model constants.

The Coffin-Manson equation shows good correlation with experiments [64].

Because there is no practical method to separate plastic strain from total strain during typical test, Engelmaier [65] proposed a new formula based on Coffin-Manson equation using total strain rather than plastic strain, using the following formula:

$$N_f = \frac{1}{2} \left(\frac{\Delta_\gamma}{2\varepsilon_f'} \right)^{\frac{1}{c}}$$
Eq. 3-9

Where ε_f' is fatigue ductility coefficient, N_f is mean cycles to failure, and c is fatigue ductility exponent.

Manson and Halford [66] were motivated to develop a more sophisticated strain based approach due to various shortcomings of available approaches.

Their model is called strain-range partitioning approach. In this model the total inelastic strain is broken into two parts consisting of plastic and creep strain components. In the case of axial tension and compression loading, the two possible inelastic components allow for a maximum of four permutations in basic cycle types: pp (plastic in tension and compression), cp (creep in tension and plastic in compression), pc (plastic in strain tension and creep in compression), cc (creep in tension and compression). To apply the strain range partitioning method, an interactive damage rule is used that relates the four separate strain ranges to life relationships.

$$\frac{1}{N_f} = \frac{F_{pp}}{N_{pp}} + \frac{F_{cc}}{N_{cc}} + \frac{F_{cp}}{N_{cp}} + \frac{F_{pc}}{N_{pc}}$$
Eq. 3-10

Where N_f is predicted cycles to failure for the given complex hysteresis loop, N_{ij} is cycles to failure for a given partitioned strain range of type ij (pp, cc, pc, or cp), and F_{ij} is fraction of total

inelastic strain range that is actually of type ij. This method has been applied widely for many alloys and often resulted in very good correlation with experimental data.

3.2.3. Energy based approaches

Energy based models are the largest group of fatigue [67]. Cyclic hysteresis energy is believed to be a comprehensive metric of cyclic fatigue damage as it includes both stress and strain hysteresis. Energy based models can be used to predict fatigue failure based on hysteresis loops. These models are divided into two groups; unified and partitioned energy. One of the most widely used models is Darvaeux Model [68], which uses the accumulated inelastic strain energy density per thermal cycle, and correlates crack initiation time and crack growth to the average energy as follows:

$$N_0 = K_1(\Delta W_{avg})^{K_2} \qquad \text{Eq. 3-11}$$

$$\frac{da}{dN} = K_3(\Delta W_{avg})^{K_4} \qquad \text{Eq. 3-12}$$

Where N_0 is the number of cycles to initiation and K_1, K_2, K_3, and K_4 are crack constants. ΔW_{avg} is volume-weight average of total inelastic work density accumulated per cycle. Another example is Akay's model that was proposed based on total energy [69]

$$N_f = \left(\frac{\Delta W_{Total}}{W_0}\right)^{\frac{1}{K}} \qquad \text{Eq. 3-13}$$

In which the ΔW_{Total} is the total strain energy, N_f is mean cycles to failure, and W_0 and K are fatigue coefficients.

Similar to strain range partitioning damage model, energy based partitioning damage model separates the damage caused by plastic and creep deformation. Inspired by the point that plastic and creep deformation result in different types of material damage as seen in various partitioned damage models such as, Strain Range Partitioning [63], a mechanism based damage model was proposed. This model assumes that cyclic fatigue damage is due to a combination of creep deformation mechanisms, plastic deformation mechanisms, and elastic deformation mechanisms. This model predicts cyclic creep fatigue damage based on deviatoric energy densities: U_e (elastic), W_p (plastic), and W_c (creep) for a typical load cycle. The damage due to each of these deformation mechanisms is determined by using a power law as provided in the following equations:

$$U_e = U_{e0} N_{fe}^b \qquad\qquad \text{Eq. 3-14}$$

$$W_p = W_{p0} N_{fp}^C \qquad\qquad \text{Eq. 3-15}$$

$$W_c = W_{c0} N_{fP}^d \qquad\qquad \text{Eq. 3-16}$$

The total energy is obtained by superposition of these contributions.

$$\text{Total Energy} = U_e + W_p + W_c = U_{e0} N_{fe}^b + W_{p0} N_{fp}^C + W_{c0} N_{fP}^d \qquad\qquad \text{Eq. 3-17}$$

Where U_{e0}, W_{p0}, and W_{c0} represent the intercept of the elastic, plastic, and creep energy density plots versus cycles to failure, on a log-log plot; while exponents b, c, and d are their corresponding slopes. These constants are material properties. The variables N_{fe}, N_{fp}, and N_{fc} represent the cycles to failure due to elastic, plastic, and creep damage respectively. Subscripts e, p and c refer to elastic, plastic, and creep damage, respectively.

The total number of cycles to failure N_f is then calculated using the following equations by estimating the total cyclic damage as a superposition of the three individual damage mechanisms (elastic, plastic and creep):

$$D_{total} = D_e + D_p + D_c \qquad\qquad\qquad \text{Eq. 3-18}$$

$$\frac{1}{N_f} = \frac{1}{N_{fe}} + \frac{1}{N_{fp}} + \frac{1}{N_{fc}} \qquad\qquad\qquad \text{Eq. 3-19}$$

Where, D is cyclic fatigue damage.

As plastic deformation is expected in IAB, either strain based or energy based damage modeling approach are suitable.

Chapter 4. Bridge geometry

An integral abutment bridge described in reference [25] was used as a case study in this paper. The bridge length was varied for five different cases with lengths of 400, 600, 800, 1200, and 1800 ft. The span of the bridge was kept constant at 50 ft. A cross section of the bridge is shown in Figure 4-1. The bridge consists of a seven inch-thick concrete slab that is supported by six girders. There is a two-foot overhang on each side of the bridge. There are eleven piles supporting the bridge abutment.
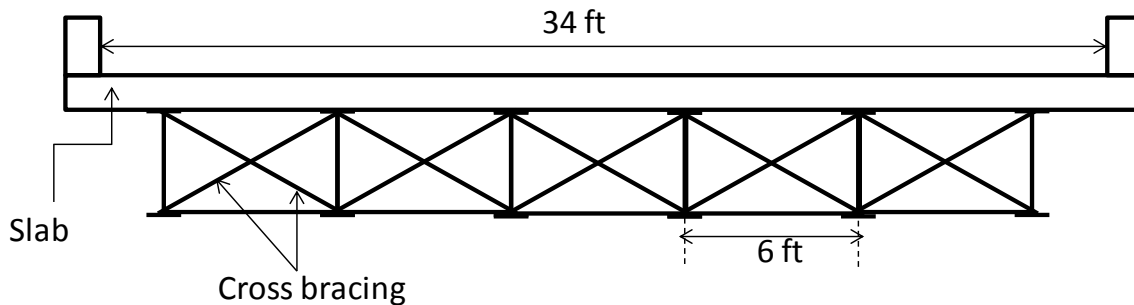
Figure 4-1: Cross section of the bridge slab, girders, and cross bracings.

Girders, cross bracing, and piles are beams of W30X132, L6X6, and HP10X42 respectively. The piles are placed such that the bending occurs around their strong axis. Figure 4-2(a) shows a two-dimensional top view of the abutment with piles location and orientation. Piles are oriented such that as thermal load is applied they rotate around their strong axis. A study conducted by Dicleli et al. [16] showed that a strong axis delays fatigue. As indicated by Decleli et al., "The larger bending capacity of the piles about their strong axis relative to the bending capacity about their weak axis allows the bridge to accommodate larger cyclic displacement before fatigue failure of the pile takes place." Therefore, if the analysis conducted in this study shows that

fatigue occurs in a case with a strong axis, then fatigue can definitely be expected in the case with a weak axis. There is no agreement between different states on the orientation of piles and in general both orientations are used in all different states. The Federal Highway Load Resistance Factor Design for integral abutment bridge [71] indicates that H-piles in any orientation in IABs are satisfactory. As quoted in this document, "For H-piles, there is no commonly used orientation of the piles. In the past, H-piles have been placed both with their strong axis parallel to the girder's longitudinal axis and in the perpendicular direction. Both orientations provide satisfactory results." Therefore, a strong axis is used in this analysis.

A three-dimensional image of the abutment and piles is shown in Figure 4-2 (b). The piles length is 41 ft of which 1 ft is within the abutment. The total width of the abutment is equal to the width of the bridge and equal to 34 ft. Due to symmetry, this figure only shows half of the abutment.
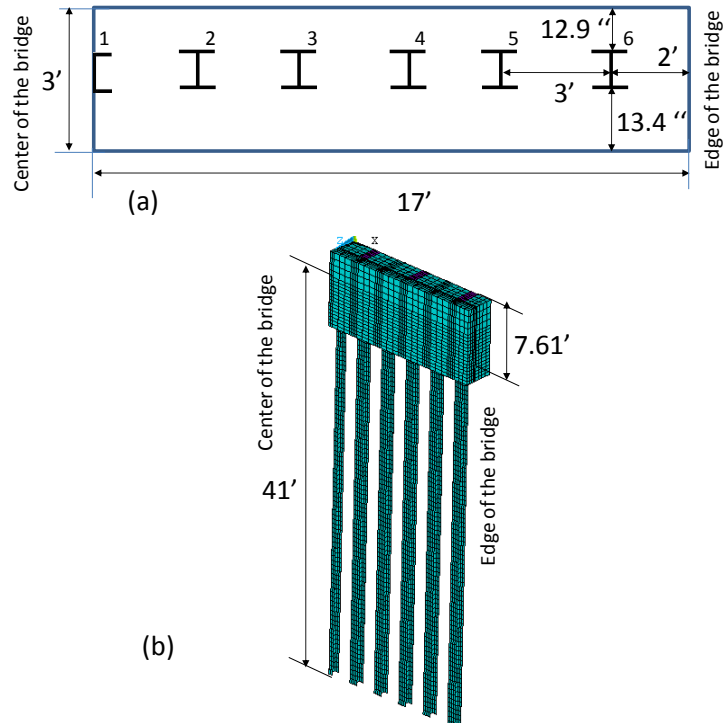
Figure 4-2: (a) View of the half of the abutment from top showing dimensions of abutment, the piles and their location, (b) three-dimensional finite element model of piles and abutment showing the depths of abutment and piles.

Girders cross bracing and piles are beams of W30X132, L6X6, and HP10X42, respectively. The dimensions of the girders, piles and cross bracings are given in Figure 4-3.

W30*132

HP10*42

L6*6*1

W30X132			HP10X42			L6X6X1		
A =	38.9	in.^2	A =	12.4	in.^2	A =	11.00	in.^2
d =	30.3	in.	d =	9.7	in.	d =	6	in.
tw =	0.615	in.	tw =	0.415	in.	b =	6	in.
bf =	10.5	in.	bf =	10.1	in.	t =	1	in.
tf =	1	in.	tf =	0.42	in.	k =	1.5000	in.
k(des) =	1.65	in.	k(des) =	1.13	in.	wt./ft. =	37.40	plf.
k(det) =	1.875	in.	k(det) =	1.125	in.	eo =	0.92	in.
k1 =	1.125	in.	k1 =	0.8125	in.	Ix =	35.40	in.^4
T =	26.5	in.	T =	7.5	in.	Sx =	8.55	in.^3
gage =	5.5	in.	gage =	5.5	in.	rx =	1.790	in.
wt./ft. =	132	plf.	wt./ft. =	42	plf.	y(bar) =	1.860	in.
bf/(2*tf)	5.27		bf/(2*tf)	12		Zx =	15.400	in.^3
h/tw =	43.9		h/tw =	18.9		yp =	0.918	in.
Ix =	5770	in.^4	Ix =	210	in.^4	Iy =	35.40	in.^4
Sx =	380	in.^3	Sx =	43.4	in.^3	Sy =	8.55	in.^3
rx =	12.2	in.	rx =	4.13	in.	ry =	1.790	in.
Zx =	437	in.^3	Zx =	48.3	in.^3	x(bar) =	1.860	in.
Iy =	196	in.^4	Iy =	71.7	in.^4	Zy =	15.400	in.^3
Sy =	37.2	in.^3	Sy =	14.2	in.^3	xp =	0.918	in.
ry =	2.25	in.	ry =	2.41	in.	Iz =	15.00	in.^4
Zy =	58.4	in.^3	Zy =	21.8	in.^3	Sz =	3.53	in.^3
rts =	2.75	in.	rts =	2.77	in.	rz =	1.170	in.
ho =	29.3	in.	ho =	9.28	in.	TAN(α) =	1.000	
J =	9.72	in.^4	J =	0.813	in.^4	Qs(36) =	1.000	
Cw =	42100	in.^6	Cw =	1540	in.^6	J =	3.68	in.^4
a =	105.90	in.	a =	70.03	in.	Cw =	9.24	in.^6
Wno =	76.9	in.^2	Wno =	23.4	in.^2	a =	2.55	in.
Sw =	202	in.^4	Sw =	24.7	in.^4	ro(bar) =	3.18	in.
Qf =	72.4	in.^3	Qf =	9.41	in.^3	H =	0.640	
Qw =	215	in.^3	Qw =	23.7	in.^3			

Figure 4-3: Dimensions of girders, piles and cross bracings.

Chapter 5. Temperature variations and modeling

A large portion of displacement in the bridge is caused by temperature variations. These temperature variations can be categorized into seasonal and daily temperature changes. Thermal displacement of the bridge depends on the change of temperature, the length of the bridge and the coefficient of thermal expansion.

AASHTO Standard Bridge Specifications (1996) [5] recommends that the rise and fall of the temperature be fixed with respect to the temperature at the time of installation for the locality where the structure is built. It also recommends that consideration be given to the lag between the air temperature and the inside temperature of massive concrete structures. Generalized yearly temperature variations for different bridge materials and for different climates are as follows:

- For metal structures: in moderate climate: 0 to 120° F and in cold climate: -30 to 120° F.
- For concrete structures: in moderate climate: 30° F temperature rise and 40° F temperature fall in cold climate: 35° F temperature rise and 45° F temperature fall.

However, in this recommendation, AASHTO does not consider the fatigue in abutment bridges and does not discuss the number of cycles that the bridge piles can stand under this temperature range.

Bridge displacements are affected by both daily and seasonal temperature changes. In order to implement the temperature load in the finite element model, we need to mathematically model the temperature variations. However, first the temperature data needs to be obtained for the specific region in which the bridge is located or will be built. The case study presented in this dissertation is located in the harsh climate of Wasatch Mountain region. Therefore, the

temperature data for that region is obtained. The next section elaborates on the process and temperature data.

5.1. Obtaining temperature data

The raw data including seasonal and daily temperatures have been obtained for Logan UT from Utah State Climate Center for 11 years from 1998 to 2009. Utah typically experiences large seasonal and daily temperature variations that expedite the fatigue process. The maximum and minimum daily temperature data for 10 years are shown in Figure 5-1. As seen in this figure the seasonal temperature range could be as large as 135° F, which even exceeds the temperature range specification of concrete given in AASHTO. As mentioned before, this recommendation does not include consideration for cyclic fatigue of piles. The daily temperature difference (ΔT) within 24 hours for 10 years is shown in Figure 5-2. As seen here the temperature difference can be as much as 56°F within 24 hours. This means that a fairly large temperature cycle could happen over many cycles of daily variations. Note that the number of daily cycles is much larger than the number of seasonal cycles. So the smaller amplitude of daily cycles does not translate into less fatigue probability. The maximum daily variations occur during the summer time.
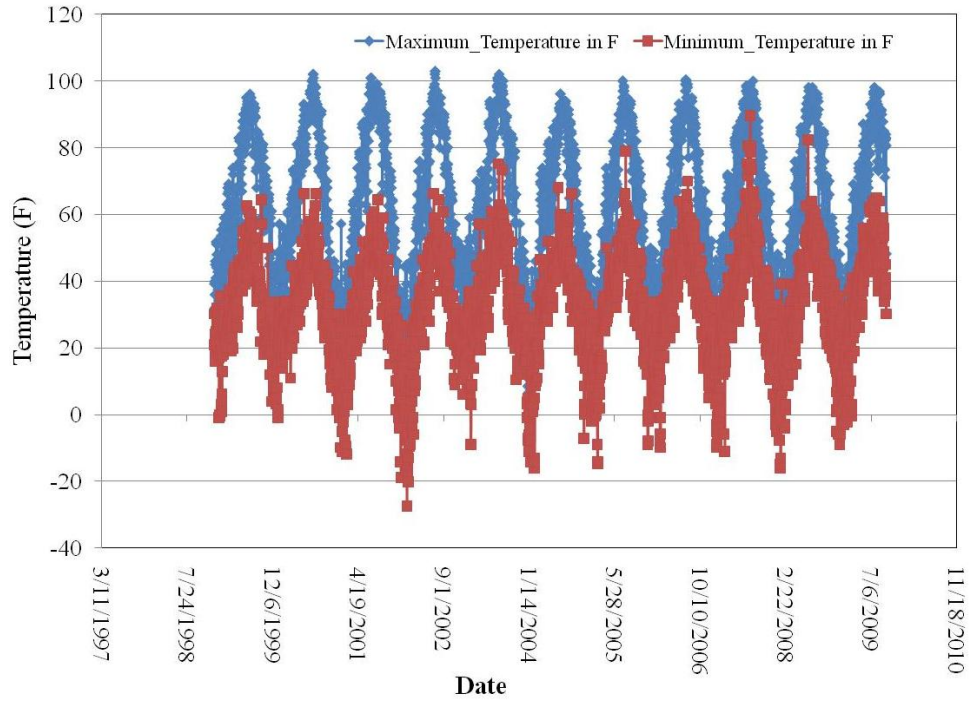
Figure 5-1: Maximum and minimum daily temperatures from 1998 to 2009 for Logan, Utah [70].
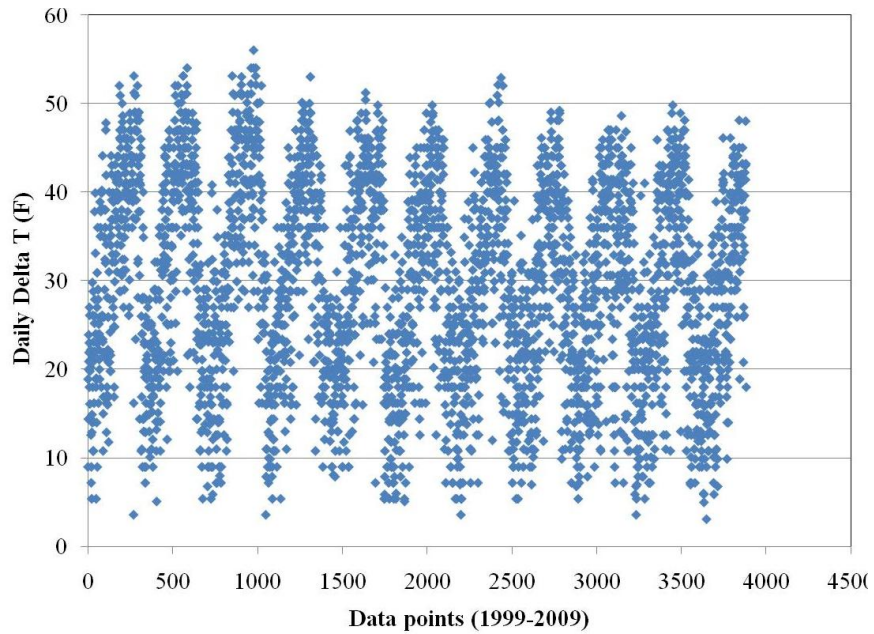
Figure 5-2: Daily temperature difference for 10 years.

Figure 5-3 shows hourly temperatures for the month of August of 2007. In this month the maximum temperature difference was 49 °F. According to the data shown in Figure 5-2 the temperature difference between night and day is much larger during the summer than winter.
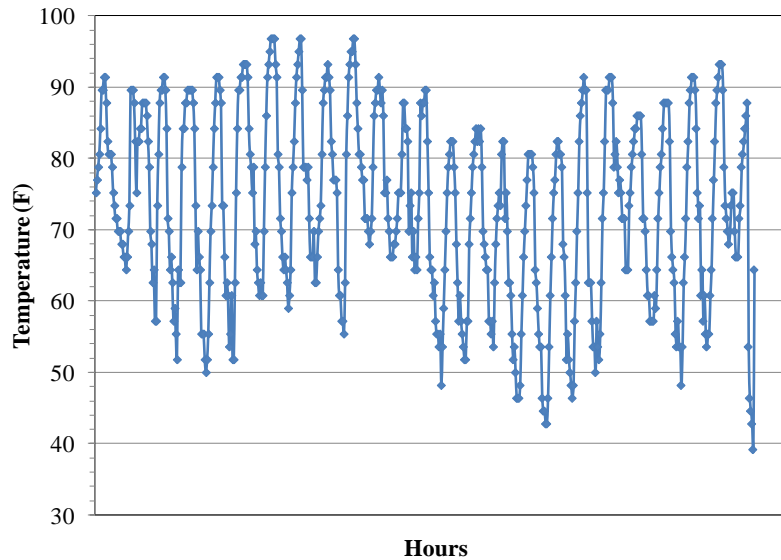
Figure 5-3: Hourly temperatures for the month of August of 2007, [70].

5.2. Mathematical modeling of temperature variations

Each daily variation in temperature completes a cycle of expansion and contraction, and the cycles repeat over time. The greatest expansion takes place during summer days, while the greatest contraction occurs during winter nights. These extreme temperature variations control the extreme displacements of integral bridges. The life cycle of the bridge will include many days with different ΔT. It is virtually impossible to predict these variations for such a large number of days. Referring to the historical data may give some estimate or trend on these values. However, with global warming issues, the historical data may not be as trustworthy for future predictions. To simplify the matter, a sine model can be used to model the temperature cycle

over one month. For the daily temperature change the model is [3]:

$$T = T_{d,amp} \sin\left(\frac{HR*2\pi}{24}\right) + T_{d,m} \qquad \text{Eq. 5-1}$$

Where $T_{d,amp}$ is the daily temperature amplitude and $T_{d,m}$ is the average daily temperature. HR varies between zero to twenty four (indicative of 24 hours in the day).

According to this model, the hourly temperature can be predicted if daily temperature amplitude and average daily temperature for each month are known. However, as mentioned the ΔT is different in each day of the month. So historically, what people have done to stay on a safe side, is to consider $T_{d,amp}$ to be the largest value that can happen and $T_{d,m}$ to be the historic average. One very conservative way is to find the highest and lowest temperatures in that month and determine the difference between them and consider that as $T_{d,amp}$. This method will give a very large ΔT that in many cases is much larger than a ΔT happening over one daily cycle. One example is shown in Figure 5-4. As seen in this figure the amplitude of temperature is much larger than the daily amplitudes. This model may be close to historical data in very harsh climates with large daily temperature variations, but for this region is considered too conservative.
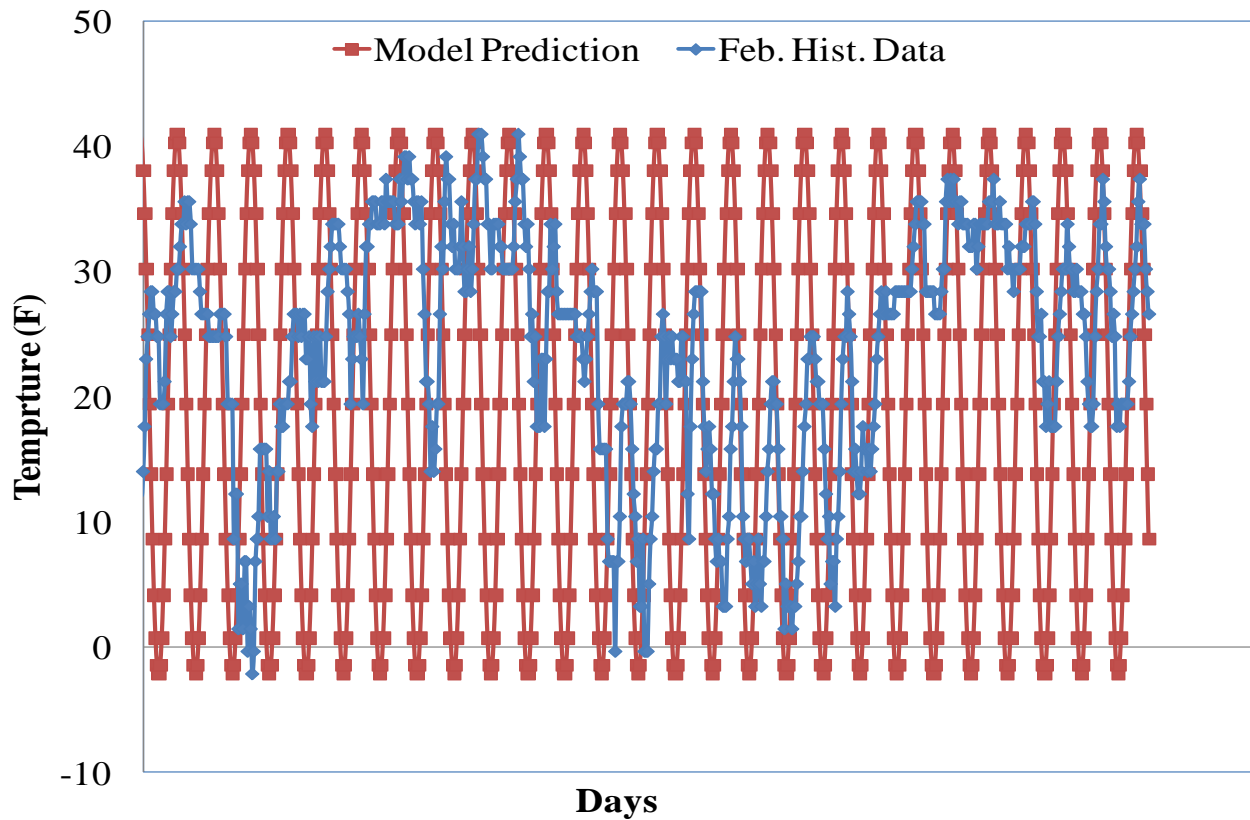
Figure 5-4: The model prediction based on temperature differences between the highest and
lowest points in the month of February comparison with historical data observed in
that month.

Another method that can be used is to determine the daily temperature amplitudes and select the
largest daily amplitude. Using this model the data of September of 2005 was used to develop
Figure 5-5. This model shows much better correlation with the historical data and is not overly
conservative. The cycle modeled using this method covers all the cycles and is still conservative.
Therefore, this is the daily temperature model that is used in our analysis. Historical data shows
that average daily amplitude is 27°F and historic mean daily temperature is 54.5°F.
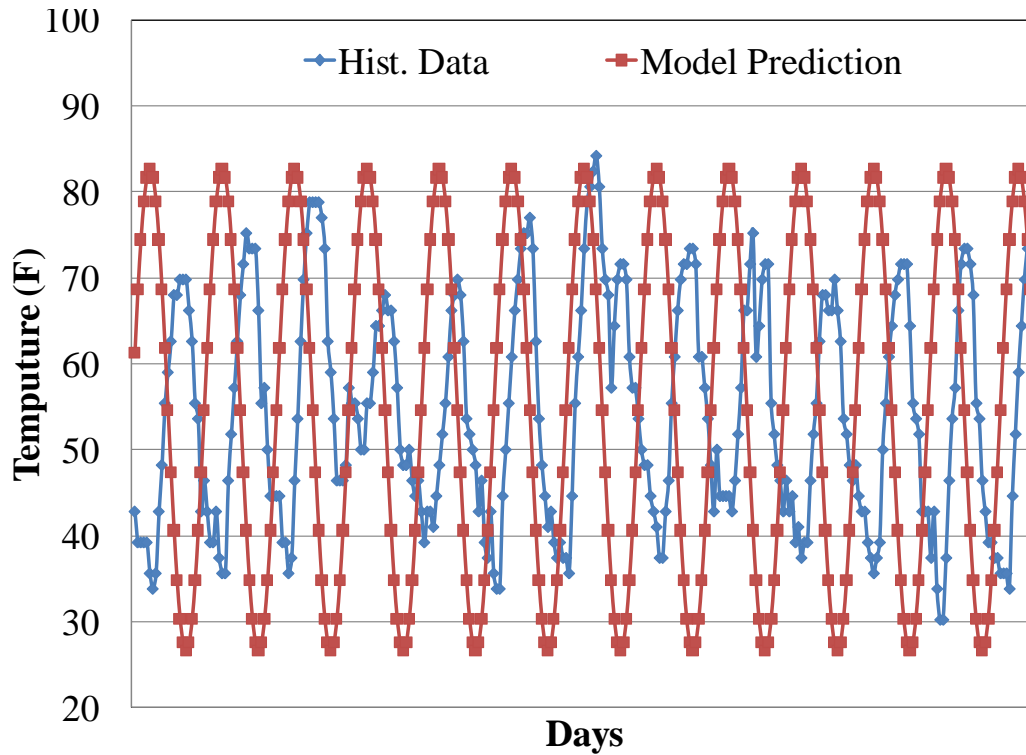
Figure 5-5: The model developed using the maximum amplitude of daily temperature

comparisons with historical data observed in the month of September 2005.

5.3. Modeling seasonal temperature variations

Seasonal temperature variations are naturally much larger than the daily temperature variations. Similar to what was done in daily temperature modeling in modeling seasonal temperature variations the largest temperature amplitude observed over 10 years of data was used to develop a similar sinusoidal model as seen in Figure 5-6. The formula used for the seasonal model is slightly different from the daily temperature cycle. The formula for the seasonal model is shown in Eq. 5-2:

$$T_s = T_{s,amp} \, \sin\left(\frac{t_d}{365} 2\pi - t_0\right) + T_{s,m} \qquad \text{Eq. 5-2}$$

$$T_{s,amp} = \frac{T_{S,max} - T_{s.min}}{2}$$ 　　　　　　　　　　　　　　　Eq. 5-3

$$T_{s,m} = \frac{T_{S,max} + T_{s.min}}{2}$$ 　　　　　　　　　　　　　　　Eq. 5-4

Where $T_{s,amp}$ is the seasonal temperature amplitude and $T_{s,m}$ is the seasonal mean temperature and t_d represents the number of the day for which the temperature is calculated. It varies between one to 365 days and t_0 is an adjustment factor that can be varied to match the model to historical data.
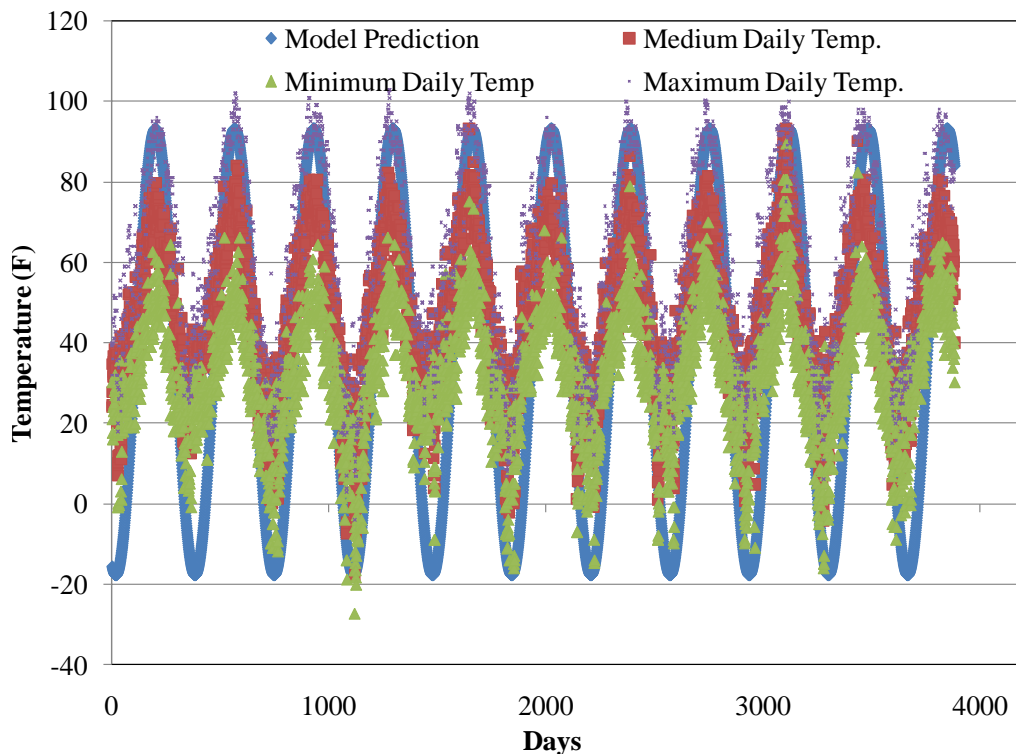
Figure 5-6: Model prediction in comparison with medium, minimum and maximum seasonal

temperature changes.

This modeling strategy was used to model 11 year temperature data. The results are shown in Figure 5-6. This figure shows several data, minimum daily temperature, maximum daily

53

temperature, mean daily temperature and the model predictions. As seen in this figure the model prediction falls between the maximum and minimum daily temperature. Maximum daily temperature and minimum daily temperatures may exceed this model in one side. However the total temperature amplitude from winter to summer on one cycle does not exceed the model. Although this model is not as conservative as the daily temperature variation model, it should still be valid because the number of cycles are much smaller than daily temperature variations. For the data, the maximum seasonal amplitude, $T_{s,amp}$, is 38°F and the historic average, $T_{s,m}$, is 55°F.

Chapter 6. Three-dimensional finite element model

Three-dimensional nonlinear finite element analysis is conducted using ANSYS 13. Due to symmetry and to reduce the computation time, a quarter of the bridge was modeled. The model includes the non-linear effect of the material plasticity of steel piles.

6.1. Finite element mesh and boundary condition

The entire model was meshed using plane and hexahedral elements. The concrete slabs, piles and girders were meshed using the two dimensional shell element (SHELL181) with the corresponding thickness of concrete slabs, flange and webs. SHELL181 is suitable for analyzing thin to moderately-thick shell structures. It is a four-node element with six degrees of freedom at each node: translations in the x, y, and z directions, and rotations about the x, y, and z-axes. SHELL181 is well-suited for linear, large rotation, and/or large strain nonlinear applications. Change in shell thickness is accounted for in nonlinear analyses [72]. Cross bracings were modeled using the one dimensional beam element (BEAM188). BEAM188 is suitable for analyzing slender to moderately stubby/thick beam structures. The element is based on Timoshenko beam theory [73]. The concrete abutment and soil are modeled using three-dimensional twenty-node solid elements of SOLID185. SOLID185 is used for 3-D modeling of solid structures. It is defined by eight nodes having three degrees of freedom at each node: translations in the nodal x, y, and z directions. The element has plasticity, hyperelasticity, stress stiffening, creep, large deflection, and large strain capabilities [72].

The number of elements for the whole structure (superstructure and substructure) is 285,000. Because of symmetry and to reduce the computational time and resources, only a quarter model

is built and meshed. The geometry of the quarter model and the boundary conditions are shown in Figure 6-1. Symmetry boundary conditions are applied on the symmetry planes: $z = 0$ on symmetry surface 1 and $x = 0$ on symmetry surface 2. The bottom of the soil is fixed in the y and z directions to simulate the end-bearing type pile. The soil thickness in the positive z direction (backfill soil thickness) is assumed to be 3 ft and its thickness in the negative z direction behind the piles is assumed to be 10 ft. Assuming that these soil layers are thick enough, the free surfaces of the soil are assumed to be stationary in the z direction as the piles move. Therefore, the displacement perpendicular to these free areas (displacement in the z direction) are assigned zero value as the boundary condition. Since all the elements are either 4-node, 8-node or 20-node elements, they are all compatible and there is no need for intermediate elements between different parts of the bridge. However, since shell nodes have 6 degrees of freedom and solid nodes have 3 degrees of freedom, contact elements are needed in between shell and solid elements. Gravity is applied in the y direction (red arrow in the Figure 6-1). The supports are provided in the y direction underneath the slab at 50 ft distances. The y displacement at these constraints is zero.
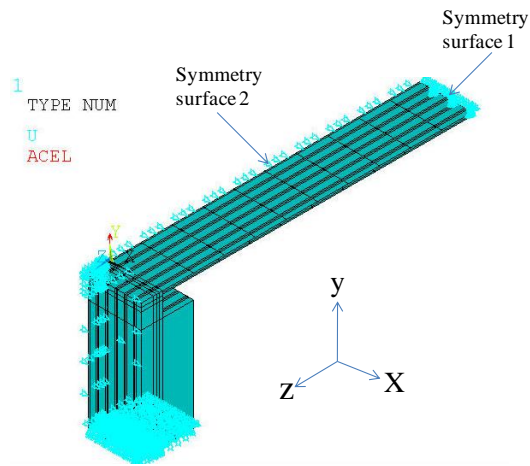
Figure 6-1: Geometry of the quarter of the bridge and the boundary conditions.

Figure 6-2 shows the soil material meshed using SOLID185. The soil surrounds the piles not visible in this picture. The model also includes backfill soil behind the abutment. Figure 6-3 shows the concert slab, which is meshed with planar elements (SHELL188) and the concrete abutment, which is meshed with SOLID185 element. Figure 6-4 shows a partial image of piles meshed with shell elements. The shell elements are defined differently such that the flange and the web are modeled with their own corresponding thicknesses.

Figure 6-5 shows all the metallic parts of the bridge including girders, piles and cross bracings.
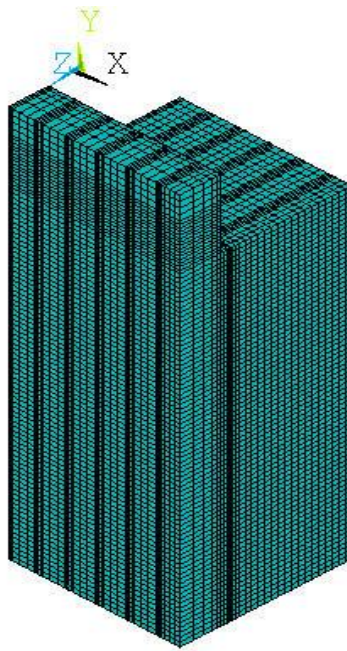
Figure 6-2: Soil material meshed using SOLID185 element.
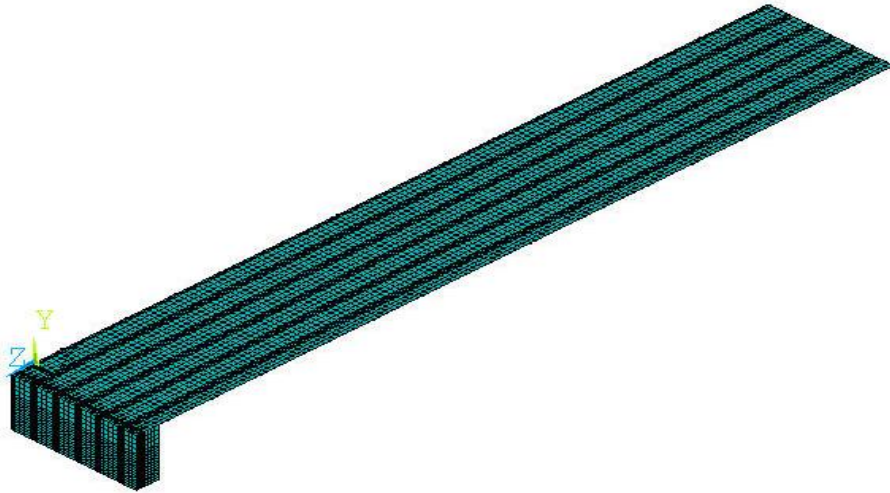
Figure 6-3: Concrete slab and abutment meshed with shell (SHELL188) and solid elements (SOLID185).
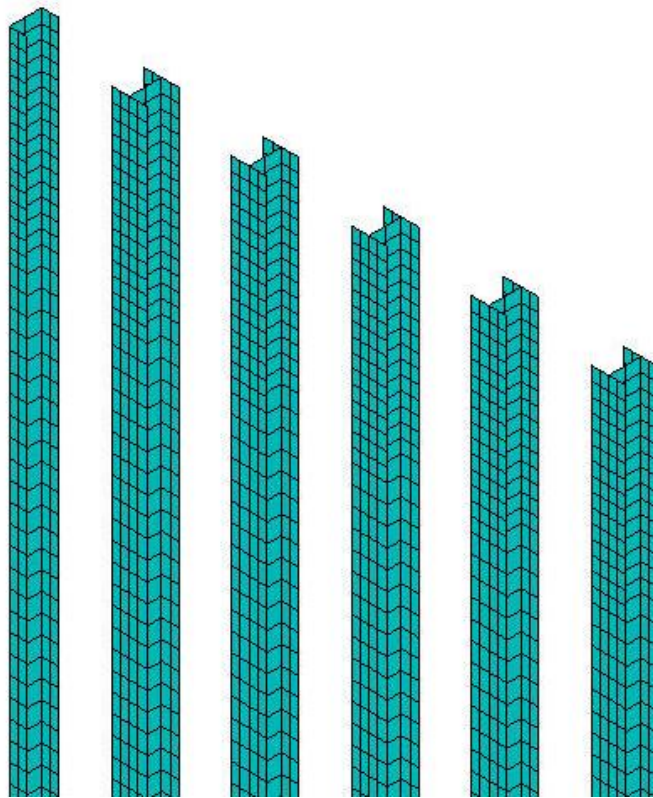
Figure 6-4: Piles meshed using shell element (SHELL188).
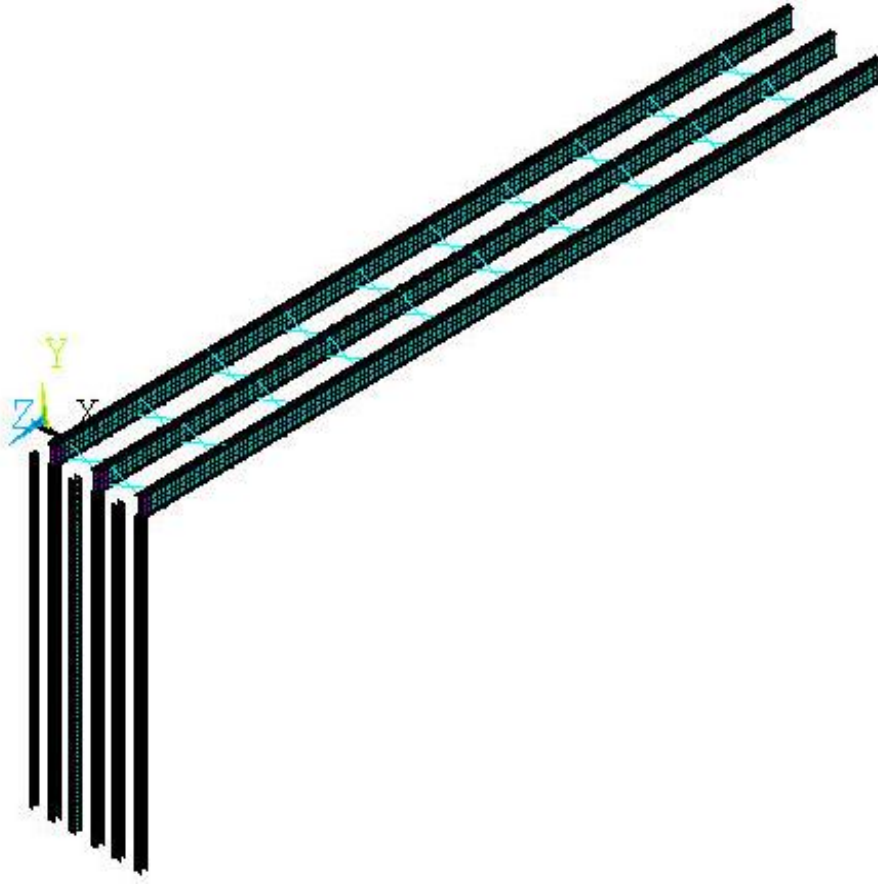
Figure 6-5: Metallic parts of the bridge.

6.2. Material properties and constitutive models

The main materials used in this bridge are concrete and steel. Concrete is assumed to behave only elastically. Steel, however, is assumed to behave as elastic-plastic. Elastic properties of concrete and steel are shown in Table 6-1.

Material	Elastic Modulus (psi)	Coefficient of thermal expansion (in/in/R)	Density (slug/in³)	Poisson's Ratio
Steel	29E6	2.54E-8	8.813E-3	0.2
Concrete	3.6 E6	2.54E-8	2.608E-3	0.29

Table 6-1: Elastic properties of concrete and steel.

Steel material used in piles, girders and cross bracings are modeled as elastic-plastic material with multilinear plastic behavior using a MISO command in ANSYS. The elastic-plastic constitutive properties for steel are shown in Figure 6-6.

The elastic region can be represented simply by Hooks Law and the nonlinear rate-independent inelastic region can be represented using a logarithmic function as follows:

$$\sigma = 10490\varepsilon^{0.2127} \hspace{4cm} \text{Eq. 6-1}$$

Where ε is the summation of elastic (ε_e) and rate independent inelastic strain (ε_p).
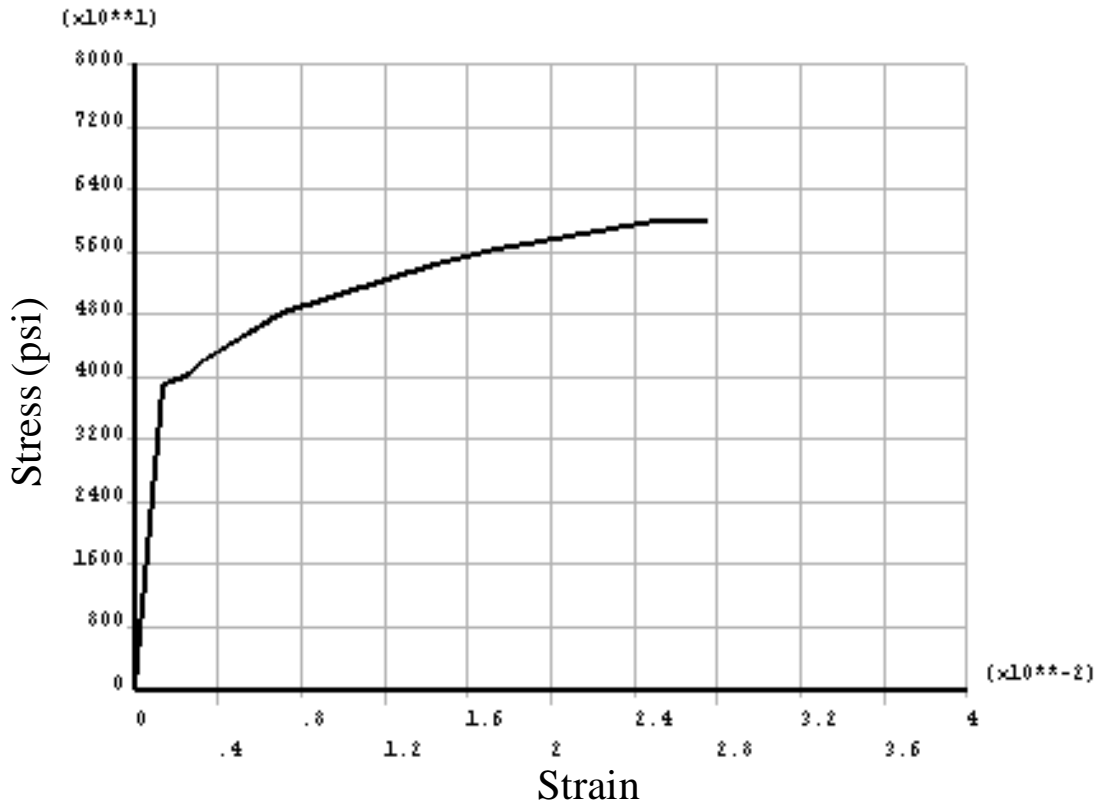
Figure 6-6: Elastic-plastic constitutive behavior of steel used in the simulation of digitized data

from Mander et al. [64].

6.3. Soil modeling

The ANSYS model includes both the superstructure and substructure (soil). Soil and powder material, however, behave differently than conventional solids. For metal plasticity (assuming von-Mises or similar yield surface), only the deviatoric stress is assumed to cause yielding. If the yield surface is plotted in principal stress space, this results in a cylinder whose axis is the hydrostatic pressure line, indicating that yielding is independent of the hydrostatic stress state. For the von-Mises yield surface, theoretically, one could have infinite hydrostatic compression, and no yielding would occur. However, soil and powder material cannot stand

tension and can only support compressive forces. Another characteristic is that the strength of these materials depends on the amount of compressive pressure. In other words, their strength and yield are pressure dependent. For example, as the depth increases in soils, the amount of shear strain needed to shear the soil increases because the compressive pressure due to soil weight increases. For this type of material usually the Drucker-Prager (DP) model is used. The DP plasticity model is different from typical metal plasticity models since it contains a dependence on hydrostatic pressure. For a linear yield surface ("linear" referring to the linear shape when plotted in the plane of effective stress vs. hydrostatic pressure), this means that if there is some hydrostatic tension, the yield strength would be smaller. Conversely, as hydrostatic compression increases, so would the yield strength. When the yield surface is plotted in principal stress space, it would look like a cone, as shown in Figure 6-7 [74].

ANSYS 13 provides three different DP constitutive models. The first type is the basic DP, which assumes perfectly plastic behavior (no strain hardening). The second type is the extended DP (EDP) model. EDP is meant to address some shortcomings of the basic DP model – namely, the use of perfectly-plastic behavior and the requirement of a linear yield surface.
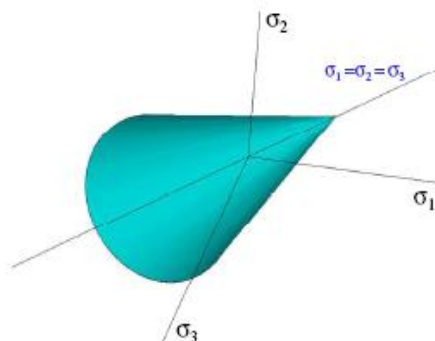
Figure 6-7: Yield surface in principal stress domain for Drucker-Prager model.

The two main characteristics that result are that (a) the yield strength changes, depending on the hydrostatic stress state and (b) some inelastic volumetric strain can occur, as defined by the flow potential. Because of these points, the DP material model is used for geomechanics or powder compaction or any other application where both hydrostatic dependence and inelastic volume strain are important.

To define the DP model, a flow potential and yield function are required. Several different types of functions are available in ANSYS (linear, power low and hyperbolic). For this analysis a linear yield function and a linear flow potential are used. Soil properties needed to define these functions in ANSYS are given in Table 6-2.

Soil parameter	Values
Modulus of elasticity (Psi)	15555
Density (Lb/ft^3)	125
Yield strength (Psi)	8
Internal friction angle	25°
Un-drained cohesion of clay (Psf)	5000

Table 6-2: Soil properties used in finite element analysis.

6.4. Global-local modeling

The finite element model of the superstructure and substructure is a very large model. This model can provide reasonable results if only rough estimates of stresses and strains in the structure are of interest. The first part of this dissertation is dedicated to understanding the behavior of the piles in the bridge and analyzing the stresses and strains in the piles. The finite

element of the whole bridge and the substructure are used initially to conduct this analysis. However, for the later sections of the dissertation, where the interest is to determine the location of fatigue crack, crack path and crack rate, we cannot use the finite element model of the whole bridge. This is due to several reasons. The mesh in this model is too coarse and is not appropriate for modeling cracks. If this model is meshed finely, the size of the model will exceed the computational capability of ANSYS. Therefore, the current model is meshed coarsely, which means the elements sizes are large, which can cause issues when exact and accurate stresses are needed in the tip of the crack. Furthermore, modeling crack requires use of "successive initiation." This technique requires runs of finite element repeatedly. Due to the large size of the bridge model, it is literally impossible with available computational resources to repeat the model for many runs as the size of each solution can easily exceed 18 Gbt of computer space. Therefore a global-local modeling approach is proposed in which the critical regions of the model are brought under the microscope and are modeled locally with a finer mesh and mesh sensitivity analysis is conducted for the local models. Global model in this analysis refers to the model of the superstructure and substructure and local model refers to the zoomed-in model of the critical region with highest level of stress and strains or the region of interest. Use of the local model will also facilitate modeling of fatigue crack initiation and propagation using the "successive initiation" technique.

Once the global model is conducted and the critical region in the pile is identified, a local model of the critical region is built and meshed with a very fine mesh. The critical region in this case is the region of the pile that is prone to fatigue crack initiation and propagation. Analyzing the stress and strains in the piles shows that the critical region is the region below the abutment. This global-local modeling strategy is shown in Figure 6-8. Part of the selected region is within the

abutment and part of it is within the soil.
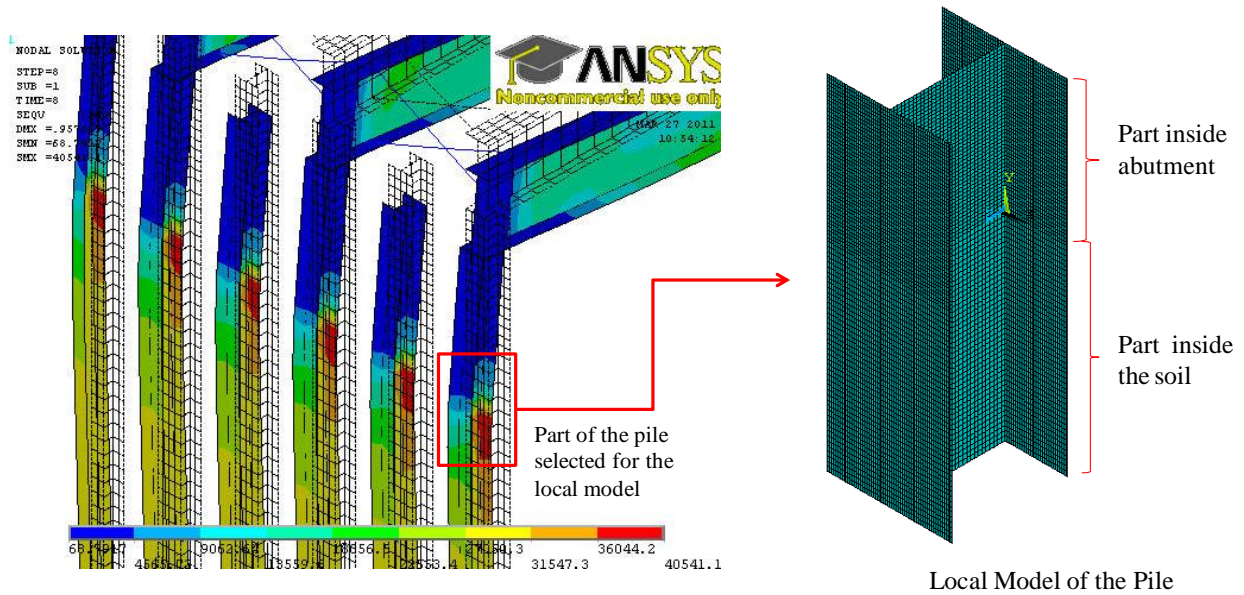
Figure 6-8: The global-local modeling strategy.

At the next step, the nodal displacement of the critical region is extracted from the global model and is applied to the local model as a boundary condition (refer to Figure 6-9). An APDL code in ANSYS is written to perform these tasks automatically. This program applies the nodal displacement taken from the global model to every node in the local model.
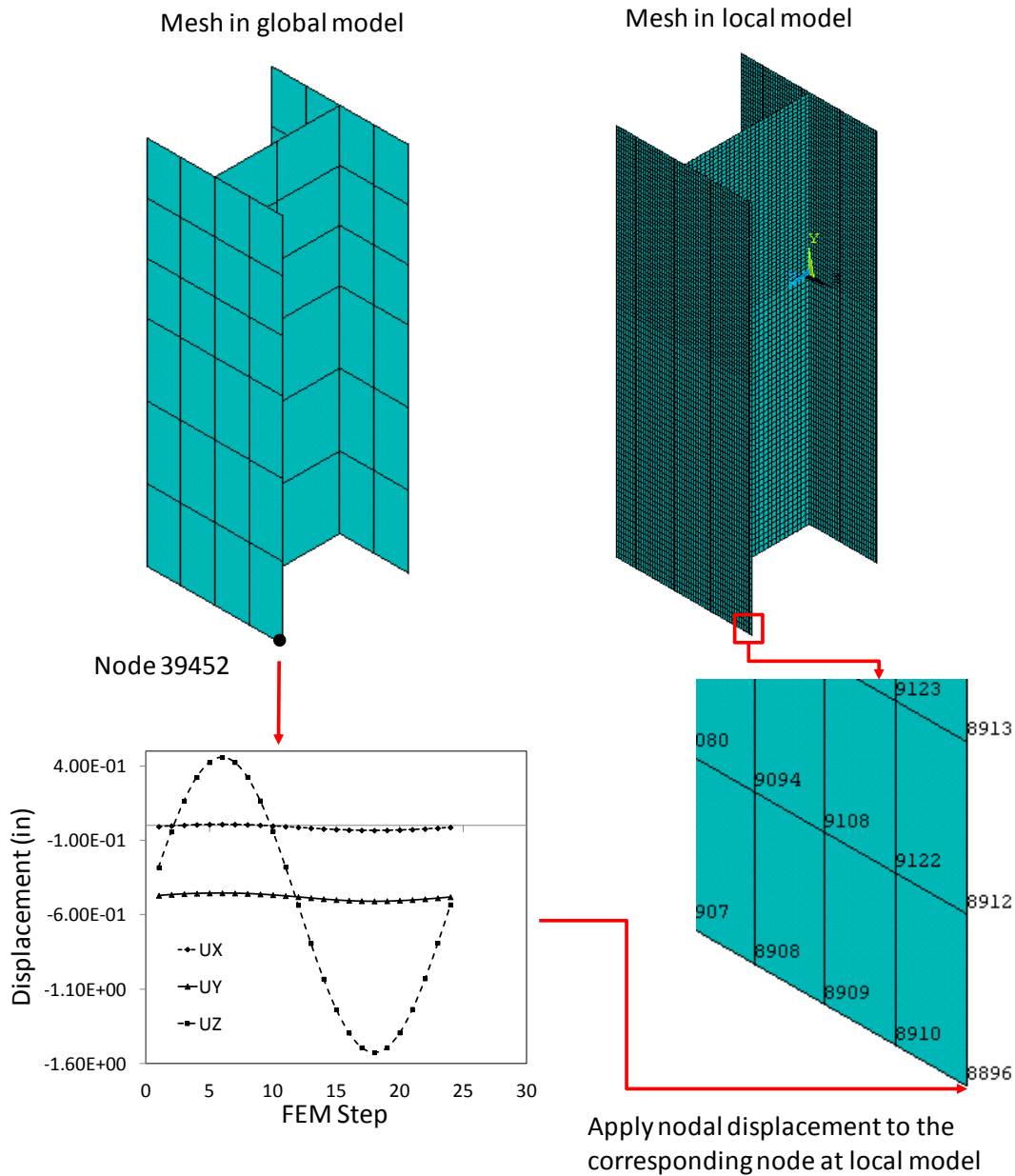
Figure 6-9: Transferring the displacement from global nodes to corresponding local nodes as

boundary conditions.

Since the global model is meshed with far coarser elements than the local model, not all the

nodes at the local model correspond to a node on the global model. Therefore, nodes without a

corresponding global mode are given a displacement determined by bilinear interpolation.

In mathematics, bilinear interpolation is an extension of linear interpolation for interpolating functions of two variables (e.g., x and y) on a regular grid. The interpolated function should not use the term of x^2 or y^2, but xy, which is the bilinear form of x and y [75].

The key idea is to perform linear interpolation first in one direction, and then again in the other direction. Although each step is linear in the sampled values and in the position, the interpolation as a whole is not linear but rather quadratic in the sample location.

Suppose that we want to find the value of the unknown function f at the point $P = (x, y)$. It is assumed that we know the value of f at the four points $Q_{11} = (x_1, y_1)$, $Q_{12} = (x_1, y_2)$, $Q_{21} = (x_2, y_1)$, and $Q_{22} = (x_2, y_2)$. Figure 6-10 shows the bilinear interpolation grid. The value of the function at point p is interpolated having the values at four points at the corners of the grid (Q_{11}, Q_{12}, Q_{21}, Q_{22}) using the following equation:

$$f(x,y)_P = \frac{f(Q_{11})}{(x_2-x_1)(y_2-y_1)}(x_2-x)(y_2-y) + \frac{f(Q_{21})}{(x_2-x_1)(y_2-y_1)}(x-x_1)(y_2-y) + \frac{f(Q_{12})}{(x_2-x_1)(y_2-y_1)}(x_2-x)(y-y_1)$$

$$+ \frac{f(Q_{22})}{(x_2-x_1)(y_2-y_1)}(x-x_1)(y-y_1) \qquad \text{Eq. 6-2}$$
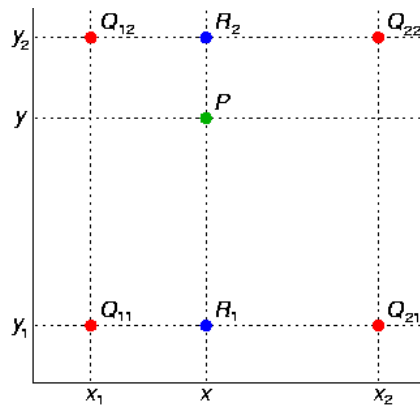
Figure 6-10: Bilinear interpolation grid [75].

67

This bilinear interpolation technique is used to determine all 6 components (U_x, U_y, U_z, ROT_x, ROT_y, ROT_z) of displacements on all the nodes of the local model. A comparison of this boundary condition transfer to the local model is presented in Figure 6-11. Notice that values of displacement in the local model completely match the values of global model.
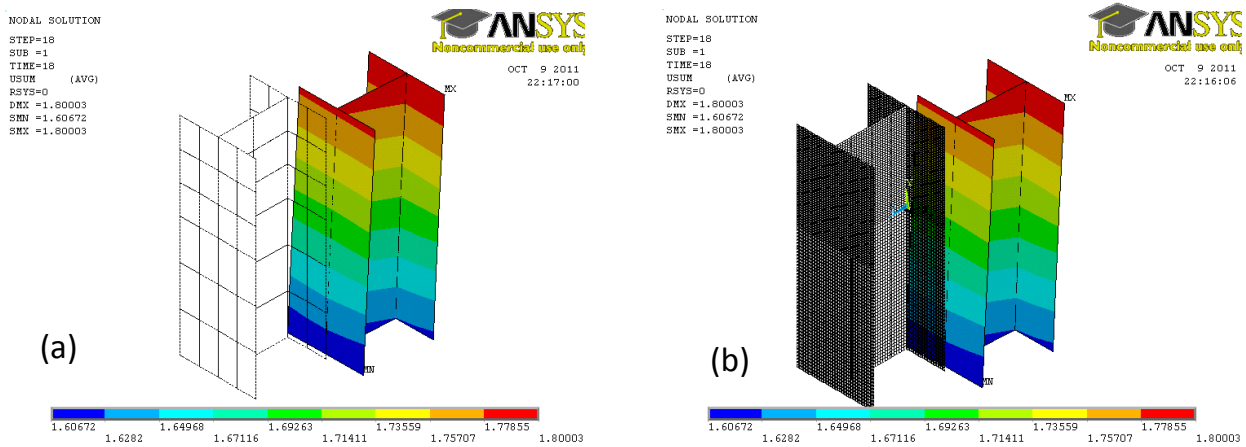
Figure 6-11: Comparison of contour plot of displacement vector in global and local model in step 18 of the daily temperature model (a) global model, (b) local model.

This displacement transfer must be done for the duration of the load, which is 24 hours for the daily cycle and 365 days for the seasonal cycle.

6.5. Successive initiation

One of the objectives of this dissertation is to investigate fatigue crack initiation and propagation in the critical pile. This is proposed to be done by separating crack initiation and propagation using a technique called "successive initiation." "Successive initiation" is a finite element technique that is used in conjunction with a continuum damage model. The method was first introduced to overcome some of the shortcomings of available fatigue life analysis

techniques. Typically fatigue life analysis for the materials and applications are done experimentally. However in many cases experimental methods are not applicable or feasible. For example, in a case of a pile buried in soil, measuring stress or strain is not practical. For such cases the FE model is used to determine the stress and strain history in the material. This stress and strain history is then used in a fatigue model to predict the fatigue life or number of cycles to failure. However, there is always uncertainty about what part of FE results would produce the most accurate predictions. This is because, typically, a distribution of stress and strains are observed over the elements in an FE model and results of one single element may prove inaccurate due to stress concentration and singularities in the FE. There is considerable argument in the engineering community over how to use FE results to determine fatigue life. Some researchers suggest averaging the values of stress or strain over all the elements in a slice of material through the cross section of the structure [76]. This technique will be denoted as an "averaging technique" in this context. This implies that the structure or material fails abruptly on after a certain number of cycles at which the whole section fails. The life obtained using the "averaging technique" includes both crack initiation and crack propagation life together and is based on the assumption that the structure fails abruptly, without attempting to predict when the damage and crack actually starts. The "averaging technique" has proved inefficient or inaccurate in some cases [76]. In reality the structure starts to weaken long before it fails. Micro-cracks and micro-voids are formed due to fatigue damage. These micro-cracks propagate as the structure continues to go through cycles of load. Eventually when these micro-cracks grow and coalesce, a large crack forms and the structure fails. The "averaging technique" does not give enough information about the damage initiation, and damage growth in the material. Neither can information be gathered about the propagation path. The "successive initiation" is introduced to

69

avoid the issues associated with the "averaging technique" by modeling crack initiation, propagation, and coalescence using a fatigue model element-wise and locally and by accumulating damage throughout the model by taking the stress and strain history of each element, updating it as the number of cycles increases and calculating its damage accumulation rate. This method was first introduced by Okura [76], Gyllenskog et al. [77], Nelson et al. [78] and Ladani [79] and has been used to model damage and crack initiation in several different applications including joint and interconnects in electronics [79], aluminum aileron lever in a T38 airplane [77], and Al-Mg bimodal grain size alloy [78]. In all of these applications, this method has been verified using experimental results or field data.

"Successive initiation" analysis involves several steps and several consecutive finite element runs. It is implemented using of FE analysis in this study. The steps in this process are listed below and are also shown in the form of a flowchart in Figure 6-12.
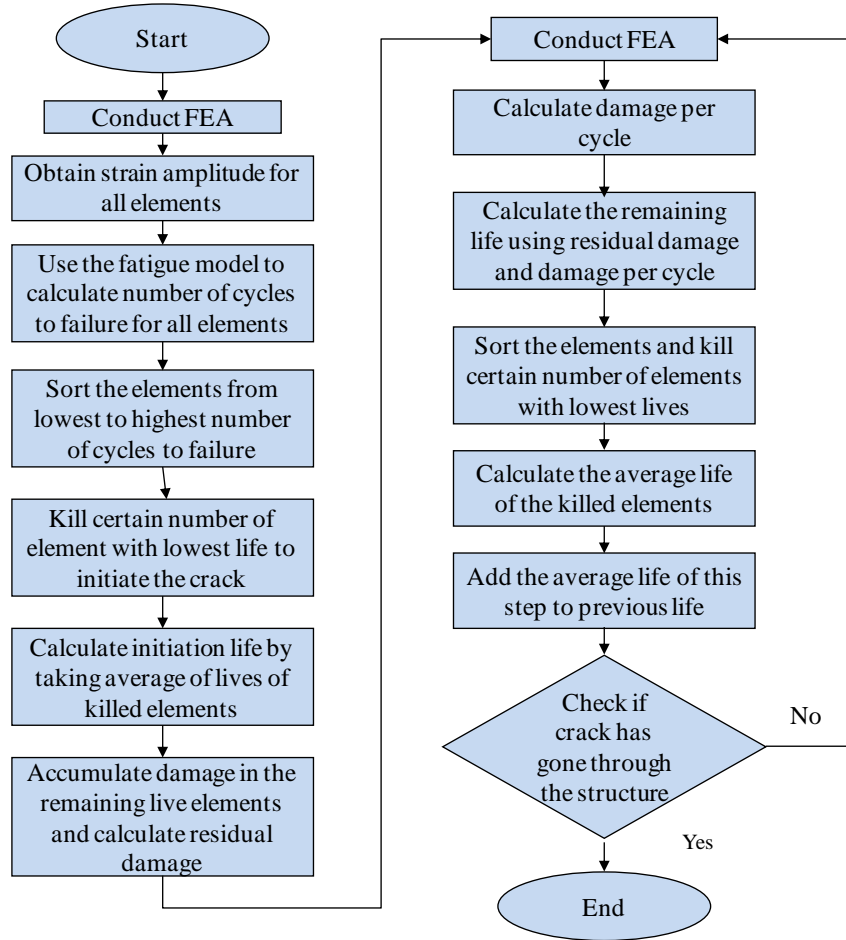
Figure 6-12: Flowchart for successive initiation technique.

1. Run FE analysis for local model.

2. Obtain the total strain amplitude for all elements in the model.

3. Calculate number of cycles to failure (fatigue life) for all elements using the fatigue model [64 & 80].

$$N_f = 2(13.35\varepsilon)^{-2.2173}$$
<div align="right">Eq. 6-3</div>

Where ε is the total strain amplitude and N_f is the number of cycles to failure.

4. Sort the elements based on the number of cycles to failure from lowest to highest number of cycles to failure.

5. Select a set of elements with the lowest number of cycles to failure.

6. Eliminate ("kill") elements with the lowest number of cycles to failure (the number of "killed" elements depends on how fast one would like to propagate the crack).

7. Calculate crack initiation life (N_{f1}), which is the average of the life of the "killed" elements.

8. Accumulate damage in the remaining live elements according to the following:

$$D_{accum} = N_{f1}.D_{cycle1} \qquad \text{Eq. 6-4}$$

Where D_{accum} is accumulated damage and D_{cycle1} is the damage per cycle for each element in run 1. Since each element has different values of stress and strain, each element will have different values of D_{cycle1}. Therefore, each element will have a different damage accumulation rate. D_{cycle1} can be obtained from the following equation:

$$D_{cycle1} = \frac{1}{N_{f1}} = \frac{1}{2(13.35\varepsilon)^{-2.2173}} \qquad \text{Eq. 6-5}$$

The strain amplitude experienced by each element is plugged into Eq. 6-5 to calculate the damage rate for each element.

9. Calculate residual damage in the remaining elements. This step is based on the assumption that each element can stand a maximum damage of 1. This means that the remaining live elements have accumulated a certain amount of damage and now can stand $D_{residual} < 1$ for the remainder of the process.

Where:

$$D_{residual} = 1 - D_{accum} \qquad\qquad\qquad\qquad \text{Eq. 6-6}$$

10. Conduct FE analysis again to find stress and strain distribution. Because some of the elements have been "killed", they cannot carry any load. Therefore, the stress and strain distribution will be different from the first run of FE and damage per cycle is different from the first run of FE.

11. Calculate damage per cycle using Eq.6-5.

12. Using this damage per cycle and the residual damage from Eq. 6-6 that we calculated from a previous FE run, the remaining life of each element is calculated using the following equation:

$$N_f = \frac{D_{residual}}{\frac{1}{2(13.35\varepsilon)^{-2.2173}}} \qquad\qquad\qquad\qquad \text{Eq. 6-7}$$

13. Sort the elements based on this new number of cycles to failure.

14. Determine the elements with the lowest number of cycles to failure.

15. "Kill" or eliminate elements with low number of cycles to failure.

16. Calculate the average life of "killed" elements, $N_{f2.}$

17. Calculate the total number of cycles by adding the number of cycles for each step.

$$N_f = N_{f1} + N_{f2} \qquad\qquad\qquad\qquad \text{Eq. 6-8}$$

18. Go back to step 8 and accumulate the damage in the remaining live elements.

19. Continue through the process to "kill" elements until crack is propagated through the material.

This method is used to find the crack initiation site and time and crack propagation path in the local model of the pile.

Chapter 7. Determination of pile stress-strain behavior and displacements

Because the lateral displacement in piles results in elastic or plastic deformation in the piles, it is crucial to determine the extent of the lateral displacement. Cyclic elastic deformation of piles results in high cyclic fatigue whereas if the displacement is large, the piles may experience plastic deformation that could result in low cycle fatigue and early failure.

Therefore, it is essential to understand the piles behavior and their mode of deformation (elastic vs. plastic). Since piles are three-dimensional structures, it is expected that three-dimensional stresses develop in them. As a result, determining the elastic or plastic deformation of piles requires utilization of plasticity theory. Determining plastic deformation (yielding) in a simple bar loaded with a uni-axial tensile load is only a matter of calculating the uni-axial stress and comparing it with the materials yield strength, whereas three-dimensional states of stress require utilization of one of the yield criteria such as Tresca or von-Mises criteria. Generally, von-Mises criteria is believed to be more accurate because it is based on deviatoric energy, which is the driving energy for shear stresses. Shear stresses are stresses that cause dislocation motion, and thus cause plastic deformation and yielding in polycrystalline metallic materials [87].

Von-Mises yield criterion can be formulated in terms of the von-Mises stress or equivalent tensile stress, σ_{eff}, a scalar stress value that can be computed from the stress tensor.

$$\sigma_y = \frac{1}{\sqrt{2}}\sqrt{\left(\sigma_{xx} - \sigma_{yy}\right)^2 + \left(\sigma_{yy} - \sigma_{zz}\right)^2 + (\sigma_{xx} - \sigma_{zz})^2 + 6\left(\tau_{yz}^2 - \tau_{xz}^2 + \tau_{xy}^2\right)} \qquad \text{Eq. 7-1}$$

Where: $\sigma_{xx}, \sigma_{yy}, \sigma_{zz}$ are normal stress components and $\tau_{yz}, \tau_{xz}, \tau_{xy}$ are the shear stress component.

In this case, a material is said to start yielding when its von-Mises stress reaches a critical value of yield strength (σ_y). It is analytically impossible to determine the three-dimensional state of stress in piles. Therefore, numerical simulations are utilized in this study to determine the components of stress tensor and, hence, the mode of deformation (elastic and plastic) in piles. In many of the simulation reports available for IABs, the steel is modeled elastically [81-84]. In some cases the models are simplified to two-dimensional models [81-84]. Elastic-plastic behavior of steel piles has not been modeled in conjunction with thermal cycling loading of bridge and bridge-soil interactions.

7.1. Stresses and strains in the pile

A parametric study was conducted in which the length of the bridge was varied in five different cases with lengths of 400, 600, 800, 1,200 and 1,800 ft. Finite element analysis results for all the cases of both seasonal and daily temperature changes show that the maximum stress in the piles occurs in the flange of the piles right below the concrete abutment. Figure 7-1 shows both deformed and un-deformed piles and the contour plot of the von-Mises stress for the case of a 1,200 ft bridge. The stress is at a maximum in the pile that is farthest from the center of the bridge (pile 6 in Figure 4-2(a)).
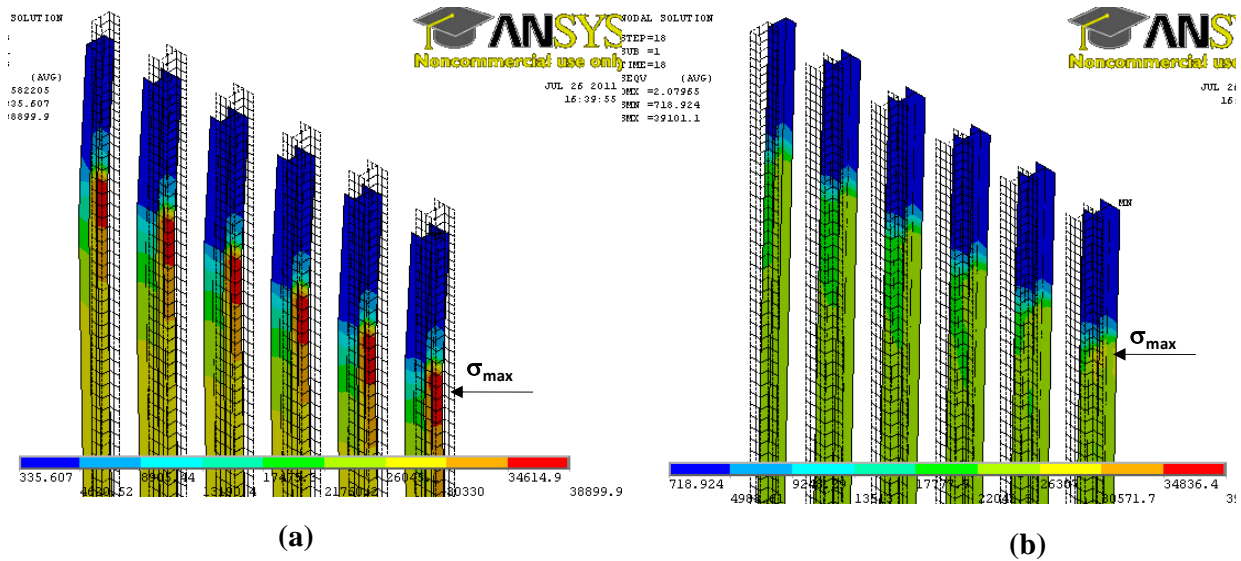
Figure 7-1: Contour plots of von-Mises stress at (a) maximum daily temperature, (b) minimum

daily temperature.

Plastic deformation is also observed in this pile, indicating that yield stress occurs in the pile. It is also observed in all the other piles, but the magnitude of it in pile 6 was the largest. Plastic deformation occurs even in the piles of the 400 ft length bridge. The plastic deformation occurs in the flange of the pile resulting in yielding of the material at this point. Figure 7-2 shows contour plots of equivalent plastic strain at pile 6 for the 1,200 ft bridge length.
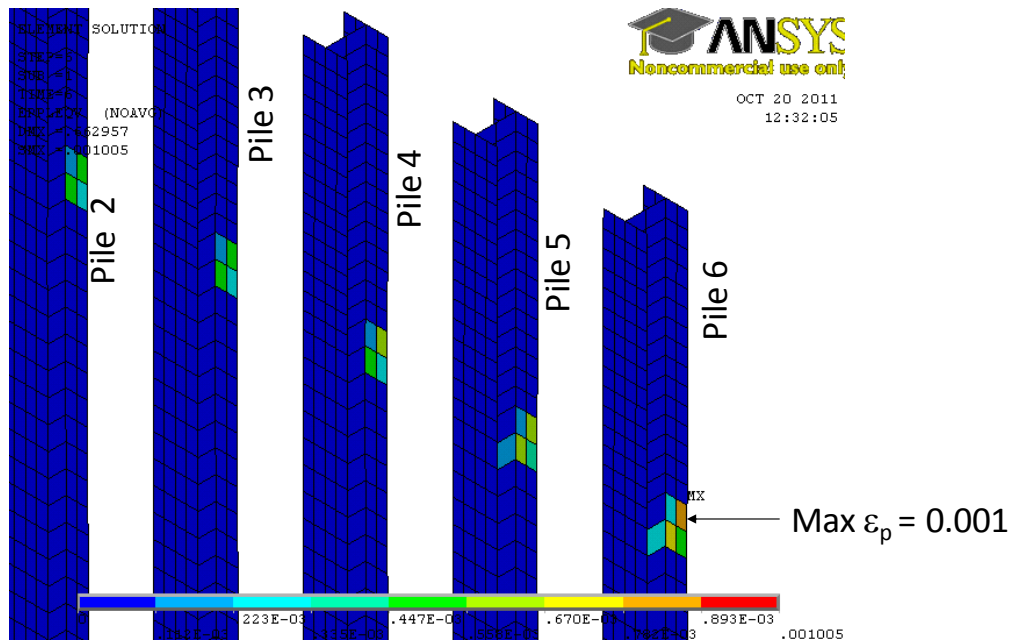
Figure 7-2: Contour plot of equivalent plastic strain at maximum daily temperature.

The plastic strain in the flange of pile 6 below the abutment at the maximum daily temperature is evaluated from finite element for all the cases and is listed in Table 7-1. The magnitude of this strain in the flange of the piles increases linearly as the length of the bridge increases, as can be seen in Figure 7-3.

Bridge Length (ft)	ε_{peq}
400	0.881E-3
600	0.914E-3
800	0.945E-3
1200	1.005E-3
1800	1.09E-3

Table 7-1: Equivalent plastic strain observed in flange of pile 6 underneath the abutment.
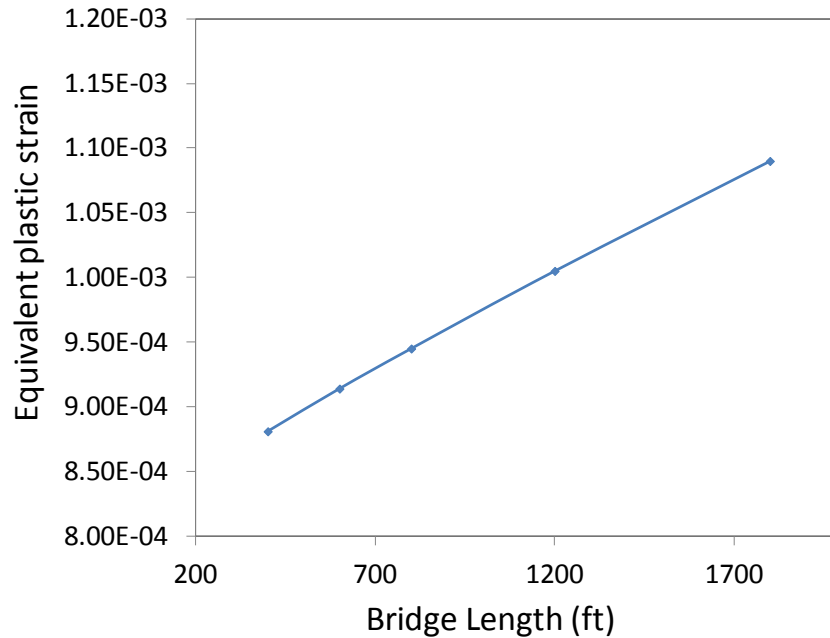
Figure 7-3: The plastic strain evaluated at the element in pile 6 right below the abutment.

The stress analysis in the pile shows that during one cycle of loading, elements experience only compression-compression. This indicates that the stresses are not completely reversed during one of load cycle (tension-compression). This is mainly because the dead and live loads on the bridge provide a large constant pressure that prevents these elements from exiting the compression side and transitioning to the tension side of the stress-strain region.

Von-Mises stress on one node in the vicinity of the maximum stress position is plotted as a function of time steps for daily and seasonal temperature variations for the case of the 1,200 ft length bridge in Figure 7-4. This figure also shows a case of no thermal expansion where the finite element model is conducted only with dead and live loads for the 1,200 ft length. No temperature variations are applied in this case. The cyclic nature of the stress can be seen in both daily and seasonal temperature cycles. Although all cases start with roughly the same value of stress, the stress increases slightly in both daily and seasonal cases.

The figure also shows the cyclic nature of the stress variation due to temperature changes. This cyclic stress is the main factor dictating fatigue life. As the amplitude of the stress increases, the fatigue life decreases. It is clear from this figure that amplitude of stress is larger in the case of seasonal temperature variations. However, one seasonal cycle occurs over one year. Therefore, the number of seasonal cycles is much smaller than daily cycles. Although the stress in the case of no thermal expansion is comparable with the maximum stress observed in both daily and seasonal cases, since the case of no thermal expansion does not experience cyclic behavior, fatigue will not occur in it.
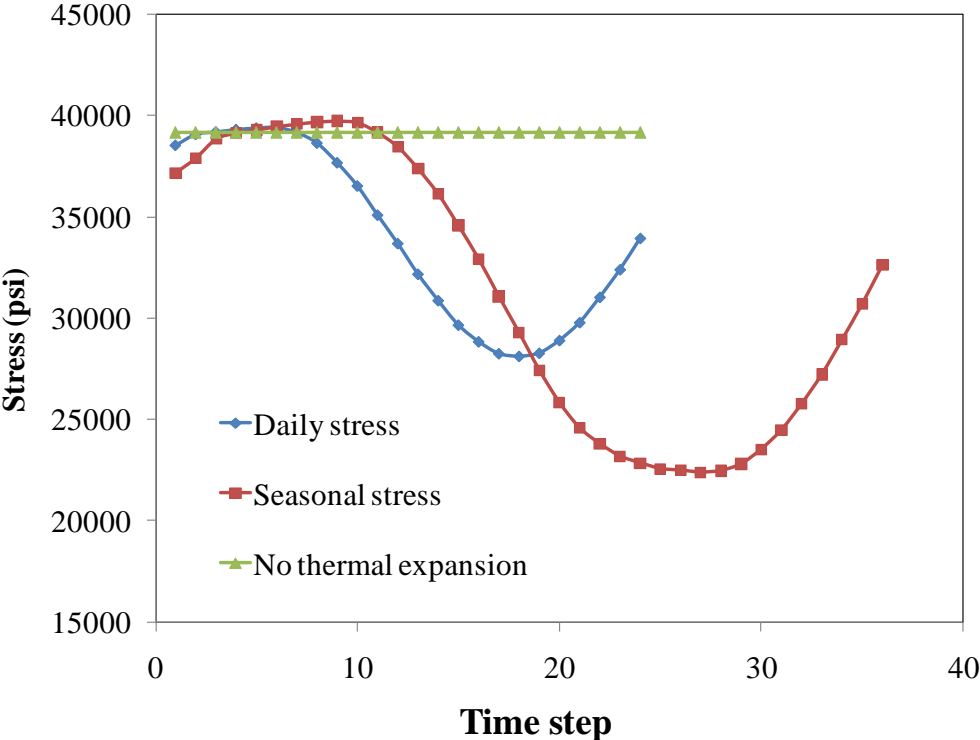
Figure 7-4: von-Mises stress observed in the node with maximum stress on maximum daily and seasonal temperature for one cycle of daily and seasonal temperature compared with a case with only dead and live loads at the same node (the unit of time step for the daily cycle is hour and the seasonal cycle is 10 days).

80

Table 7-2, shows the maximum and minimum stress obtained in pile 6 for the 1200 ft bridge analyzed.

Pile 6	Maximum stress (psi)	Minimum stress (psi)
D.L & L.L	39177	370
Max Daily	39409	300
Min Daily	36444	719
Max Seasonal	39766	316
Min Seasonal	38601	1467

Table 7-2: Comparison of maximum and minimum stresses observed in pile 6 for the case of 1,200 ft bridge.

7.2. Displacement of the pile

Maximum lateral displacement in the piles at maximum and minimum daily and seasonal temperatures are obtained from the finite element for all the cases of the parametric study. The results are listed in Table 7-3 . These displacement are plotted as a function of bridge length in Figure 7-5. It can be clearly seen that the value of deformation linearly increases with the length.

Case	Displacement (in) in FEA				Displacement (in) using ASHTOO			
(ft)	Max daily	Min daily	Max seasonal	Min seasonal	Max daily	Min daily	Max seasonal	Min seasonal
400	0.3452	-0.7875	0.4528	-1.4073	0.429	-0.429	0.858	-0.858
600	0.3760	-1.1471	0.5338	-2.0628	0.644	-0.644	1.29	-1.29
800	0.4060	-1.4979	0.6139	-2.7031	0.858	-0.858	1.72	-1.72
1200	0.4652	-2.1755	0.7712	-3.944	1.29	-1.29	2.57	-2.57
1800	0.5492	-3.1432	0.9968	-5.7328	1.93	-1.93	3.86	-3.86

Table 7-3: Displacements due to thermal load in piles in bridges with lengths varied between 400 ft to 1,800 ft.
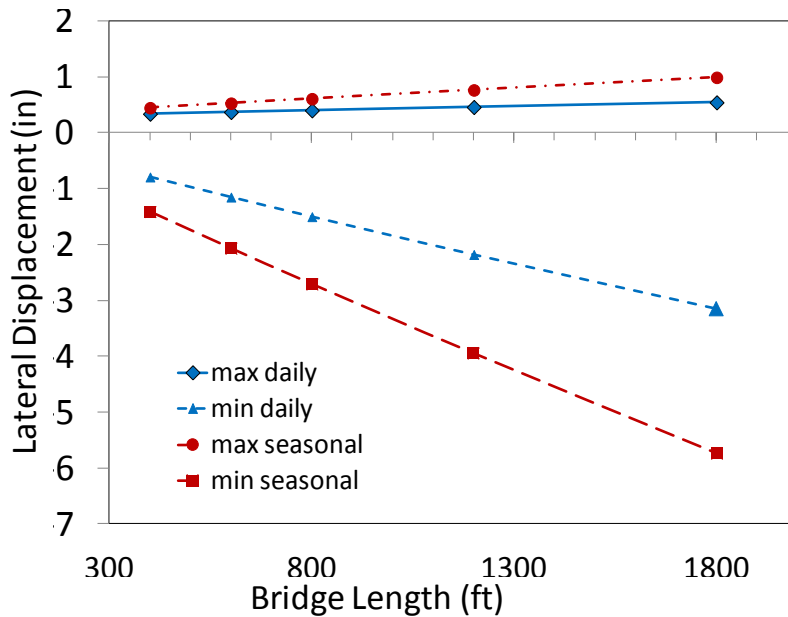
Figure 7-5: Lateral displacement of piles as function of length for seasonal and daily temperature variations.

In comparison, if the bridge was simply supported, the design thermal movement ΔT according to AASHTO [5] associated with a uniform temperature change can be obtained from:

$$\Delta_T = \alpha L(T_{MaxDesign}\text{-}T_{MinDesign}) \qquad\qquad \text{Eq. 7-2}$$

Where: L = expansion length (in), α = coefficient of thermal expansion (in./in./°F) and $T_{MaxDesign}$ and $T_{MinDesign}$ are temperature ranges for different climates. For a 1,200 ft bridge and range of temperature of 93° to -17°, the thermal movement of the bridge with length of 1,200 ft will be 0.64 in summer.

Lateral displacement of the pile 6 for a of 1,200 ft bridge due to the dead and live load is shown in Figure 7-6.

Lateral displacement of the piles and their profile at different temperatures for the case of 1,200 ft are plotted and shown in Figure 7-7 through Figure 7-10. As seen in Figure 7-7 and Figure 7-9 , the displacement at high temperatures is non-monotonic. This is consistent with what the literature has shown [23 & 85-86]. The top of the pile is pulled in due to the bending moment caused by the vertical dead (DL) and live loads (LL) on the bridge. At the same time, it is pushed out due to thermal expansion. At low temperatures, the pile's behavior is monotonic as shown in Figure 7-8 and Figure 7-10. In these cases, the direction of displacement due to thermal contraction and the dead and live loads on the bridge are the same. Therefore, these deformations are added together to create the total displacement of the piles. Lateral displacement due to the seasonal temperature cycles is larger than that due to daily temperature cycles, indicating a larger amount of plastic deformation and a lower number of cycles to failure for the seasonal temperature cycle. However, the bridge experiences many more daily temperature cycles, which

may result in failure of the piles in a shorter time.
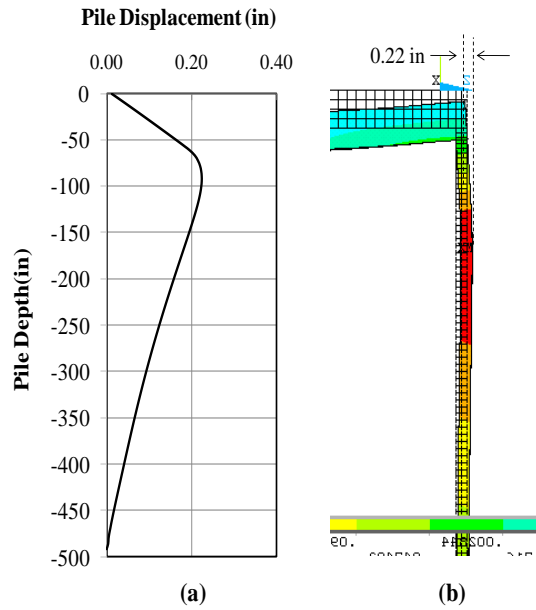
Figure 7-6: Displacement of the pile (LL & DL only).

Figure 7-7: Lateral displacement of the pile at maximum daily temperature, (a) displacement

profile of middle nodes on the pile obtained from FEM, (b) FEM illustration of

displacement in pile.
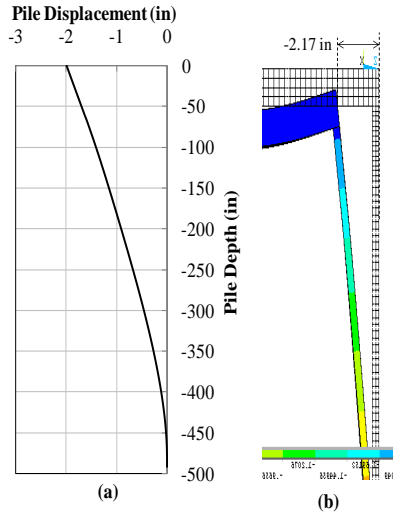
Figure 7-8: Lateral displacement of the pile at minimum daily temperature, (a) displacement

profile of middle nodes on the pile, (b) FEM illustration of displacement in pile.
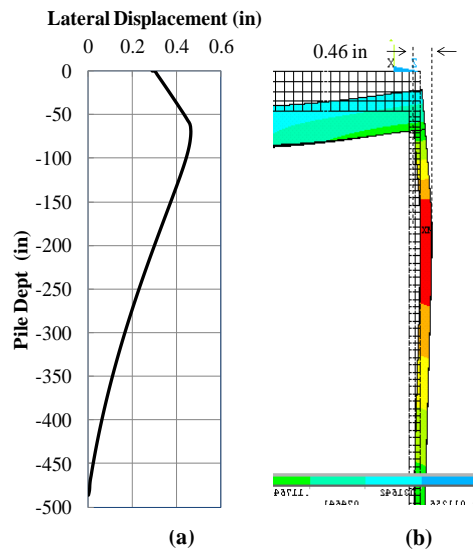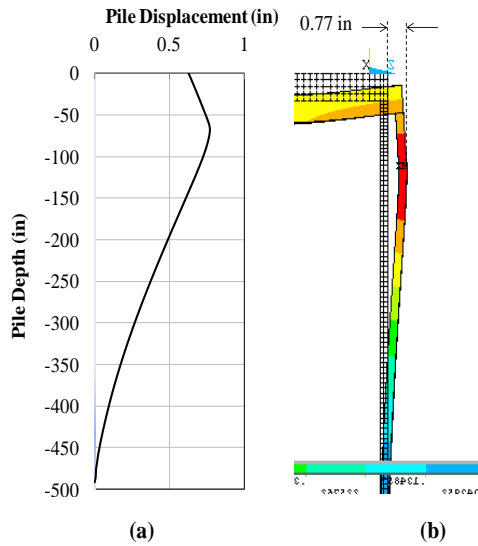

Figure 7-9: Lateral displacement of the pile at maximum seasonal temperature, (a) displacement

profile of middle nodes on the pile, (b) FEM illustration of displacement in pile.
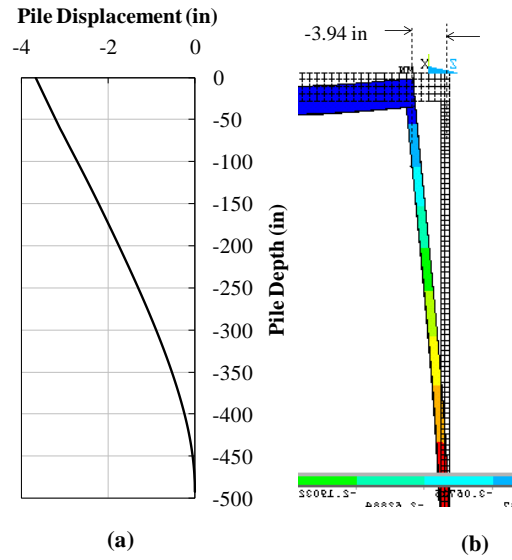
Figure 7-10: Lateral displacement of the pile at minimum seasonal temperature, (a) displacement

profile of middle nodes on the pile, (b) FEM illustration of displacement in pile.

Chapter 8. Fatigue life analysis of piles

Depending on the criticality of the application, fatigue life is typically defined differently. For example, in some aerospace applications, fatigue life is considered the number of cycles that it takes for a crack to reach the critical dimension of 0.09 x 0.06 inches [77]. In the electronic industry, however, fatigue life is define differently. For example, fatigue life for an interconnect that is subjected to cyclic mechanical load is the number of cycles that it takes for the interconnect to fail completely [90]. ASTM defines fatigue life as the number of stress cycles of a specified character that a test specimen sustains before failure of a specified nature occurs [91]. Fatigue life has never been defined in piles. Therefore, in this study a definition of fatigue life for piles is introduced. Fatigue life is defined as the number of cycles that takes for the crack length to reach a quarter of the flange length of the steel pile.

In order to determine the fatigue life of the piles, the state of stress and strains in all the elements of the pile section was determined. An appropriate fatigue model is then used to determine the fatigue life. This chapter presents such determination.

8.1. Extract stress-strain history from FE

Since piles are three-dimensional structures, it is expected that three-dimensional stresses develop in them. As mentioned earlier, von-Mises stress is needed to be able to determine if the pile experiences plastic deformation. Von-Mises stress is extracted from FE results.

In the case modeled in this study the maximum stress occurs in pile 6 right below the abutment. Figure 8-1 shows contour plot of von-Mises stress in the piles elements. Regardless of the magnitude of stress, its amplitude is the deciding factor in fatigue life. Figure 8-2 is used to

illustrate this concept.
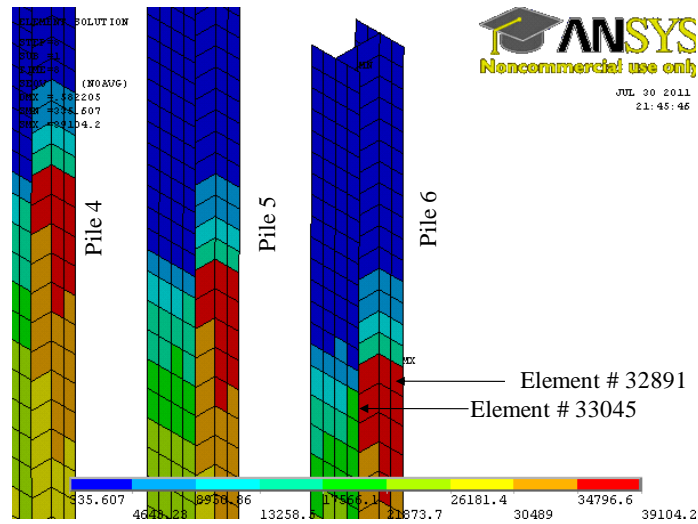
Figure 8-1: Contour plot of von-Mises stress in elements of pile.

As seen in this figure the magnitude of stress is higher in element 32891 (39,104 psi) compared to element 33045 (21,873 psi). Both of these elements are located in pile 6 and under the abutment. However, if the stress history in one cycle of loading is plotted, it can be seen that the amplitude of the stress is much higher in element number 33045 ($\Delta\sigma_2$) compared to element number 32891 ($\Delta\sigma_1$) as seen in Figure 8-2. This indicates that fatigue failure will occur faster in element 33045 even though the magnitude of stress is higher in element 32891.
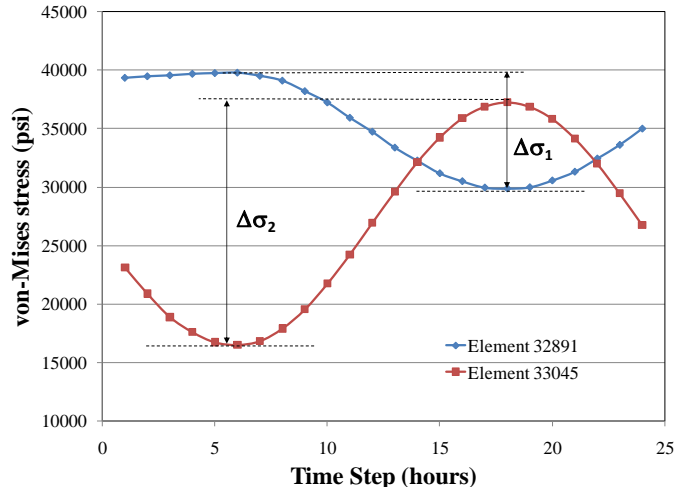
Figure 8-2: Stress history in two elements shown in Figure 8-1.

Therefore, it is important to extract the stress, strain or energy history for all the elements over one cycle of loading and determine the amplitude of it for each element.

In the case of a pile, it must be noted that piles are always under a large amount of compression stresses due to dead and live loads. Even though the thermal expansion and contraction will cause cyclic stress and will create some stress amplitude, the stress amplitude is rarely large enough to cause tensile stresses in the elements. Therefore, when the stresses are extracted, typically the sign of the largest component of stress, in this case σ_y is negative. However, regardless of the sign of the stress components, the equivalent stress or strain which is calculated using the von-Mises equation, is always positive according to Eq. 8-1. Careful analysis of the stress-strain history shows that two element numbers 32430 and 33045, which are located right below the abutment and in a diagonal location of each other on tip of the flanges of the pile 6, have the highest and comparable stress amplitudes as seen in Figure 8-3.

89
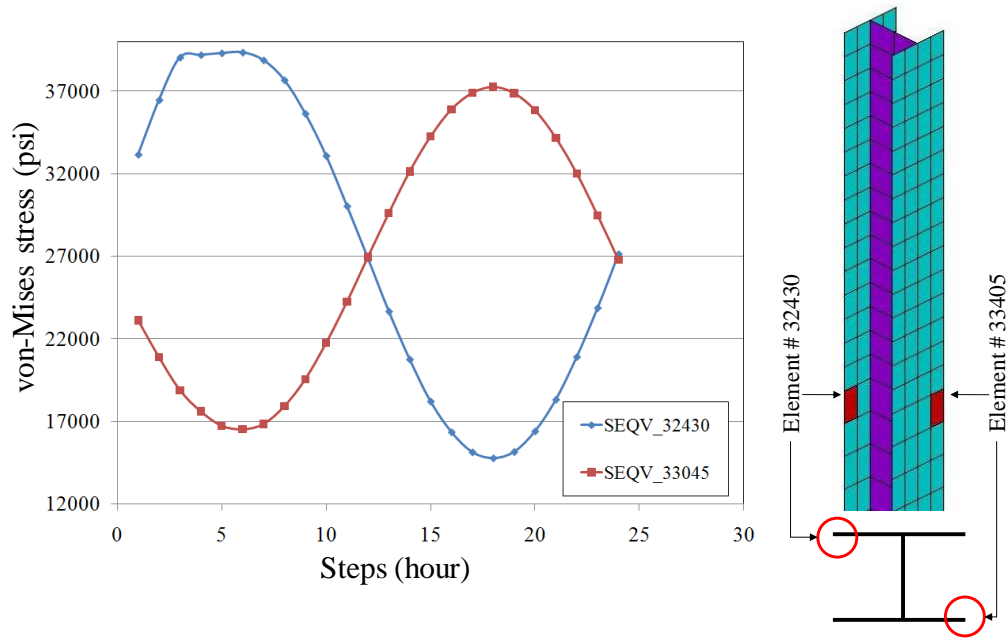
Figure 8-3: Von-Mises stress history in one cycle of loading for two elements in pile number 6 identified as critical elements.

As expected, the stress amplitude in these two elements behaves in an opposite manner. This means that when stress in one is increased, the stress in the other one is decreased. This is expected because these two elements are located on opposite sides in the pile.

This indicates that fatigue crack will most likely start from these locations. The stress or strain amplitudes from these two elements can be used to determine the fatigue life of these elements. It must be noted that failure of these two elements does not necessarily mean failure of the pile. Complete failure of the pile requires failure of all the elements across the pile section. Therefore, the life calculated using the values obtained from these two elements only indicates the extent of crack propagation. Since the stress and strain amplitude are larger in element 32430, these values are used in this paper to calculate fatigue life. It is expected that element 33045 will fail shortly after failure of element 32430.

8.2. Determine an appropriate fatigue damage model

There are several different approaches that have been used in the literature to predict the fatigue life of a structure. The type of approach depends on many factors, such as type of material, types of deformation, regime, and mode of cyclic loading. An example is the fracture mechanics approach. Fracture mechanics considers propagation of a single dominant crack through an otherwise undamaged material. This technique is more appropriate for modeling cracks in brittle material where plasticity is negligible. If material experiences plastic deformation or distributed damage, a fracture mechanics approach is not the best technique to model damage and cracks. In this case, a crack is propagated by growth, coalescence, and the interconnection of micro-cracks and voids distributed all over the stressed regions. Therefore, the use of a continuum damage model is more appropriate. As mentioned earlier, continuum damage modeling approaches have been classified into several groups: stress-based, strain-based, and energy-based approaches. In the case of steel, available models are stress-based and strain-based. Since the piles in our case experience plastic deformation and thus experience low-cycle fatigue, a strain based model is selected as the fatigue model. The fatigue life is calculated using the formula [63 & 80] :

$$\varepsilon_a = 0.0795(2N_f)^{-0.448} \qquad \qquad \text{Eq. 8-1}$$

Where ε_a is the total strain amplitude and N_f is the number of cycles to failure. This model was proposed by Koh et al. in 1991 [80] to determine the low-cycle fatigue life of high-strength steel material. The model was reexamined by Mander et al. [63] and showed 98% correlation through experiments.

8.3. Determine the fatigue life of piles

The total strain amplitude extracted from the FE model is used in Eq. 9-2 to determine the number of cycles to failure. The total strain amplitude is calculated using the following formula:

$$\varepsilon_a = \varepsilon_{ea} + \varepsilon_{pa} \qquad\qquad \text{Eq. 8-2}$$

Where ε_{ea} is the elastic strain amplitude and ε_{pa} is the plastic strain amplitude. The total strain amplitude obtained from the FE model for element 32430 in the case of the 1,200 foot long bridge is 1.23e-3. Plugging this value in the fatigue model, the number of cycles to failure would be 5,475 cycles. Dividing it by 365 (days) would give 15 years to failure for this element. This means that this element fails after 15 years and the crack starts.

Seasonal temperature variations cause much larger stress and strain amplitudes. A comparison between the stress amplitudes caused by daily and seasonal temperature variations observed in the same element in the case of a 1,200 foot long bridge is shown in Figure 8-4. As seen in this figure, the amplitude of stress due to seasonal temperature change is so large that stresses are actually tension-compression. Although the amplitude of stress/strain is much larger in the seasonal temperature variation, the frequency of this load is much lower. Each cycle of seasonal temperature variation occurs over one year. Therefore, it may take many years before the element actually fails. However, superposition of this load on top of daily temperature variations will have some effects on the life.
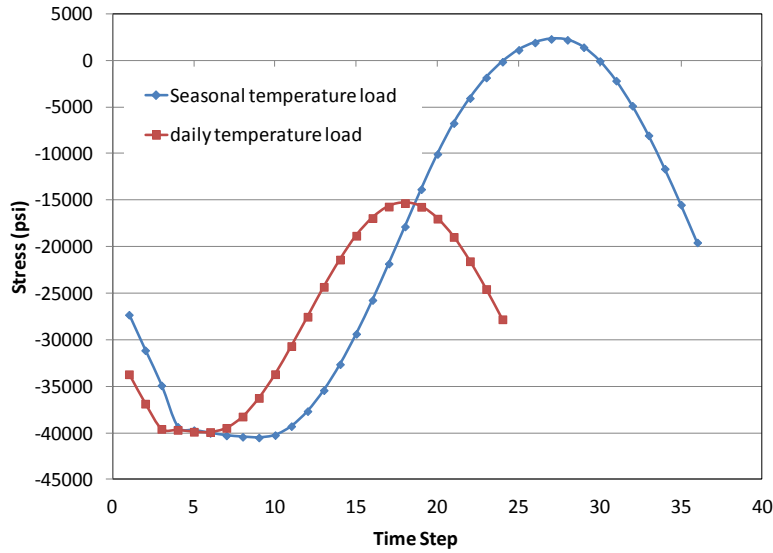
Figure 8-4: Comparison of seasonal and daily stress in y orientation in element 32430.

Superposition of daily and seasonal temperature cycles is schematically illustrated in Figure 8-5. The daily temperature cycle is shown as a higher frequency load on top of the low frequency seasonal temperature load.

To account for both daily and seasonal temperature variations, the damage caused by both of these cycles must be taken into account. This is done using the Palmgren-Miner rule (Miner [88] and Palmgren [89]) as follows:

$$\frac{N_d}{N_{fd}} + \frac{N_s}{N_{fs}} \leq 1 \qquad \text{Eq. 8-3}$$
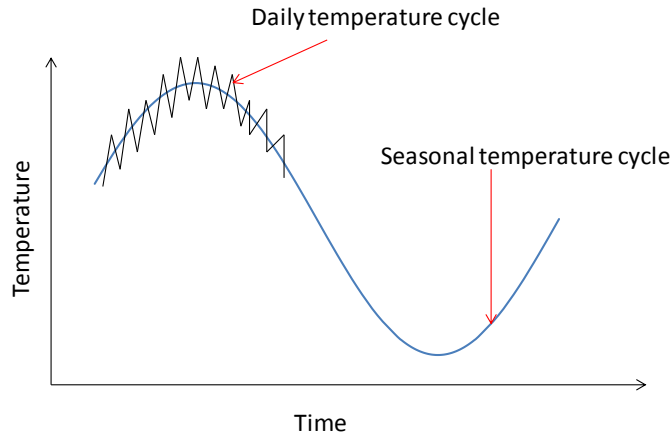
Figure 8-5: Schematic illustration of superposition of daily and seasonal temperature cycles.

Where N_d is the number of daily cycles and N_s is the number of seasonal cycles. N_{fd} and N_{fs} are the number of cycles to failure if each load was applied individually. The relationship says that if two different kinds of loads with different frequencies are applied, the summation of total damage caused by these two cyclic loads (in our case seasonal and daily cyclic loads) should be smaller than 1. If it reaches 1, the structure fails. In our case $N_d = 365\ N_s$ thus Eq. 13 becomes:

$$\frac{365N_s}{N_{fd}} + \frac{N_s}{N_{fs}} = 1 \qquad\qquad \text{Eq. 8-4}$$

In the case of the 1,200 foot long bridge, N_{fd} was calculated to be 5,475 cycles. The same technique of using the total strain amplitude for element number 32430 yields the amount of total strain amplitude of 2.08 E-3 for seasonal load and thus the total number of cycles to failure for seasonal load to be 1,701 cycles (i.e., 1,701 years). Subtracting these values in the Miner [88] equation and calculating the N_s we get 14.8 cycles (since each cycle is equivalent to one year this value is these equivalent to 14.8 years). This shows that the effect of seasonal cyclic load is not significant during the life time of the bridge compared to the effect of daily cycles. Therefore, analysis based on daily number of cycles to failure should provide accurate enough results for

94

the number of cycles to failure. Similar calculations are conducted for the all bridges with different lengths. The results are listed in Table 8-1.

Bridge length (ft)	400	600	800	1200	1800
Total strain amplitude	7.67e-4	8.88e-4	1.01e-3	1.23e-3	1.52e-3
Fatigue life (number of cycles to failure)	15,769	11,363	8,582	5,475	3,451
Fatigue life (years)	43	31	23.5	15	9.5

Table 8-1: Daily fatigue life analysis of IAB bridges with different lengths

Bridge length (ft)	400	600	800	1200	1800
Total strain amplitude	1.41e-3	1.66e-3	1.87e-3	2.08e-3	2.32e-3
Fatigue life (number of cycles to failure)	4,053	2,807	2,166	1,701	1,332
Fatigue life (years)	4,053	2,807	2,166	1,701	1,332

Table 8-2: Seasonal fatigue life analysis of IAB bridges with different lengths.

Bridge length (ft)	400	600	800	1200	1800
Total fatigue life (years)	42.7	30.8	23.2	14.8	9.3

Table 8-3: Fatigue life analysis for combined effect of daily and seasonal temperature variations for IAB bridges with different lengths.

A plot of the strain amplitude versus the length of the bridge and the predicted number of cycles to failure using the fatigue model for both daily and seasonal temperature variations are shown in Figure 8-6 and Figure 8-7. The daily strain amplitudes are relatively smaller than the seasonal amplitudes. The elastic portion of these two strain amplitudes does not change as the temperature

cycle amplitude changes. Therefore, the main contribution is from change in plastic strain amplitudes. As a result the linear trend of the strain amplitude in the daily graph becomes a nonlinear trend in the seasonal curve. As expected, the life predicted by the fatigue model follows a power law curve and is significantly smaller due to seasonal temperature variations than daily temperature variations.
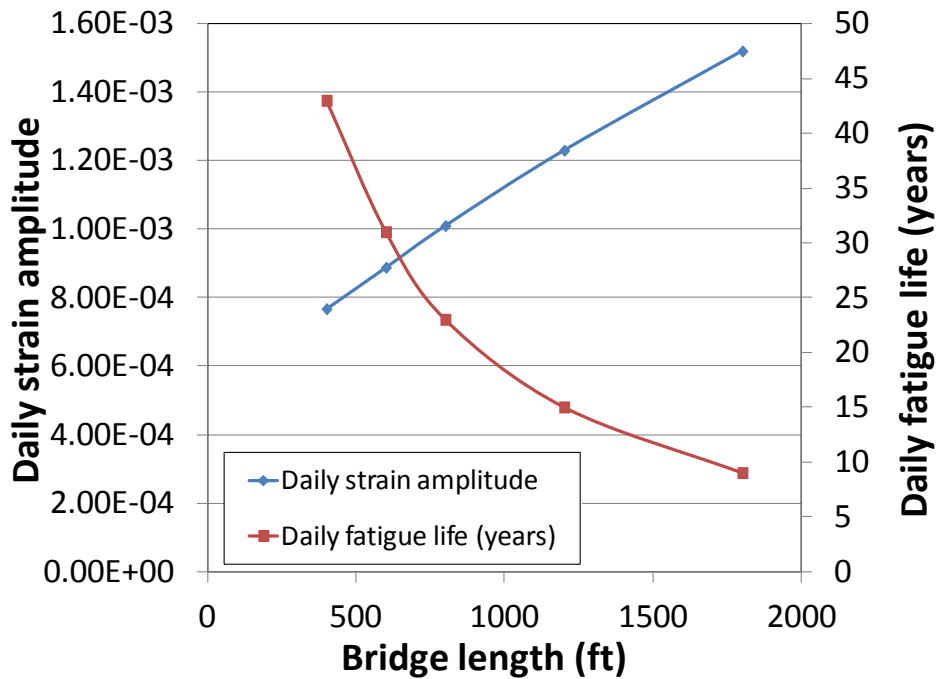
Figure 8-6: Total strain amplitude and fatigue life for daily temperature cycle versus bridge length.
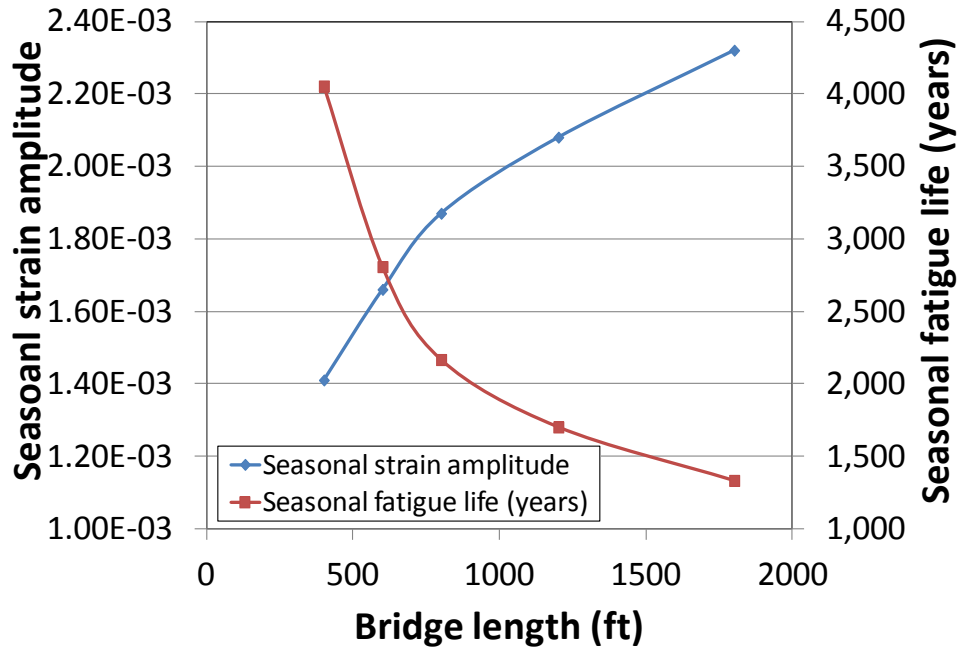
Figure 8-7: Total strain amplitude and fatigue life for seasonal temperature cycles versus bridge length.

Chapter 9. Crack initiation and propagation in piles

Figure **9-1** shows the contour plot of von-Mises stress at maximum and minimum daily temperatures. One daily temperature cycle has also been shown in this Figure 9-1(c). The stresses are higher in the part of the pile that is within the soil. A sharp change in the stress values is observed as the pile exits the abutment and enters the soil. Furthermore, the amplitude of stress is maximum at the elements right below the abutment at the tip of the flange of the pile. This indicates that the crack initiates from this point. The crack initiation site is shown in Figure 9-1 and Figure 9-2. This point has the maximum stress amplitude. The maximum stress at this point is about 41,000 psi, which occurs at the maximum daily temperature at time step 6, and the minimum stress, which occurs at the minimum temperature at step 18 is around 2,000 psi. This results in stress amplitude of 19,500 psi. There is another site located diagonally across the crack initiation site (indicated by a secondary crack initiation site in Figure 9-1 and Figure 9-2, which is also likely to have a crack soon after a crack initiates at the first location.
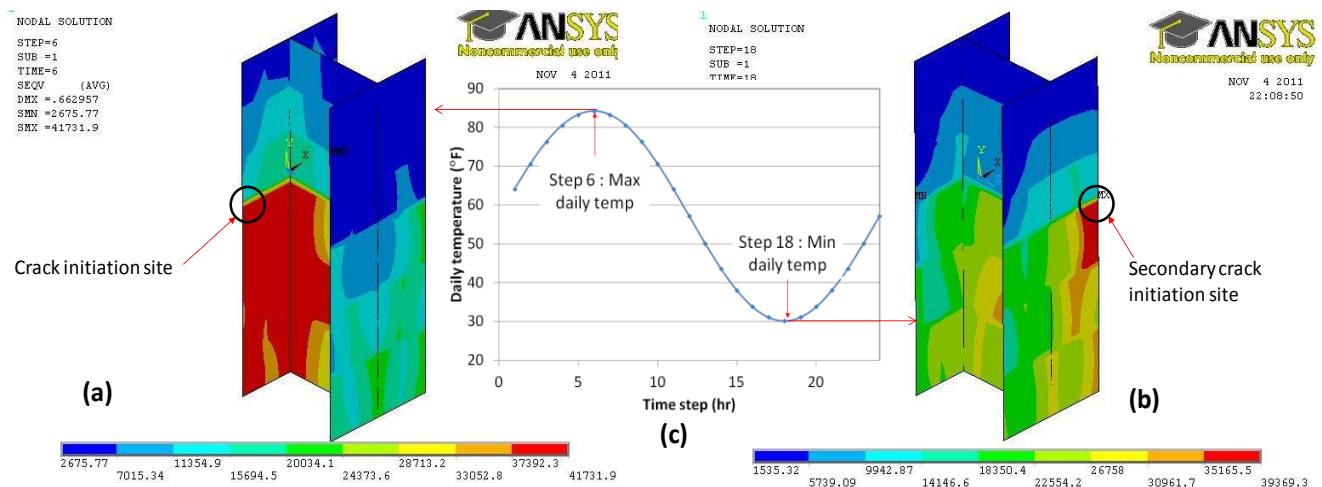
Figure 9-1: Illustration of cyclic stress amplitude, (a) contour plot of von-Mises stress at

maximum daily temperature, (b) contour plot of von-Mises stress at minimum daily

temperature, (c) one daily temperature cycle.
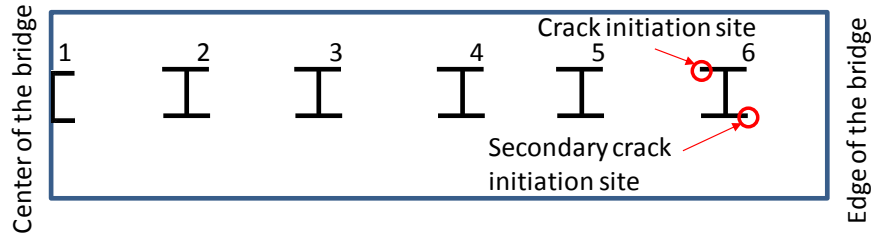
Figure 9-2: Crack initiation site shown in pile 6.

The contour plots of von-Mises stress at maximum and minimum daily temperatures are shown in Figure 9-3. As the elements are "killed" in the initiation site, their load bearing is reduced to zero and therefore these elements bear no stress. As discussed earlier, the continuation and propagation of the crack depends on the stress and strain amplitude. This amplitude is maximum in the vicinity of the crack tip and therefore the crack continues to grow towards the web of the pile.

Figure 9-3: Contour plot of von-Mises stress at the time of crack initiation (a) maximum daily temperature, (b) minimum daily temperature. Inset images in each part show the enlarged crack initiation zone.

Cracked area is plotted against the number of cycles in Figure 9-4. The crack initiates at the tip of the flange and propagates towards the web until it is well into the web of the pile. The algorithm shown and explained in Section 6.5. is implemented in ANSYS using a code written in APDL language such that at each run of FE, five elements are "killed". This is because there is a tradeoff between the accuracy of the crack path and predicted life by "killing" a smaller number of elements and the number of runs of FE. Clearly more runs of FE are required to propagate a crack to the same extent if a lower number of elements are killed in each step. However, this means longer computation time and more memory space. In this case, the program was conducted first for "killing" one element at a time, but this was found to exceed the available computational resources. Therefore, the program was adjusted to "kill" five elements at each step of the process. The program continued for 200 successive runs and total of 1000 elements were "killed". The program was stopped at the 200th run due to limited computational space.
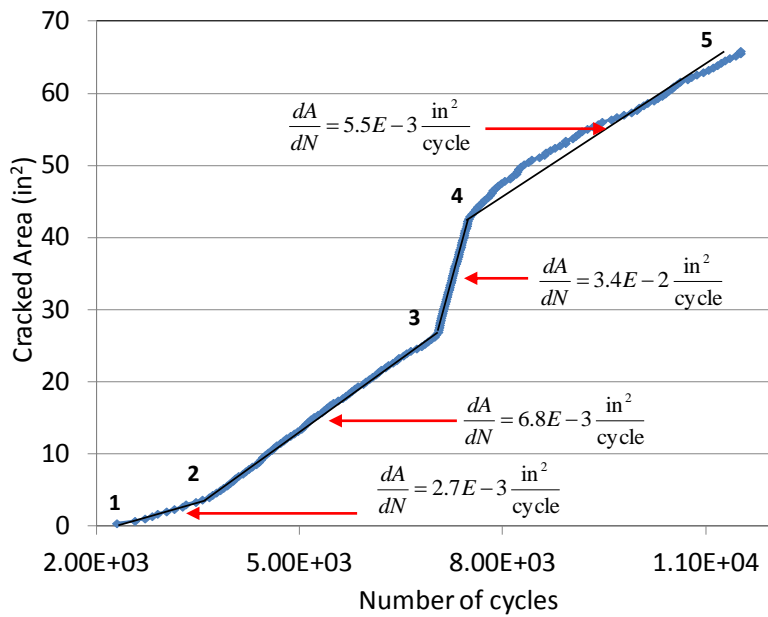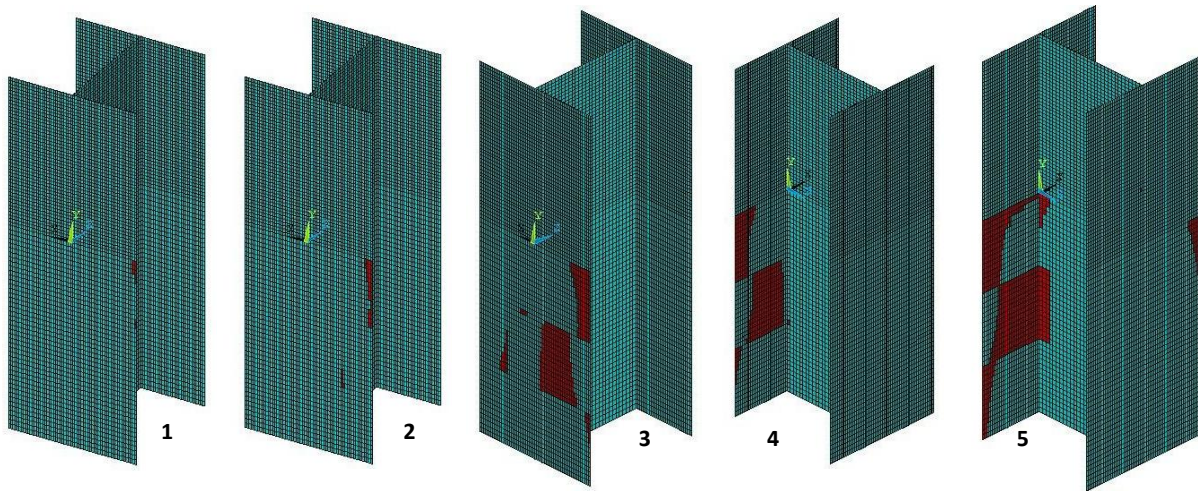
Figure 9-4: Crack propagation area versus the number of cycles.

The cracked area in Figure 9-4 is obtained by multiplying the number of "killed" elements by the area of a single element. The crack propagation rate is obtained by obtaining the slope of the curve. Several stages are identified based on the crack propagation rate. These stages, associated propagation rate and FE images associated with each stage (showing the crack at the start of each stage) are shown in this figure. The crack initiates after 2,300 cycles of daily loads, which

corresponds to 6.5 years. It initially propagates through the flange with a rate of 2.7 E-3 in^2/cycle. At point 2, another crack starts in the flange and the total propagation rate increases more than twice to 6.8 E-3 in^2/cycle. The crack propagation rate increase five times at point 3, to 3.4 E-2 in^2/cycle as several other cracks initiate. At cycle number 7,475, which corresponds to 20 year of life, cracks reach the web of the pile. This is shown by point 4 in this figure. As soon as the cracks reach the web, however, the propagation rate decreases to 5.5 E-3 in^2/cycle. This indicates that the flange may be less fatigue resistant. The number of cycles at which the program was stopped was 11,518 cycles, which corresponds to 31.5 years. This indicates that in this particular case, the crack may initiate within the first decade, but may not propagate through the whole pile section for several decades.
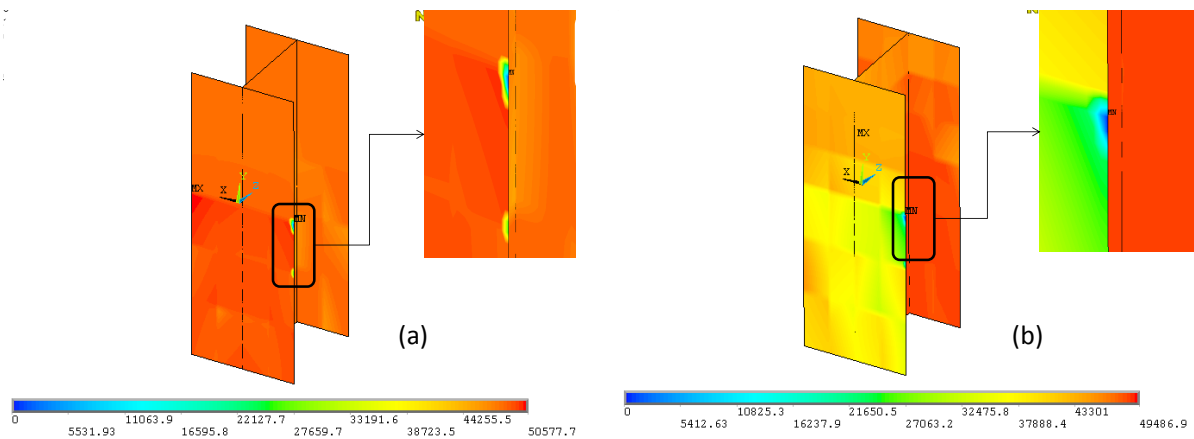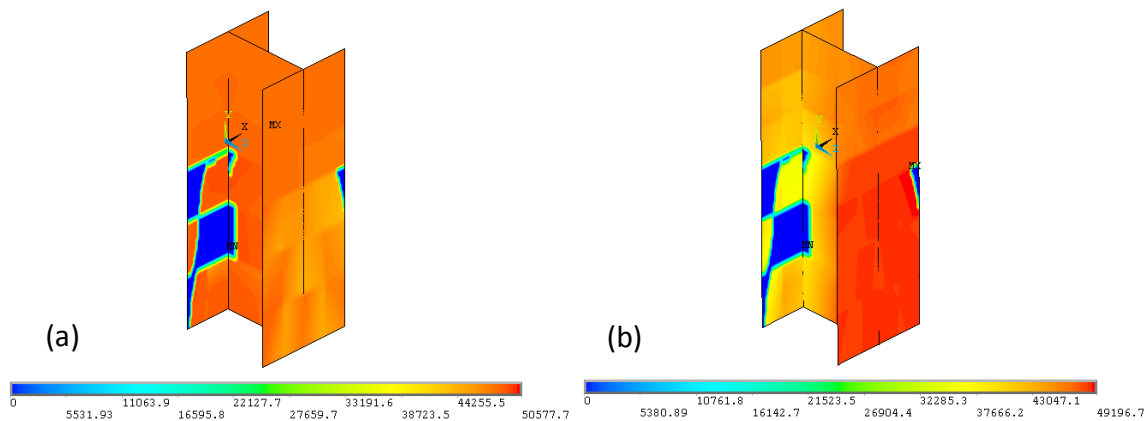

Figure 9-5: Contour plot of von-Mises stress at the end of crack propagation, (a) maximum daily temperature, (b) minimum daily temperature, Inset images in each part show the enlarged crack initiation zone.

Figure 9-5 shows the contour plot of von-Mises stress at the end of the simulation when the crack reaches the web at maximum and minimum daily temperatures. The cracked regions are unable to bear any loads and therefore show zero stress. This figure clearly shows that a crack

has also initiated from the secondary crack initiation site as well.

Several factors may affect these results, including the length of the bridge and orientation of the pile. A parametric study conducted for the global model showed that as the length of the bridge increases the displacement in the piles increases. This could result in larger stress and strain amplitudes that result in shorter fatigue life. Therefore, in longer bridges these rates may increase and in shorter bridges it is expected that these rates decrease. It was shown that the fatigue life is longer in piles oriented around their strong axis [16]. Therefore, if the orientation of piles changes to a weak axis, these rates are expected to increase. The location of crack initiation and propagation path may also change in this case. Crack initiation points and the propagation paths are shown in Figure 9-6. All the cracks start in the part of the pile below the abutment. Most of them start in flange 1. Only one crack, C6, starts in the web of the pile. After the cracks in flange 1 reach the web, cracks start in flange 2 (the secondary crack initiation site shown in Figure 9-1 and Figure 9-2. Cracks mostly develop more towards the web of the pile.
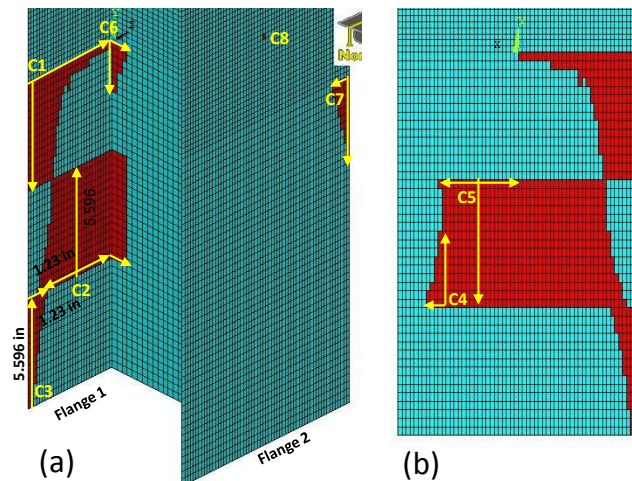
Figure 9-6: Crack initiation sites and propagation paths, (a) isometric view of the pile, (b) back view of the pile.

Chapter 10. Conclusion and summary

Non linear three-dimensional finite element analysis of the bridge superstructure and substructure under the cyclic thermal loading, due to seasonal and daily temperature variations was conducted. A global-local modeling strategy in conjunction with "successive initiation" was used to determine the fatigue crack location, initiation time, and propagation path and propagation rate. The analysis reveals several important points in this structure as follows:

- Plastic strain is observed underneath the abutment in the flange of the pile in both daily and seasonal temperature cycles for bridges with lengths of 400 ft and longer. This indicates the possibility of yielding and low cycle fatigue failure in the case study presented here.

- Low cycle fatigue can start with a small crack at the tip of the flange. The small cracks will then propagate towards the web of the pile. As a crack propagates under further cyclic loads, the load-bearing area of the pile decreases. This results in higher stresses at the tip of the crack and faster propagation rates. The crack at this point acts as a plastic hinge. Eventually this crack will result in failure of the pile.

- The thermal displacement of the piles and plastic deformation in them increase linearly as the length increases. Observation of plastic deformation indicates the possibility of low cycle fatigue.

- Pile displacement in summer and during the high temperature time of the day behaves non-monotonically with respect to the depth. Thermal variations add some more displacement in addition to the existing displacement. Pile displacement in winter and during the low temperature time of the night is mostly monotonic. This occurs mainly

because the deformation due to dead and live loads and temperature variations are in the same direction.

- Fatigue life was found to be about 42 years in a 400 foot long bridge and the decreases to 9.5 years in a 1,800 foot long bridge.

- When the length of the bridge increases, the total strain amplitude increases, which results in an exponential reduction of fatigue life.

- Plastic strain was observed in a bridge as short as 400 ft. The strain amplitude due to seasonal temperature variations was found to be much larger than the strain amplitude due to daily temperature variations. As a result, the seasonal fatigue life was found to be much smaller than daily fatigue life.

- Because the frequency of the daily cycles are much larger, the dominant case of fatigue failure is found to be the daily temperature cycles.

- The Palmgren-Miner rule was used to find the combination effect of daily and seasonal cycles. It was concluded that the contribution of seasonal cycles is negligible.

- The crack simulation showed that the fatigue crack may initiate in the first decade of the bridge life.

- The crack is more likely to initiate below the abutment and in the flange of the pile.

- More than one crack could initiate at a time and the rate of crack propagation may change as more cracks initiate in the flange.

- The crack propagation rate reduced as it reached the web of the pile.

- Even though cracks may start in the first decade, they may not propagate long enough to cause the pile to fail until several decades later.

- Even if the crack resulted in the failure of a single pile it may not result in the failure of the whole bridge.

- These results were applicable for the case studied and would vary if any of the materials, geometry, or loading changed. It is expected that a crack will propagate slower in shorter bridges and faster in longer bridges. But this can only be verified through further analysis of different cases.

Chapter 11. Contributions and future work

11.1. Contributions

Contributions of this dissertation include:

- Knowledge and insight on lateral deformation of piles in IABs and the stress and strain distribution in the piles.

- Finite element codes can be generalized to any bridge with different materials and different lengths.

- Determination of the type of deformation (plastic vs. elastic) in piles and understanding the effect of length on the amount of deformation.

- Determination of the critical pile in the pile group and critical location in that pile that is more prone to fatigue damage cracks and failure.

- Understanding the effect of bridge length on stress and strain distribution due to thermal load in the steel piles.

- Estimating fatigue life of piles in IABs under thermo-mechanical cyclic loads.

- Determining the effect of length on the thermo-mechanical fatigue life of the piles in IABs.

- Understanding the contribution of daily and seasonal temperature variations on fatigue life of the IABs.

- Knowledge of the significance of fatigue damage for IABs with lengths greater than conventional lengths.

- A guideline for fatigue analysis of the piles in IABs that can be used for new designs or

existing bridges.

- Insights on the mechanics of fatigue crack initiation and propagation.

- Knowledge of crack initiation location, crack propagation path and rate.

- A continuum damage modeling methodology used for the first time in piles of IABs to determine the crack location, path and rate. This methodology can easily be generalized to determine the fatigue crack damage for any part of the bridge that experiences cyclic loading and fatigue.

This study was conducted for a specific case of an IAB located in the harsh climate of the Wasatch Mountains. Nevertheless, some of the findings can be easily applied to other cases of IABs.

11.2. Future work

This study was specific to the steel H piles. However, many bridges are built using concrete piles or new types of composite materials. The methodology presented in this study can easily be applied to determine fatigue resistance and fatigue life of other types of piles or different pile materials.

One may also conduct the analysis for different climates. Clearly, milder climates will result in longer fatigue life and harsher climates will result in a shorter fatigue life. This analysis was conducted for a stiff clay soil type. The results of past experiments [2] show that stiffer soil causes larger loads on the piles that could result in shorter fatigue life. It is expected that soft clay and sand would increase the fatigue life. However, this has not been systematically studied. This could be a good research topic for future work.

The fatigue modeling and crack propagation methodology proposed in this study can be used for any part of the bridge that experiences cyclic loading. Therefore, there are many more potential applications for which this methodology can be implemented.

Appendix A: Ansys APDL

! An representative ansys commands used for the analysis.

/prep7

ET,1, SHELL181

ET,2, BEAM188

ET,3, SOLID185

ET,4, MPC184,1,1

L=400   !half of the bridge in ft

!MATERIAL PROPERTIES OF CONCRETE

!MPTEMP,1,298

MP, EX, 1, 3.6E6 ! psi elastic modulus Concrete slab

MP, ALPX, 1, 10E-6   !coefficient of thermal expansion /c

MP, DENS, 1, 0.063   !density lb/in3

MP,NUXY,3,0.2   !poissons ratio

!MPTEMP,1,298

!MATERIAL PROPERTIES OF STEEL

MP, EX, 2, 29E6 ! psi Steel girder, pile, bracing

MP, ALPX, 2, 12.6E-6   !/C

MP, DENS, 2, 0.28   !lb/in3

MP,NUXY,2,0.29

E2=29E6

TB,MISO,2,, , ,

TBTEMP,298,1   !Temperature 1

TBMODIF,1,1,0.001344

TBMODIF,1,2,E2*0.001344

TBMODIF,2,1,0.00241

TBMODIF,2,2,40000

TBMODIF,3,1,0.002744

TBMODIF,3,2,40909

TBMODIF,4,1,0.003115

TBMODIF,4,2,41818

TBMODIF,5,1,0.007054

TBMODIF,5,2,48181

TBMODIF,6,1,0.01443

TBMODIF,6,2,54545

TBMODIF,7,1,0.017436

TBMODIF,7,2,56363

TBMODIF,8,1,0.02501

TBMODIF,8,2,60000

 !Material properties for sand

!MPTEMP,1,298

MP, EX, 3, ! Loose sand

MP,NUXY,3,0.27

MP, DENS, 3, 9.893E-4

!TB,DP,3

!TBDATA,1,0,30,0   ! Cohesion = 0 (use consistent units),

! Angle of internal friction = 30 degrees,

! Dilatancy angle = 0 degrees

!1 megapascal = 145.037 738 01 pound/square inch

!assuming the modulus of 50 MPa

!Material properties for Clay

!MPTEMP,1,298

MP, EX,4,15555 ! Very stiff clay

MP,NUXY,4,0.27

MP, DENS, 4,0.002232   !(125/32.174)lb/ft3....convert to lb/in3

!TB, Lab, MAT, NTEMP, NPTS, TBOPT, EOSOPT, FuncName

!TB,DP,4

!TBDATA,1,13.8,25,0

!TBDATA,1,13.8,25,0   ! Stiff clay with c=2000 psf, internal angle of friction =25

! Angle of internal friction = 30 degrees,

! Dilatancy angle = 25 degrees

!Dimensions of girder

*SET,wfg , 10.545

*SET,hfg , 30.31

*SET,twg , 0.615

*SET,tfg , 1

SECTYPE, 1, shell

SECDATA, tfg,2

sectype,2,shell

secdata,twg,2

!Dimensions of h-pile

*SET,wfh , 10.075

*SET,hfh , 9.70

*SET,twh , 0.415

*SET,tfh , 0.420

SECTYPE,3, shell

SECDATA,tfh,2

SECTYPE,4, shell

SECDATA,twh,2

sectype,5, shell

secdata,7,1

!Dimensions of cross-bracing

*SET,Axb,11

*SET,Ixxb,35.5

*SET,yxb,1.86

*SET,Iyyb,Ixxb

*SET,xxb,yxb

SECTYPE, 6, beam, L, crossbracing

SECDATA,6,6,1,1

*SET,gird , 6*12 ! girder spacing

*SET,tsl , 7 !thickness of slab

*SET,extra , 2*12 !overhang

*SET,spansl , 10*12

!Keypoints for slab

K,1,-(extra+2*gird+(gird/2)),0,0

K,2,-(2*gird+(gird/2)+(wfg/2)),0,0

K,3,-(2*gird+(gird/2)+0*(wfg/2)),0,0

K,4,-(2*gird+(gird/2)-(wfg/2)),0,0

K,5,-(2*gird)-(wfg/2),0,0

K,6,-(2*gird),0,0

K,7,-(2*gird)+(wfg/2),0,0

K,8,-(gird+(gird/2)+(wfg/2)),0,0

K,9,-(gird+(gird/2)+0*(wfg/2)),0,0

K,10,-(gird+(gird/2)-(wfg/2)),0,0

K,11,-(gird)-(wfg/2),0,0

K,12,-(gird),0,0

K,13,-(gird)+(wfg/2),0,0

K,14,-(gird/2)-(wfg/2),0,0

K,15,-(gird/2)+0*(wfg/2),0,0

K,16,-(gird/2)+(wfg/2),0,0

K,17,-(wfg/2),0,0

K,18,0,0,0

K,19,(wfg/2),0,0

K,20,(gird/2)-(wfg/2),0,0

K,21,(gird/2)+0*(wfg/2),0,0

K,22,(gird/2)+(wfg/2),0,0

K,23,gird-(wfg/2),0,0

K,24,gird,0,0

K,25,gird+(wfg/2),0,0

K,26,gird+(gird/2)-(wfg/2),0,0

K,27,gird+(gird/2)+0*(wfg/2),0,0

K,28,gird+(gird/2)+(wfg/2),0,0

K,29,2*gird-(wfg/2),0,0

K,30,2*gird,0,0

K,31,2*gird+(wfg/2),0,0

K,32,2*gird+(gird/2)-(wfg/2),0,0

K,33,2*gird+(gird/2)+0*(wfg/2),0,0

K,34,2*gird+(gird/2)+(wfg/2),0,0

K,35,extra+2*gird+(gird/2),0,0

*SET,z ,-spansl

K,36,-(extra+2*gird+(gird/2)),0,z

K,37,-(2*gird+(gird/2)+(wfg/2)),0,z

K,38,-(2*gird+(gird/2)+0*(wfg/2)),0,z

K,39,-(2*gird+(gird/2)-(wfg/2)),0,z

K,40,-(2*gird)-(wfg/2),0,z

K,41,-(2*gird),0,z

K,42,-(2*gird)+(wfg/2),0,z

K,43,-(gird+(gird/2)+(wfg/2)),0,z

K,44,-(gird+(gird/2)+0*(wfg/2)),0,z

K,45,-(gird+(gird/2)-(wfg/2)),0,z

K,46,-(gird)-(wfg/2),0,z

K,47,-(gird),0,z

K,48,-(gird)+(wfg/2),0,z

K,49,-(gird/2)-(wfg/2),0,z

K,50,-(gird/2)+0*(wfg/2),0,z

K,51,-(gird/2)+(wfg/2),0,z

K,52,-(wfg/2),0,z

K,53,0,0,z

K,54,(wfg/2),0,z

K,55,(gird/2)-(wfg/2),0,z

K,56,(gird/2)+0*(wfg/2),0,z

K,57,(gird/2)+(wfg/2),0,z

K,58,gird-(wfg/2),0,z

K,59,gird,0,z

K,60,gird+(wfg/2),0,z

K,61,gird+(gird/2)-(wfg/2),0,z

K,62,gird+(gird/2)+0*(wfg/2),0,z

K,63,gird+(gird/2)+(wfg/2),0,z

K,64,2*gird-(wfg/2),0,z

K,65,2*gird,0,z

K,66,2*gird+(wfg/2),0,z

K,67,2*gird+(gird/2)-(wfg/2),0,z

K,68,2*gird+(gird/2)+0*(wfg/2),0,z

K,69,2*gird+(gird/2)+(wfg/2),0,z

K,70,extra+2*gird+(gird/2),0,z

MAT,1

!Creating the areas for the slab

*do,i,1,34,1

A,i,i+1,i+36,i+35

*enddo

!Keypoints for girders (front)

K,71,-(2*gird+gird/2)-(wfg/2),0,0

K,72,-(2*gird+gird/2)+0*(wfg/2),0,0

K,73,-(2*gird+gird/2)+(wfg/2),0,0

K,74,-(2*gird+gird/2)+0*(wfg/2),-hfg/2,0

K,75,-(2*gird+gird/2)-(wfg/2),-hfg,0

K,76,-(2*gird+gird/2)+0*(wfg/2),-hfg,0

K,77,-(2*gird+gird/2)+(wfg/2),-hfg,0

K,78,-(gird+gird/2)-(wfg/2),0,0

K,79,-(gird+gird/2)+0*(wfg/2),0,0

K,80,-(gird+gird/2)+(wfg/2),0,0

K,81,-(gird+gird/2)+0*(wfg/2),-hfg/2,0

K,82,-(gird+gird/2)-(wfg/2),-hfg,0

K,83,-(gird+gird/2)+0*(wfg/2),-hfg,0

K,84,-(gird+gird/2)+(wfg/2),-hfg,0

K,85,-(gird/2)-(wfg/2),0,0

K,86,-(gird/2)+0*(wfg/2),0,0

K,87,-(gird/2)+(wfg/2),0,0

K,88,-(gird/2)+0*(wfg/2),-hfg/2,0

K,89,-(gird/2)-(wfg/2),-hfg,0

K,90,-(gird/2)+0*(wfg/2),-hfg,0

K,91,-(gird/2)+(wfg/2),-hfg,0

K,92,gird/2-(wfg/2),0,0

K,93,gird/2+0*(wfg/2),0,0

K,94,gird/2+(wfg/2),0,0

K,95,gird/2+0*(wfg/2),-hfg/2,0

K,96,gird/2-(wfg/2),-hfg,0

K,97,gird/2+0*(wfg/2),-hfg,0

K,98,gird/2+(wfg/2),-hfg,0

K,99,gird+gird/2-(wfg/2),0,0

K,100,gird+gird/2+0*(wfg/2),0,0

K,101,gird+gird/2+(wfg/2),0,0

K,102,gird+gird/2+0*(wfg/2),-hfg/2,0

K,103,gird+gird/2-(wfg/2),-hfg,0

K,104,gird+gird/2+0*(wfg/2),-hfg,0

K,105,gird+gird/2+(wfg/2),-hfg,0

K,106,2*gird+gird/2-(wfg/2),0,0

K,107,2*gird+gird/2+0*(wfg/2),0,0

K,108,2*gird+gird/2+(wfg/2),0,0

K,109,2*gird+gird/2+0*(wfg/2),-hfg/2,0

K,110,2*gird+gird/2-(wfg/2),-hfg,0

K,111,2*gird+gird/2+0*(wfg/2),-hfg,0

K,112,2*gird+gird/2+(wfg/2),-hfg,0

!Keypoints for girders (back)

K,113,-(2*gird+gird/2)-(wfg/2),0,z

K,114,-(2*gird+gird/2)+0*(wfg/2),0,z

K,115,-(2*gird+gird/2)+(wfg/2),0,z

K,116,-(2*gird+gird/2)+0*(wfg/2),-hfg/2,z

K,117,-(2*gird+gird/2)-(wfg/2),-hfg,z

K,118,-(2*gird+gird/2)+0*(wfg/2),-hfg,z

K,119,-(2*gird+gird/2)+(wfg/2),-hfg,z

K,120,-(gird+gird/2)-(wfg/2),0,z

K,121,-(gird+gird/2)+0*(wfg/2),0,z

K,122,-(gird+gird/2)+(wfg/2),0,z

K,123,-(gird+gird/2)+0*(wfg/2),-hfg/2,z

K,124,-(gird+gird/2)-(wfg/2),-hfg,z

K,125,-(gird+gird/2)+0*(wfg/2),-hfg,z

K,126,-(gird+gird/2)+(wfg/2),-hfg,z

K,127,-(gird/2)-(wfg/2),0,z

K,128,-(gird/2)+0*(wfg/2),0,z

K,129,-(gird/2)+(wfg/2),0,z

K,130,-(gird/2)+0*(wfg/2),-hfg/2,z

K,131,-(gird/2)-(wfg/2),-hfg,z

K,132,-(gird/2)+0*(wfg/2),-hfg,z

K,133,-(gird/2)+(wfg/2),-hfg,z

K,134,gird/2-(wfg/2),0,z

K,135,gird/2+0*(wfg/2),0,z

K,136,gird/2+(wfg/2),0,z

K,137,gird/2+0*(wfg/2),-hfg/2,z

K,138,gird/2-(wfg/2),-hfg,z

K,139,gird/2+0*(wfg/2),-hfg,z

K,140,gird/2+(wfg/2),-hfg,z

K,141,gird+gird/2-(wfg/2),0,z

K,142,gird+gird/2+0*(wfg/2),0,z

K,143,gird+gird/2+(wfg/2),0,z

K,144,gird+gird/2+0*(wfg/2),-hfg/2,z

K,145,gird+gird/2-(wfg/2),-hfg,z

K,146,gird+gird/2+0*(wfg/2),-hfg,z

K,147,gird+gird/2+(wfg/2),-hfg,z

K,148,2*gird+gird/2-(wfg/2),0,z

K,149,2*gird+gird/2+0*(wfg/2),0,z

K,150,2*gird+gird/2+(wfg/2),0,z

K,151,2*gird+gird/2+0*(wfg/2),-hfg/2,z

K,152,2*gird+gird/2-(wfg/2),-hfg,z

K,153,2*gird+gird/2+0*(wfg/2),-hfg,z

K,154,2*gird+gird/2+(wfg/2),-hfg,z

MAT,2

!Creating areas of girders

*do,i,71,96,7

A,i,i+1,i+43,i+42

*enddo

*do,i,72,107,7

A,i,i+1,i+43,i+42

*enddo

*do,i,75,110,7

A,i,i+1,i+43,i+42

*enddo

*do,i,76,111,7

A,i,i+1,i+43,i+42

*enddo

*do,i,72,107,7

A,i,i+2,i+44,i+42

*enddo

*do,i,74,109,7

A,i,i+2,i+44,i+42

*enddo

A,99,100,142,141

a,106,107,149,148

! Creating cross bracing

*do,i,72,100,7

L,i,i+7,5

L,i,i+11,5

L,i+4,i+7,5

L,i+4,i+11,5

*enddo

!Properies for slab

aSEL,S,LOC,Y,0

asel,u,,,35,44

asel,u,,,69,70

AATT,1,,1,,5

ALLSEL,ALL

! properties for girders (flange)

allsel,all

asel,s,,,39,56

asel,a,,,35,38

asel,a,,,69,70

!AATT, MAT, REAL, TYPE, ESYS, SECN

AATT,2,,1,,1

!properties for girders (web,extra)

allsel,all

asel,s,,,57,68

AATT,2,,1,,2

!properties for bracings

lsel,s,,,219,220

lsel,a,,,223,224

lsel,a,,,227,228

lsel,a,,,231,232

lsel,a,,,235,236

lesize,all,,,4

LATT,2,,2,,,,6

LMESH,all

!..

 !nummrg,all

!girder lenth in abutment glib

allsel,all

glib =22.6

MAT,2

k,1600,0,0,glib

!nustr,line,2000

l,18,1600

adrag,112,126,,,,,238

adrag,188,204,,,,,238

adrag,148,170,,,,,238

!making the pile in the middle of bridge

numstr,kp,2000

k,,0,-hfg,22.6

k,,0,-hfg,12.9

k,,5.2725,-hfg,22.6

k,,5.2725,-hfg,12.9

k,,-5.2725,-hfg,22.6

k,,-5.2725,-hfg,12.9

l,2002,2000

l,2000,2004

l,2000,2001

l,2001,2003

l,2001,2005

!entering the key points for the end of the pile

k,,-5.2725,-91.31,12.9

l,2005,2006

!creating the pile inside the abutment

adrag,257,258,,,,,259

adrag,256,255,,,,,259

adrag,254,,,,,,259

!creating the end point for the pile

numstr,kp,2010

k,,-5.2725,-522.31,12.9

!nummrg,all

l,2009,2015

!lsel,s,,,260,263,3

!lsel,a,,,265,268,3

!lsel,a,,,270

adrag,263,,,,,,273

adrag,265,268,,,,,273

adrag,260,,,,,,273

adrag,270,,,,,,273

!nummrg,all

!creating pile distance 36 under the girdir

pd=36

asel,s,,,77,86

agen,2,all,,,-pd

!nummrg,all

!allsel,all

numcmp,all

```
KWPAVE,191

asel,s,,,71,76

asbw,all

allsel,all

!nummrg,all

!properties of the girdirs flang

asel,s,,,97,100

asel,a,,,103,104

asel,a,,,107,108

AATT,2,,1,,1

!properties of the girdires web

asel,s,,,101,102

asel,a,,,105,106

AATT,2,,1,,2

!properties of the piles, mat 2,mesh types 1, real 5

asel,s,,,77,96

!AATT, MAT, REAL, TYPE, ESYS, SECN

aatt,2,,1,,3

!.............................................................

!staring to assign segments to lines for mesh

!Mesh areas and lines so far

!slab span length divided to 15

LSEL,s,line,,6,99,3

lsel,a,,,2,6,4

LESIZE,all,,,15

!assign line size to the small areas of the slab
```

lsel,s,,,5,7,2

lsel,a,,,8,10,2

LSEL,a,line,,14,16,2

LSEL,a,line,,17,19,2

LSEL,a,line,,23,25,2

LSEl,a,line,,26,28,2

lsel,a,,,32,34,2

lsel,a,,,35,37,2

lsel,a,,,41,43,2

lsel,a,,,44,46,2

lsel,a,,,50,52,2

lsel,a,,,53,55,2

lsel,a,,,59,61,2

lsel,a,,,62,64,2

lsel,a,,,68,70,2

lsel,a,,,71,73,2

lsel,a,,,77,79,2

lsel,a,,,80,82,2

lsel,a,,,86,88,2

lsel,a,,,89,91,2

LESIZE,all,,,2

!assign line size to the large areas of slab

LSEL,s,line,,1,3,2

LSEL,a,line,,11,13,2

LSEL,a,line,,20,22,2

LSEL,a,line,,29,31,2

LSEl,a,line,,38,40,2

lsel,a,,,47,49,2

lsel,a,,,56,58,2

lsel,a,,,65,67,2

lsel,a,,,74,76,2

lsel,a,,,83,85,2

lsel,a,,,92,94,2

lsel,a,,,101,103,2

LESIZE,all,,,3

lsel,s,,,102

lsel,a,,,4

lesize,all,,,15

!assign line segments to the girdirs

lsel,s,,,105,121,2

lsel,a,,,124,133,3

lsel,a,,,135,165,2

lsel,a,,,168,198,3

lsel,a,,,214,217,3

lsel,a,,,4

lsel,a,,,102

LESIZE,all,,,15

lsel,s,,,140,166,2

lsel,a,,,167,169,2

lsel,a,,,170,172,2

lsel,a,,,173,175,2

lsel,a,,,176,178,2

lsel,a,,,179,181,2

lsel,a,,,182,184,2

lsel,a,,,185

lsel,a,,,187,188

lsel,a,,,190,191

lsel,a,,,193,194

lsel,a,,,196

lsel,a,,,197,199,2

lsel,a,,,210,211

lsel,a,,,200,209

lsel,a,,,241,243,2

lsel,a,,,104,122,2

lsel,a,,,123,125,2

lsel,a,,,126,128,2

lsel,a,,,129,131,2

lsel,a,,,132,138,2

lsel,a,,,212,213

lsel,a,,,215,216

lsel,a,,,239,242,3

lsel,a,,,244,247,3

lsel,a,,,249,252,3

lsel,a,,,254,258

lsel,a,,,260,263,3

lsel,a,,,265

lsel,a,,,268,270,2

lsel,a,,,274,277,3

lsel,a,,,280,282,2

lsel,a,,,285,288,3

lsel,a,,,290,294,2

lsel,a,,,295,299,2

lsel,a,,,301,302

lsel,a,,,304,313,3

lsel,a,,,315,318,3

lsel,a,,,320,324

lsel,a,,,325,331

lsel,a,,,332,339

lsel,a,,,340,343

lsel,a,,,95,97,2

lsel,a,,,98,100,2

lsel,a,,,136,138,2

lsel,a,,,215,216

lesize,all,,,2

!dividing the lines of piles so that I wont get irregular mesh

lsel,s,,,259,261,2

lsel,a,,,262,266,2

lsel,a,,,267,271,2

lsel,a,,,272

lsel,a,,,289,293,2

lsel,a,,,296,300,2

lsel,a,,,303,305,2

lesize, all,,,15

lsel,s,,,273,275,2

```
lsel,a,,,276,278,2

lsel,a,,,279,283,2

lsel,a,,,284,286,2

lsel,a,,,287

lsel,a,,,306,308,2

lsel,a,,,309,311,2

lsel,a,,,312,316,2

lsel,a,,,317,319,2

lesize,all,,,77

!copying the girdirs, slab and cross brasings

!esla,s

!esll,a

!cm,slab,elem

z=-120

!define the length of the bridge. L=120*(i+1). Define i. i=29 represents L=300 ft

*do,i,1,9,1

allsel,all

asel,s,,,1,70

AGEN,2,all,,,0,0,i*z

lsel,s,,,219,220

lsel,a,,,223,224

lsel,a,,,227,228

lsel,a,,,231,232

lsel,a,,,235,236

LGEN,2,all,,,0,0,i*z

*enddo
```

```
ALLSEL,all

AMESH,all

nummrg,kp

WPAVE,0,0,0

CSYS,0

!.................................................

!NEED TO CREATE THE ABUTMENT NOW

Mat,1

allsel,all

asel,s,,,101,102

asel,a,,,105,106

asel,a,,,89

vdrag,all,,,,,,170

nummrg,kp

Mat,1

asel,s,,,737,742,5

asel,a,,,746,750,4

asel,a,,,753

aatt,1,1,1

vdrag,all,,,,,,47

nummrg,kp

Mat,1

asel,s,,,758

asel,a,,,763,767,4

asel,a,,,771,774,3

aatt,1,1,1
```

vdrag,all,,,,,,258

nummrg,kp

Mat,1

asel,s,,,79

asel,a,,,784,788,4

asel,a,,,792,795,3

vdrag,all,,,,,,257

nummeg,kp

Mat,1

allsel,all

asel,s,,,800,805,5

asel,a,,,809,813,4

asel,a,,,816

aatt,1,1,1

vdrag,all,,,,,,56

nummeg,kp

mat,1

asel,s,,,89

asel,a,,,101,102

asel,a,,,105,106

vdrag,all,,,,,,239

nummrg,kp

mat,1

asel,s,,,77,78

asel,a,,,87,88

asel,a,,,757

asel,a,,,820

vdrag,all,,,,,,325

nummrg,kp

k,,0,0,36

lstr,164,1811

mat,1

asel,s,,,80,81

asel,a,,,90,91

vdrag,all,,,,,,2592

!nummrg,kp

asel,s,,,832,836,4

asel,a,,,818

vdrag,all,,,,,,2602

asel,s,,,811,815,4

asel,a,,,790,794,4

vdrag,all,,,,,,2602

asel,s,,,755

asel,a,,,769,773,4

vdrag,all,,,,,,2602

asel,s,,,748,752,4

asel,a,,,853,857,4

vdrag,all,,,,,,2602

!...

asel,s,,,847,851,4

asel,a,,,842

asel,a,,,855,858,3

```
asel,a,,,863,867,4

asel,a,,,872,876,4

asel,a,,,891,896,5

asel,a,,,901,906,5

aatt,1,1,1

!------------------------............//////////////////////

!This is the end of creation of one part of abutment that needs to be copied and pasted several times

!copying the elements of abutment and pile and making the rest of the piles

gd=72

*do,i,1,3,1

asel,s,,,77,108

agen,2,all,,,i*gd

*enddo

*do,i,1,3,1

vsel,s,,,1,54

vgen,2,all,,,i*gd

*enddo

*do,i,1,2,1

asel,s,,,77,108

agen,2,all,,,-i*gd

*enddo

*do,i,1,2,1

vsel,s,,,1,54

vgen,2,all,,,-i*gd

*enddo

vsel,s,,,168,187
```

vsel,a,,,193,194

vsel,a,,,197,200

vsel,a,,,203,212

vclear,all

vdele,all,,,1

asel,s,,,1031,1040

asel,a,,,1631

asel,a,,,1695

asel,a,,,1700

asel,a,,,1727,1733,6

aclear,all

adele,all,,,1

asel,s,,,1564,1570,6

asel,a,,,1575,1580,5

asel,a,,,1584

asel,a,,,1705

asel,a,,,1744

asel,a,,,1793

asel,a,,,1797

vdrag,all,,,,,,101

asel,s,,,2234,2239,5

asel,a,,,2243,2247,4

asel,a,,,2250

asel,a,,,2269

asel,a,,,2296

asel,a,,,2361,2364,3

vdrag,all,,,,,,1

!soil modeling

mat,4

asel,s,loc,y,-91.31

vdrag,all,,,,,,308

k,10000,0,0,84

lstr,1811,10000

mat,4

lesize,3170,,,5

asel,s,loc,z,36

vdrag,all,,,,,,5561

mat,4

vsel,s,mat,,4

asel,s,ext

asel,r,loc,z,0

vdrag,all,,,,,,102

nummrg,all

allsel,all

LSEL,S,TYPE,,2

LCLEAR,ALL

LATT,2,,2,,,,6

LMESH,all

NSL=L/10

*DO,J,10,NSL-1,1

asel,s,,,1,70

```
AGEN,2,all,,,0,0,j*z

lsel,s,,,219,220

lsel,a,,,223,224

lsel,a,,,227,228

lsel,a,,,231,232

lsel,a,,,235,236

LGEN,2,all,,,0,0,j*z

*enddo

!b.c.

ALLSEL,ALL

!asel,s,loc,z,84

!asel,a,loc,z,-120

!da,all,UX,0

!da,all,UY,0

!da,all,UZ,0

LSEL,S,LOC,Y,-522.31

DL,ALL,,Uy,0

DL,ALL,,Uz,0

allsel,all

lsel,s,loc,z,-L*12

dl,all,,uz,0

allsel,all

ACEL,0,32.174,0

VSEL,S,LOC,X,-0.01,-300

vclear,all

VDELE,ALL
```

```
ASEL,S,LOC,X,-0.01,-300

aclear,all

ADELE,ALL

LSEL,S,LOC,X,0,-300

LCLEAR,ALL

LDELE,ALL

ESEL,S,CENT,X,0,-300

EDELE,ALL

nsel,s,loc,x,0,-300

ndele,all

ASEL,S,LOC,X,0

DA,ALL,ux,0

LSEL,S,LOC,X,0

DL,ALL,,ux,0

ALLSEL,ALL

L1=L*12-20

NS=(L*12)/400

nsel,s,loc,z,-L1,-L*12

*do,j,1,NS-1,1

NS1=j*400-20

nsel,a,loc,z,-NS1,-j*400

*ENDDO

nummrg,all

d,all,uy,0

allsel,all

SELTOL,1E-6
```

nsel,s,loc,z,-L*12,-L*12

nsel,r,loc,x,0

nsel,r,loc,y,0

d,all,all,0

allsel,all

nummrg,all

Bibliography

1. Stephens, R.I. and Fatemi, R.A. *Metal Fatigue in Engineering, 2nd* second edition, John Wiley and Sons, Inc. p. 33, 2001.

2. Arsoy, S. "Experimental and Analytical Investigations of Piles and Abutments of Integral Bridges," PhD Dissertation, Virginia Institute of Technology Blacksburg, VA, pp. 161-163, 2000.

3. Hallmark, R. "Low-cycle Fatigue of Steel Piles in Integral Abutment Bridges," Thesis, Department of Civil and Environmental Engineering, Division of Structural Engineering, Luleå University of Technology, Swiss, p. 15, 2006.

4. Wiss, J. "Synthesis of Technical Information for Jointless Bridge Construction," Technical Report, Elstner Associates, Inc., State of Vermont Agency of Transportation, pp. 25-36, June 2002.

5. AASHTO, "A Standard Specifications for Highway Bridges," 16th edition, American Association of State Highway and Transportation Officials, Washington, DC, p. 677, 1996.

6. Peter, M. "Reducing Brittle and Fatigue Failures in Steel Structures," ASCE Publications, Technology & Engineering, Reston, VA, pp. 1-38, 2010.

7. White, H. "Integral Abutment Bridges: Comparison of Current Practice Between European Countries and the United States of America," Special Report 152, Transportation, Research and Development Bureau, New York State Department of Transportation, p. ii, 2007.

8. New York State Department of Transportation. "Bridge Manual, 3rd Edition," New York, 2005.

9. Burke, M.P., "Integral Bridges," Transportation Research Record 1275, Transportation

Research Board, National Research Council, Washington, DC, pp. 53-61, 1990.

10. Husain, I. and Bagnariol, D. "Design and Performance of Jointless Bridges in Ontario," Transportation Research Record, Transportation Research Board, National Research Council, Washington, DC, pp. 109-121, 2000.

11. Amde, M., Wolde, T., Greimann, L. and Yang, P.S. "End-Bearing Pile in Jointless Bridges," Journal of Structural Engineering, ASCE, Vol. 114, No. 8, pp. 1870-1884, 1988.

12. Soltani, A. and Kukreti, A.R. "Performance Evaluation of Integral Abutment Bridges," Transportation Research Record 1371, Transportation Research Board, National Research Council, Washington, DC, pp. 17-25, 1992.

13. Amde, A. M., Klinger, J.E. and White, E.J. "Performance of Jointless Bridges," Journal of Performance of Construction Facilities, ASCE, Vol. 2, No. 2, pp. 111-125, 1988.

14. Maruri, R.F. and Petro, S.H. "Integral Abutments and Jointless Bridges Survey Summary," FHWA Conference on Integral Abutments and Jointless Bridges, Baltimore, MD, March 16-18, pp. 12-29, 2005.

15. Idaho Transportation Department "Design Guidelines for Integral Abutment," Article 11.6.1.3, pp.1-5, 2008.

16. Dicleli, M. and Albhaisi, S.M. "Maximum Length of Integral Bridges Supported on Steel H-Piles Driven in Sand," Engineering Structures, Vol. 25, pp. 1491–1504, 2003.

17. Abendroth, R.E. and Greimann, L.F. "Field Testing of Integral Abutments," Iowa DOT Project HR-399, Iowa State University and Iowa Department of Transportation, Ames, IA, 2005.

18. Connal, J. "Integral Abutment Bridges Australian and US Practice," Austroads 5th

Bridge Conference, Hobart, Australia, pp. 19-21, May 2004.

19. Huckabee, P. "Plastic Design of Steel HP-Piles for Integral Abutment Bridges," FHWA Conference, Integral Abutment and Jointless Bridges, Baltimore, MD, pp. 270-280, March 2005.

20. Conboy, D. and Stoothoff, E. "Integral Abutment Design and Construction: The New England Experience," The 2005 FHWA Conference, Integral Abutment and Jointless Bridges, Baltimore, MD, pp. 50-60, March 2005.

21. Yannotti, A. Alampalli, S. and White, H. "Experience with Integral Abutment Bridges," New York State Department of Transportation, FHWA Conference, Integral Abutment and Jointless Bridges, Baltimore, MD, pp. 41-49, March 2005.

22. Weakley, K. "VDOT Integral Bridge Design Guidelines," FHWA Conference, Integral Abutment and Jointless Bridges, Baltimore, MD, pp. 61-70, 2005.

23. Huang, J., French, C. and Shield, C. "Behavior of Concrete Integral Abutment Bridges," Final Report, Minnesota Department of Transportation, Research Service Section, St. Paul, MN, 2004.

24. Dicleli, M. and Albhaisi, S. "Effect of cyclic thermal loading on the performance of steel H piles in integral bridges with stub abutments," Journal of Constructional Steel Research, Vol. 60, pp. 161-182, 2004.

25. Thanasattayawibul, N. "Curved Integral Abutment Bridges," PhD Dissertation, Civil and Environmental Engineering, University of Maryland, College Park, MD, pp. 72-81, 2006.

26. Wolde, T., Amde, M.M. and Klinger, J.E. "The State of the-Art in Integral Abutment Bridge Design and Construction," AW087- 313-046, FHWA/MD-87/04, pp. 12-28, 1987.

27. Wolde, T., Amde, M.M. and Greimann, L.F. "General Design Details for Integral

Abutment Bridges," Journal of Civil Engineering Practice, BSCE/ASCE, ISSN: 0886-9685, Vol. 3, No. 2, pp. 7-20, 1988.

28. MSL Engineering Limited for the Health and Safety Executive. "A Study of Pile Fatigue During Driving and In-Service and of Pile Tip Integrity," Offshore Technology Report, UK, pp. 4-21, 2001.

29. Dunker, K.F. and Abu Hawash, A. "Expanding the Use of Integral Abutments in Iowa," Proceedings of the 2005 Mid-Continent Transportation Research Symposium, Ames, IA, pp. 4-13, August 2005.

30. US Department of Transportation, Federal Highway Administration. "Allowable Stresses in Piles," Final Report, pp.15-25, 1983.

31. Jorgensen, J.L. "Behavior of Abutment Piles in an Integral Abutment in Response to Bridge Movements," Transportation Research Board, National Academy of Sciences, No. 903, pp. 72-79, 1983.

32. Girton, D.D., Hawkinson, T.R. and Greimann, L.F. "Validation of Design Recommendations for Integral Abutment Piles," Journal of Structural Engineering, ASCE, Vol. 117, No. 7, pp. 2117-2134, July 1991.

33. Hoppe, E.J. and Gomez, J.P. "Field Study of an Integral Backwall Bridge," Virginia Transportation Research Council, VTRC 97-R7, p. 47, October 1996.

34. Lawver, A., French, C. and Shield, C.K. "Field Performance of Integral Abutment Bridge." Transportation Research Record 1740, Transportation Research Board, National Research Council, Washington, DC, pp. 108-117, 2000.

35. Alizadeh, M. and Davisson, M.T. "Lateral Load Tests on Piles Arkansas River Project," Journal of the Soil Mechanics and Foundations Division, ASCE, Vol. 96, No. SM 5,

Proc. Paper 7510, pp. 1583-1603, September 1970.

36. Matlock, H., Ingram, W.B., Kelley, A.E. and Bogard, D. "Field Tests of the Lateral Load Behavior of Pile Groups in Soft Clay," Proceedings, Offshore Technology Conference, Houston, TX, Vol. IV, Paper No. 3871, pp. 163-174, May 1980.

37. Meimon, Y., Baguelin, F. and Jezequel, J.F. "Pile Group Behavior Under Long Time Lateral Monotonic and Cyclic Loading," Proceedings, Third International Conference, Numerical Methods in Offshore Piling, Nantes, US, pp. 285-302, May 1986.

38. Brown, D.A., Reese, L.C. and O'Neill, M.W. "Cyclic Lateral Loading of a Large Scale Pile Group, " Journal of Geotechnical Engineering, ASCE, Vol. 113, No. 11, pp. 1326-1343, November, 1987.

39. Greimann, L.F., Abendtroth, R.E., Johnson, D.E. and Ebner, P.B. "Pile Design and Tests for Integral Abutment Bridges," Final Report, Iowa Department of Transportation, Project HR-273, Ames, Iowa, pp. 12-16, 1987.

40. Brown, D.A., Morisson, C. and Reese, L.C. "Lateral Load Behavior of Pile Group in Sand," Journal of Geotechnical Engineering, ASCE, Vol. 114, No. 11, pp. 1261-1276, November 1988.

41. Rice, J.R. "A Path Independent Integral and the Approximate Analysis of Strain Concentration for Notches and Cracks," Journal of Applied Mechanics, Vol. 35, pp. 379-386, 1968.

42. Wells, A.A. "Application of Fracture Mechanics At and Beyond General Yielding," British Welding Journal, Vol. 10, pp 563-570, 1963.

43. Kanvinde, A.M. and Deierlein, G.G. "Continuum Based Micro Models for Ultra Low Cycle Fatigue Crack Initiation in Steel Structures," Proceedings, ASCE Structures

Congress and Exposition, New York, NY, doi: 10.1061/40753(171), p. 192, 2005.

44. Kachanov, LM. *Introduction to Continuum Damage Mechanics.* Netherlands, Dordrecht, Martin Nijhoff Publishers, pp.10-21, 1986.

45. Rabotnov, Y. "Creep Rupture," In: Hetenyi M., Vincenti W., Editors. *Applied Mechanics.* Proceedings of the 12th International Congress of Applied Mechanics, Stanford. Springer-Verlag, Berlin, Germany, pp. 342–349, August 1968.

46. Chaboche, J. and Lesne, P.A. "Non-Linear Continuous Fatigue Damage Model," Journal Fatigue Fracture Engineering Material Structure, Vol. 1, pp. 1–17, 1988.

47. Dufailly, J. and Lemaitre J. "Modeling Very Low Cycle Fatigue," International Journal of Damage Mechanics, Vol. 4, pp. 153–170, 1995.

48. Hayhurst, D. "Creep Rupture Under Multiaxial States of Stress," Journal of Mechanics and Physic Solids, Vol. 20, pp. 381–90, 1972.

49. Cocks, A. Leckie, F. "Creep Constitutive Equations for Damaged Materials," Journal of Advanced Applied Mechanics, Vol. 25, pp. 239–294, 1987.

50. Kruch, S., Chaboche, J. and Lesne, P. "A New Damage Approach for Creep Crack Growth Prediction," In: Zyczkowski M., Editor. *Creep in Structures*, IUTAM Symposium Cracow/Poland, Berlin/Heidelberg, Germany: Springer Verlag, pp. 355–362, 1990.

51. Lemaitre, J. and Plumtree, A. "Application of Damage Concepts to Predict Creep Fatigue Failures," Journal of Engineering Material and Technology, Vol. 101, pp. 284–292, 1979.

52. Chaboche, J. "Continuous Damage Mechanics, A Tool to Describe Phenomena Before Crack Initiation," Journal of Nuclear Engineering Design, Vol. 64, pp. 233–247, 1981.

53. Lemaitre, J.A. "Continuous Damage Mechanics Model for Ductile Fracture," Journal of

Engineering Material and Technology, Vol. 107, pp. 83–89, 1985.

54. Rousselier, G. "Ductile Fracture Models and Their Potential in Local Approach of Fracture," Journal of Nuclear Engineering Design, Vol. 105, pp. 97–111, 1987.

55. Lemaitre, J. and Marquis, D. "Modeling Elasto Plasticity Damage and Ageing as Coupled Behaviors in Engineering Materials," In: Tooth A. and Spence J., Editors. Applied Solid Mechanics, 2nd Meeting, Glasgow/ London, UK, Elsevier, pp. 277–302, 1997.

56. Lämmer, H., and Tsakmakis, C.H. "Discussion of Coupled Elastoplasticity and Damage Constitutive Equations for Small and Finite Deformations," International Plasticity, Vol.16, No. 5, pp. 495–523, 2000.

57. Frear, D.R., Jones, W.B. and Kinsman, K.R. "Solder Mechanics; A State of the Art Assessment," Minerals, Metals & Material Society, Warrendale, PA, pp. 29-104, 1991.

58. Srinivas, V., Ramanjaneyulu, K. and Jeyasehar, C. "Multi-stage Approach for Structural Damage Identification Using Modal Strain Energy and Evolutionary Optimization Techniques," Structural Health Monitoring, Vol. 10, No. 2, pp. 219-230, 2011.

59. Whitten, L., Schulza, E. and Udda, J. "Single and Multiaxis Fiber Grating Based Strain Sensors for Civil Structure Applications," Oregon Department of Transportation Research, pp. 1-9. 1998.

60. Gea, H.C. and Luo, G.H. "Stress Based and Strain Based Methods for Predicting Optimal Orientation of Orthotropic Materials," Structural and Multidisciplinary Optimization,Vol. 26, pp. 229–234, 2004.

61. Coffin, L.F. "A Study of the Cyclic Thermal Stresses on a Ductile Metal," Transactions of ASME, Vol. 76, pp. 931-950, 1954.

62. Manson, S.S. "Fatigue: A Complex Subject-some Simple Approximations,"

Experimental Mechanics, Vol. 5, No. 7, pp. 193-226, 1965.

63. Kilinski, T.J., Lesniak, J.R. and Sandor, B.I. "Modern Approaches to Fatigue Life Prediction of SMT Solder Joints," In: Lau J.H., Editor, Solder Joint Reliability Theory and Applications, Van Nostrand Reinhold, NY, Chapter 13, pp. 384-405, 1991.

64. Mander, J.B., Panthaki, F.D. and Kasalanat, A. "Low-cycle Fatigue Behavior of Reinforcing Steel," Journal of Materials in Civil Engineering, Vol. 6, No. 4, pp. 453-468, November, 1994.

65. Engelmaier, W. "Fatigue Life of Leadless Chip Career Solder Joints During Power Cycling," IEEE Transactions on Components, Hybrids, and Manufacturing Technology, Vol. CHMT-6, No. 3, pp. 232-237, 1983.

66. Manson, S.S., Halford, G.R. and Hirschberg, M.H. "Creep Fatigue Analysis by Strain Range Partitioning," ASME Symposium, Design for Elevated Temperature Environments, pp. 12-28, 1971.

67. Lee, W.W., Nguyan, L.T. and Selvaduray, G.S. "Solder Joint Fatigue Models: Review and Applicability to Chip Scale Packages," Microelectronics Reliability, Vol. 40, pp. 231-244, 2000.

68. Darveaux, R., Benerji, K., Mawer, A. and Dody, G. *Durability of Plastic Ball Grid Array assembly*, Ball Grid Array Technology, Lau, J. Editor, McGraw Hill Inc, New York, NY, pp. 86-95, 1995.

69. Akay, H., Zhang, H. and Paydar, N. "Experimental Correlation of an Energy Based Fatigue Life Prediction Method for Solder Joints," Advances in Electronic Packaging, Proceeding of the Pacific Rim/ASME International Intersociety of Electronic and Photonic Packaging Conference, Interpack, Vol. 2, pp. 1567-1574, 1997.

70. Utah State University, Utah State Climate Center, http://climate.usurf.usu.edu/, reviewed 2009.

71. U.S. Department of Transportation, Bridge Technology, Design. "Comprehensive Design Example for Prestressed Concrete (PSC) Girder Superstructure Bridge, pp122-127," Step 2011.

72. ANSYS, "Material Data Tables," Version 13, 2011.

73. Beer, F. and Johnson, E.R. *Mechanics of Materials, Third Edition*, McGraw Hill Publication, pp. 54-61, 2002.

74. Sheldon, I. "Sheldon's ANSYS.NET Tips and Tricks: Drucker-Prager Model," Memo Number STI:08/02., ANSYS Revision 11.0.2008, pp. 34-41, 2008.

75. http://en.wikipedia.org/wiki/Bilinear_interpolation.

76. Okura, J.H. "Effect of Temperature and Moisture on Durability of Low Cost Flip Chip on Board (FCOB) Assemblies", PhD Dissertation, Department of Mechanical Engineering, University of Maryland, College Park, MD, pp. 95-98, 2001.

77. Gyllenskog, J. and Ladani, L. "Fatigue Crack Initiation and Propagation in Aileron Lever Using Successive Initiation Modeling Approach," AIAA Journal of Aircraft, Vol. 49, No. 8, pp. 1387-1395, August 2011.

78. Nelson, S., Ladani, L., Topping, T. and Lavernia, E. "Fatigue and Monotonic Loading Crack Nucleation and Propagation in Bimodal Grain Size Aluminum Alloy," Acta Materialia, Vol. 59, pp. 3550–3570, 2011.

79. Ladani, L. "Reliability Estimation for Large Area Solder Joints Using Explicit Modeling of Damage," IEEE Transactions on Device and Materials Reliability (T-DMR), Vol. 8, No. 2, pp. 375-386, June 2008.

80. Koh, S.K. and Stephens, R.I. "Mean Stress Effects on Low Cycle Fatigue for a High Strength Steel," Fatigue Fracture of Engineering Materials and Structures, Vol. 14, No. 4, pp. 413-428, 1991.

81. Amde, A.M., Chini, S.A. and Mafi, M. "Model Study of H-Piles Combined Loading," Geotechnical and Geological Engineering, Vol. 15 pp. 343-355, 1997.

82. Ellis, E.A. and Springman, S.M. "Modelling of Soil Structure Interaction for a Piled Bridge Abutment in Plane Strain FEM Analyses," Computers and Geotechnics, Vol. 28, pp. 79-98, 2001.

83. Kalayc, E., Civjan, S., Breña, A., Sergio F. and Allen, C.A. "Load Testing and Modeling of Two Integral Abutment Bridges in Vermont, US," Structural Engineering International, Vol. 21, No 2, pp. 181-188, May 2011.

84. Pétursson, H., Collin, P., Veljkovic, M. and Andersson, J. "Monitoring of a Swedish Integral Abutment Bridge," Structural Engineering International, Vol. 21, No. 2, pp. 175-180, May 2011.

85. Huang, J., Shield, C. and French, C. "Parametric Study of Concrete Integral Abutment Bridges," Journal of Bridge Engineering, Vol. 13, No. 5, pp. 511-526, September 2008.

86. Huang, J., Shield, C. and French, C. "Time-Dependent Behavior of a Concrete Integral Abutment Bridge," Transportation Research Record, Journal of the Transportation Research Board, 0361-1981, Special Volume CD 11-S, pp 299-309, Tuesday, June 17, 2008.

87. Von-Mises, R. "Mechanik der Festen Körper im Plastisch Deformablen Zustand. Göttin. Nachr," Math. Phys., Vol. 1, pp. 582–592, 1996.

88. Miner, M.A. "Cumulative Damage in Fatigue," Journal of Applied Mechanics, Vol. 12,

pp. 159-164, 1945.

89. Palmgren, A. "Die Lebensdauer von Kugellagern," Zeitschrift des Vereins Deutscher Ingenieure, Vol. 68, pp. 339-341, 1924.

90. Ladani, L. and Razmi, J. "Probabilistic Design Approach for Cyclic Fatigue Life Prediction of Microelectronic Interconnects," IEEE Transactions on Advanced Packaging, Vol. 33, No. 2, pp. 559-568, May 2010.

91. Ralph, R.I. and Henry, F.O., "*Metal Fatigue in Engineering*," Second edition, John Wiley & Sons, Inc. p. 69, ISBN 0-471-51059-9, 2001.